

**DESIGN OF BIOCOMPATIBLE ASPARAGINE-GRAPHENE OXIDE
FREE CHLORINE SENSORS FABRICATED USING SOLUTION-
BASED PROCESSING**

DESIGN OF BIOCOMPATIBLE ASPARAGINE-GRAPHENE OXIDE
FREE CHLORINE SENSORS FABRICATED USING SOLUTION-
BASED PROCESSING

By

JUNAID SIDDIQUI, B.A.Sc.

A Thesis Submitted to the School of Graduate Studies in Partial Fulfilment of the Requirements
for the Degree of Master of Applied Science

McMaster University © Copyright by Junaid Siddiqui, October 2022

McMaster University

Master of Applied Science (2022)

Hamilton, Ontario

(Electrical and Computer Engineering)

TITLE: Design of Biocompatible Asparagine-Graphene Oxide Free
Chlorine Sensors Fabricated Using Solution-Based Processing

AUTHOR: Junaid Siddiqui
M.A.Sc. University of Waterloo, Waterloo, Canada

SUPERVISOR: Dr. M. Jamal Deen

NUMBER OF PAGES: 97, xix

Lay Abstract

Free chlorine is used to disinfectant sources of water, and eliminate pathogens. The World Health Organization (WHO) maintains strict amounts of free chlorine in water due to its widespread usage owed to its low cost and persistence in water systems. Too little, and it will not be an effective disinfectant, and too much and the high consumption of free chlorine increases the risk cancer or the formation of hazardous chemicals. Recently, free chlorine sensors that measure an electrical response proportional to the amount of free chlorine are gaining interest for fast, accurate, and repeatable measurements.

This thesis focuses on the design, fabrication, and evaluation of these sensors made using biodegradable materials in a solution-based fabrication processes with the aim of working towards large-scale fabrication of a printable ink. First, we review the results achieved by the sensors within recent literature. Second, we present the design of a sensor that aims to achieve environmentally friendly goals and maintain competitive performance characteristics. The, the sensor is tested under various conditions with its performance quantified under different conditions. Third, the sensor is characterized using a neural network to measure its performance and identify sources of improvement for future designs. Finally, we incorporate the sensor with an android app to measure free chlorine in remote water systems.

Abstract

Chlorine is used as a powerful disinfectant in water-related industries and in the food industry to remove bacteria and other harmful contaminants. We present a solution-based fabrication process for a biodegradable electrochemical free chlorine sensor using asparagine that is functionalized onto graphene oxide (GO). An ink solution of the GO functionalized with asparagine was fabricated then deposited onto a screen-printed carbon electrode (SPCE) using a spin-coater. The sensor showed high a sensitivity of $0.30 \mu\text{A ppm}^{-1}$ over a linear range of 0 to 8 ppm with a hysteresis-limited resolution of 0.2 ppm, very high selectivity in the presence of commonly interfering ions, and an operating voltage well below the reduction potential of dissolved oxygen. The sensor response time to achieve a steady state was 50 s, and it showed little change in its drift response over 16 h and over a temperature range of 10 to 45 °C. From the development of the free chlorine sensor, over 9000 datapoints were collected and used for training a neural network model to quantify and characterize factors affecting the free chlorine sensor performance. A readout system was designed with a printed circuit board and an android app to simplify free chlorine sensing for an end user.

Acknowledgements

I would first like to express my gratitude to Dr. M. Jamal Deen for supervising my research. I did not originally plan to pursue graduate studies, but upon meeting Dr. Deen during my 4th year, he presented me an offer to pursue a path where I could gain invaluable personal and technical skills. My ability to communicate about my research with other researchers was polished through our regular research meetings which gave me the confidence to speak about my technical expertise. Through these meetings and through continuous feedback in presentations and technical papers, Dr. Deen's guidance enabled me to refine my ability to return to basics and renew the planning, research, and execution process for every task I may carry out. Dr. Deen's technical and theoretical expertise in sensors, and research as a whole, honed my skills in the problem-solving process, and allowed me to develop skills that would give me a significant edge in the industry, no matter what I choose to do whether it is sensors, machine learning, or in electronics. I am extremely grateful for the guidance and opportunities presented throughout my research. I would also like to thank Dr. Ognian Marinov for his guidance during the noise measurements in for my thesis, and my committee members Dr. Ravi Selvaganapathy and Dr. Matiar Howlader for taking the time to review my thesis and providing valuable and insightful comments on my research.

I also had the privilege of working with some great researchers in Dr. Deen's team during these two years of study: Arif ul Alam, Mahtab Taheri, Mohammad Nami, Amir Hallajzadeh, Wei Jiang, Ryan Scott, Xuanyu Qian, Junzhi Liu, Ronald Luo, Sumit Majumder, Abu Ilius Faisal, Sophini Subramaniam, Mahdi Naghshvarianjahromi, and others. Of my colleagues, Arif ul Alam, and Wei Jiang deserve recognition for being mentors during my time as a graduate

student. Mahtab Taheri and Mohammad Nami deserve recognition for their ongoing and unwavering assistance in my research work. For this, I am very grateful.

The completion of this work was also aided by the McMaster ECE technical staff. Tyler Ackland's assembly of the circuit boards for our designs were also very important for the completion of the work.

Lastly, I would like to thank my sisters, my parents, and my teachers for their support during this work. I dedicate my thesis to them.

Table of Contents

Lay Abstract	iii
Abstract	iv
Acknowledgements	v
Table of Contents	vii
List of Figures	x
List of Tables	xv
List of Abbreviations	xvi
List of Symbols	xviii
Declaration of Academic Achievement	xix
Chapter 1 Introduction	1
1.1. Importance of Water Quality	1
1.1.1. Importance of Free Chlorine Sensing	1
1.2. Research Background	3
1.2.1. Sensing of Free Chlorine	3
1.2.2. Machine Learning	7
1.2.3. Research Challenges	10
1.3. Research Contributions	12
1.4. Thesis Organization	14
Chapter 2 Review of Free Chlorine Sensors	16
2.1. Fundamental Concepts.....	16
2.2. Experimental Methods.....	19
2.2.1 Voltammetry	19
2.2.2. Amperometry	25
2.2.3. Potentiometry	30
2.2.4. Chemiresistivity	32
2.2. Fabrication Methods	35
2.2.1. Chemical Functionalization	36
2.2.2. Electrochemical Functionalization	39
2.2.3. Chemical Vapor Deposition	41
2.2.4. Simple and Cost-Effective Fabrication methods	43
2.3. Conclusion	44

Chapter 3 Design Parameters of Asparagine-Functionalized Graphene Oxide Free Chlorine Sensors & Predictive Modeling	46
3.1. Material Parameters	46
3.1.1. Graphene Oxide	48
3.1.2. Asparagine	49
3.2. Fabrication	51
3.2.1. Solution-Based Processing.....	52
3.2.2. Ink Deposition.....	55
3.3. Neural Networks Design for Predictive Modelling	56
3.3.1. Neural Network Inputs.....	57
3.3.2. Datasets.....	59
3.3.3. Validation Process	60
3.4. Conclusion	65
Chapter 4 Experimental Results of Asparagine-Functionalized Graphene Oxide Free Chlorine Sensors & Predictive Modeling	68
4.1. Experimental Setup	68
4.1.1. Chemicals and Reagents	68
4.1.2. Apparatus	68
4.1.3. Preparation of the Electrode.....	69
4.1.4. Preparation of Samples	70
4.2. Results and Discussions	71
4.2.1. Mechanism	71
4.2.2. Hysteresis	74
4.2.3. Drift.....	74
4.2.4. Interference	75
4.2.5. Temperature	76
4.2.6. Figure of Merit	77
4.3. Neural Network Modelling	79
4.3.1. Optimal Model Selection	79
4.3.2. NN Training	80
4.3.3. Input Parameter Performance.....	81
4.4. Conclusion.....	90
Chapter 5 Conclusions and Future Work	92
5.1. Conclusions	92
5.2. Future Work	95

References.....	99
Appendix A Copyright Permissions	116
Appendix B Code Bases.....	120
Machine Learning Code Base.....	120
Firmware Code Base.....	120
Android App.....	120

List of Figures

Figure 1-1: Graphic showing the effects of free chlorine concentrations that are too low or too high, and the uses of water properly disinfected within the acceptable limits.	3
Figure 1-2: DPD-chlorine reaction product [35].....	5
Figure 1-3: Comparing inputs and outputs between classical programming and machine learning [43]......	8
Figure 1-4: (a) NN diagram showing the direction of data flow from input layer, across hidden layers, to the output layer [43]; (b) Diagram of NN with 5 nodes in the input layer (\mathbf{x}), 7 nodes in the first hidden layer ($\mathbf{h}^{(1)}$), 4 nodes in the second hidden layer ($\mathbf{h}^{(2)}$), and 1 node in the output layer (\mathbf{o}).	10
Figure 2-1: (a) Models of the electric double layer region where anions are adsorbed to the surface of the electrode [55]; (b) a plot of the diffusion coefficients of HOCl and OCl ⁻ at different temperatures, the regular operational temperature range, and normal range measured with sensors [16].	18
Figure 2-2: (a) 3-electrode setup used for voltammetry and amperometry, and (b) linear sweep voltammetry voltammogram with $E_{p/2}$ and E_p showing the voltages at the half-peak and peak current responses [66].	19
Figure 2-3: (a) LSV voltammogram of CGO–SnO ₂ electrode reducing NaOCl (concentrations of $i - vi$ 0, 0.1, 0.9, 4.01, 8.05, 10.08 ppm) [73]; (b) LSV voltammograms overlaid from the BDD electrode, across a pH 4–10 in 96.4 ppm free chlorine solutions; scan rate 0.1 V s ⁻¹ . Dashed arrow points to decreasing pH values [67].	23
Figure 2-4: (a) CV Potential waveform plot with E_i and E_f showing the minimum and maximum potentials applied, respectively, and t_λ showing the midpoint of one cycle [66]; (b) CV voltammogram showing oxidation and reduction peaks and their potentials, E_o and E_r , respectively, and forward and backward peak currents, I_{pf} and I_{pb} , respectively [66]; (c) CV voltammogram of PDPE in 744 ppm NaOCl at a scan rate of 0.05 V s ⁻¹ [74]; (d) Selectivity measurements on PDPE in the presence of NO ₃ ⁻ (7.3 ppm), SO ₄ ²⁻ (13.5 ppm), CO ₃ ²⁻ (11.3 ppm), HCO ₃ ⁻ (14.5 ppm), Cl ⁻ (1.8 ppm) ions at V_{app} 1.5 V [74].	24

Figure 2-5: (a) A potential step at t_0 used in chronoamperometry measurements [77]; (b) The growth of the diffusion layer and its thickness over time [77]; (c) Resulting current as a function of time [77].	27
Figure 2-6: The chronoamperometry process for (a) $t = 0$ before the potential step where the free chlorine (green) is dispersed in the solution, (b) just after the potential step, there is a spike in current as the solute in contact with the surface of the electrode reacts immediately, forming the products of the reaction, and begins developing the electric double layer (dashed lines), and (c) at steady state shows the flow of the products (yellow) and free chlorine (green) and the electric double layer (dashed lines); (d) simultaneous pH and free chlorine measurement at varying pH (4 to 10) and free chlorine concentrations (0, 2, and 4 ppm) [39].	30
Figure 2-7: Two-electrode setup for potentiometric measurements; The chemical reaction shows the reduction of free chlorine using a ferrocene-based electrode [84].	32
Figure 2-8: (a) Schematic of chemiresistive sensor with two electrodes and sensitive material deposited in between; (b) SEM images of Whatman no. 1 filter paper modified with PEDOT:PSS [93]; (c) SEM images of Whatman no. 1 filter paper modified with PEDOT:PSS/graphene nanohybrid ink [93]; (d) Nanohybrid ink-modified paper-based sensor signal responses in solutions with different concentrations of free chlorine [93]; (e) Linear relationships between the measured responses of the nanohybrid ink sensor material for different lengths of time, the normalized resistance and the logarithmic concentration of free chlorine [93]; (f) Overoxidation reaction scheme of PEDOT by NaClO showing the opening of conjugated double bonds and reducing its conductivity as a result [96].	34
Figure 2-9: Chemical structures of functional groups used in functionalizing carbon-based materials for fabricating electrochemical free chlorine sensors. (PCAT: phenyl capped polyaniline tetramer; ABAPE: 4-Aminophenylboronic acid pinacol ester).	38
Figure 2-10: (a) Schematic of amine compound undergoing an electrochemical reaction under an applied potential	40
Figure 2-11: Fabrication schematic and mechanism of CVD process.	42
Figure 2-12: Stepwise fabrication of (a)-f) pencil graphite electrode and then g)-l) drawn on paper with an insulating polymer layer applied to define the desired surface area [74]. m) The preparation process of carbon paste electrode modified with ferrocene [84].	44

Figure 3-1: Schematic diagram of a (a) graphene oxide sheet, (b) graphene sheet, (c) CNT, and d) diagram of graphene sheets reducing free chlorine molecules.	49
Figure 3-2: Chemical diagram of (a) amino-acid base form and (b) asparagine.....	50
Figure 3-3: Proposed reaction products of asparagine with GO where (a) the COOH group is covalently bonded to the GO sheet, and (b) the α -amino is covalently bonded to one of the carboxylic acid groups on the GO sheet.	53
Figure 3-4: Proposed forward and backward reaction products of asparagine-GO in the presence of OCl^- where (a)-(b) the $-\text{NHCl}$ group is formed at α -amino group and the amide group due to the presence of high pH, and the reversible reaction due to the presence of OH^- being the catalyst for base-catalyzed hydrolysis.....	54
Figure 3-5: Diagram of the spin-coater and use with an SPCE. The SPCE is taped to the rotating chuck using double sided tape such that the conductive area of the electrode is directly above the center of chuck. The control unit and control knob are used to set the rotating speed and duration.	56
Figure 3-6: Individual node in a NN with respective input nodes (x), output nodes (y), weights on each connection (w) and biases (b).....	57
Figure 3-7: NN architecture with 10 nodes in the input layer, 1 node in the output layer, (a) 8 nodes in both hidden layers, and (b) 16 nodes in both hidden layers; (c) ReLU activation function used in the nodes of the hidden layer.	62
Figure 3-8: K-fold Cross Validation method where four identical blank NNs are created. The training data is divided into four equal parts or folds, and used to train and test the models such that three folds (blue) are used to train the model and the last fold (black) is used to test the model. The weights, biases, and other NN parameters are given by w , and the test errors are given by ϵ . The final error is given by calculating the average of the errors of all four tested models.	64
Figure 3-9: Flowchart that details each step and task carried out from importing and formatting the raw sensor data (purple), evaluating, and testing (blue) various different NN architectures (orange), then isolating the parameters and evaluating the MAE and PCC of each parameter to quantify their impact on the sensors' performances (yellow).	65

Figure 4-1: Experimental setup including laptop with potentiostat software, EmStat potentiostat, 3-electrode configuration with counter electrode (CE), reference electrode (RE), working electrode (WE), and a beaker with the free chlorine solution.....	69
Figure 4-2: Fabrication steps of the asparagine-GO free chlorine sensor.....	70
Figure 4-3: ColorQ PRO 7 Hand-Held Photometer commercial DPD-based colorimetric test kit with accompanying test tubes and chlorine reagents.	71
Figure 4-4: (a) Varying free chlorine measurements measured using chronoamperometry, from low to high concentrations of free chlorine; (b) The current response of 3 different free chlorine sensors measured at 50 s to show the reproducibility of the sensors.....	72
Figure 4-6: (a) Response current of chronoamperometry measurements at 50 s to show hysteresis behavior of sensor with free chlorine measurement cycling from low to high (blue) then high to low (orange) for (a) asparagine-GO (b) GO (c) SPCE; (d) Cyclic voltammetry response of the SPCE, plain GO, and GO-asparagine (FCI = free chlorine).	73
Figure 4-6: (a) Current response at 50 s vs. free chlorine concentration to show the hysteresis behavior of the sensor from 3 increasing and decreasing concentrations, and (b) drift measured with asparagine-GO free chlorine sensor in tap water over 16 h.....	74
Figure 4-8: Insensitivity to commonly interfering ions and sensor response to an equal volume of free chlorine after introducing ions. Details for ion addition are shown in the graph.....	76
Figure 4-8: Change in current due to change in temperature with constant source of tap water..	77
Figure 4-9: (a) MAE of validation curve of the optimal model and (b) a zoomed in image showing its evolution after 100 epochs.....	81
Figure 4-10: (a) Evolution of MAE and PCC on full dataset over duration of free chlorine measurement; Correlation plots of the model’s performance on all the sensors at (b) t = 1 s, c) t = 10 s, (d) t = 25 s, e) t = 42 s to show the evolution of spread and the accuracy of the model at different points in time.....	83
Figure 4-11: Correlation plot comparing the model performance on predicted free chlorine concentration of sensors fabricated (a) without and (b) with spin coating.....	85
Figure 4-12: Correlation plot comparing the model performance on predicted free chlorine concentration of sensors fabricated (a) with decreasing and (b) increasing free chlorine concentrations during the measuring cycles.	86

Figure 4-13: Correlation plot of the model’s performance at $t = 40$ s for sensors used for (a) one, (b) two, and (c) three cycles..... 88

Figure 4-14: (a) Evolution of MAE and PCC over time on sensors used after 1, 2, and 3 cycles; correlation plot of the model’s performance at $t = 40$ s for sensors used for (b) one, (c) two, and (d) three cycles..... 89

List of Tables

Table 3-1: Amines used to functionalize to GO, their chemical structures, and hazards	51
Table 4-1: Comparison of fabrication, sensitivity, range, hysteresis, selectivity, and response time of amperometric sensors made with graphene-based or carbon-based substrates.....	79
Table 4-2: Validation MAE and PCC of NNs (PCC on top; MAE below).	80
Table 4-3: PCC and MAE values of sensor data when isolating the ‘Increasing ppm’ parameter and again according to ‘Spin Coating’. (PCC top, bold; MAE bottom).....	86

List of Abbreviations

ABAPE	4-Aminophenylboronic acid pinacol ester
AFM	Atomic force microscopy
Ag	Silver
AgCl	Silver chloride
Al ₂ (SO ₄) ₃	Aluminum Sulphate
Au	Gold
C	Carbon
CA	Chronoamperometry
CaCl ₂	Calcium chloride
CE	Counter Electrode
Cl ⁻	Chloride Ion
Cl ₂	Chlorine gas
CNT	Carbon Nanotubes
CO ₃ ²⁻	Carbonate ion
-COOH	Carboxyl Group
Cu	Copper
CuCl ₂	Copper (II) chloride
CV	Cyclic Voltammetry
CVD	Chemical Vapor Deposition
DI	Deionized (water)
DPD	<i>N,N</i> -diethyl- <i>p</i> -phenylenediamine
EDL	Electric Double Layer
FoM	Figure of Merit
GO	Graphene Oxide
H ₃ O ⁺	Hydronium Ion
HCO ₃ ⁻	Biocarbonate ion
HOCl	Hypochlorous acid
Hz	Hertz
IHP	Inner Helmholtz plan
KNO ₃	Potassium nitrate
K ₂ CO ₃	Potassium carbonate
KCV	K-Fold Cross Validation
LOD	Limit of Detection

MAE	Mean Absolute Error
MgCl ₂	Magnesium chloride
ML	Machine Learning
NaCl	Sodium chloride
NaHCO ₃	Sodium bicarbonate
NaOH	Sodium hydroxide
Na ₂ SO ₄	Sodium sulphate
(NH ₄) ₂ SO ₄	Ammonium sulphate
NN	Neural Network
O ₂	Oxygen
OCl ⁻	Hypochlorite ion
OH ⁻	Hydroxide ion
-OH	Hydroxyl group
OHP	Outer Helmholtz plane
PCAT	Phenyl capped polyaniline tetramer
PCC	Pearson correlation coefficient
PEDOT:PSS	poly(3,4-ethylenedioxythiophene): poly(styrenesulfonate)
Pt	
ppm	Parts per million
ppb	Parts per billion
RE	Reference Electrode
RPM	Revolutions per minute
rGO	Reduced Graphene Oxide
SO ₄ ²⁻	Sulphate ion
WE	Working Electrode
WHO	World Health Organization
ZnNO ₃	Zinc (II) nitrate

List of Symbols

E	Reduction potential [eV]
$E_{HOCl,Cl^-/OH^-}^0$	Formal reduction potential of $HOCl$ to OH/Cl^- [eV]
R	Gas Constant [$J \cdot mol^{-1} \cdot K^{-1}$]
T	Absolute temperature [K]
F	Faraday's Constant [$C \cdot mol^{-1}$]
I	Current response from sensors [μA]
D	Diffusion of free chlorine ions in solution [$m^2 \cdot s^{-1}$]
C_{HOCl}^*	Initial concentration of $HOCl$ in solution [$mol \cdot mL^{-1}$]
A	Sensor surface area [mm^2]

Declaration of Academic Achievement

This thesis was written by Junaid Siddiqui under the supervision and guidance of Dr. M. Jamal Deen from McMaster University.

- **Chapter 1:** I present an overview of fundamental free chlorine sensing principles, machine learning and neural networks, and a sensor readout system for displaying free chlorine measurements.
- **Chapter 2:** I present a detailed review of the sensing methods used by electrochemical free chlorine sensors, and then discuss the various fabrication processes used to create the sensors.
- **Chapter 3:** I designed a novel and environmentally friendly electrochemical free chlorine sensor made using and biodegradable materials in a solution-based fabrication process. I designed a neural network using industry standard neural network modelling tools and K-fold Cross Validation.
- **Chapter 4:** I carried out detailed measurements to extract the performance characteristics of the free chlorine sensors and characterized the testing and performance parameters using neural network models.
- **Chapter 5:** I designed a PCB, built an Android app and wrote firmware to interface between them and the free chlorine sensors. I carried out measurements for measuring the noise in sensors to characterize their longevity and performance characteristics. Tyler Ackland was responsible for assembling the PCB.
- **Chapter 6:** Based on the literature review and design experience, I discussed several key research challenges for the coming years. Although free chlorine sensors face challenges with fouling, interference, and repeatability, free chlorine sensors are expected to make drastic improvements in the near future.

Chapter 1 *

Introduction

1.1. Importance of Water Quality

Having access to safe and potable water is a necessary condition to human development and good health. It is considered to be one of the most effective means in ensuring healthy living, and reducing poverty [1]. However, only 74% of the world's population have access to potable water and still 2 billion people continue to consume water from sources that are not safely managed, 282 million people with limited access to safe water, and 122 million people using untreated surface water sources [1]. The contaminants in the untreated water vary, with some of the most immediately dangerous contaminants being microorganisms which can cause either cholera or dysentery [2], [3]. Many technologies exist to remove these types of organic contaminants where the water becomes potable through the addition of chemicals. As the added disinfecting chemicals are so ubiquitous, consistently monitoring the quantities of these substances in water systems becomes equally critical in its importance in ensuring public safety and health.

1.1.1. Importance of Free Chlorine Sensing

Free chlorine is a strong oxidizing agent that is used to disinfectant and remove disease-causing bacteria that can be found in drinking water, pool water, or waste-water [2], [3]. The chlorine compound can bond with and destroy the outer surface of many water-borne-diseases

* Part of this work will be submitted for consideration for publication in RSC Advances as: J. Siddiqui, M. Taheri, M. Nami, M. J. Deen, Carbon-Based Electrochemical Free Chlorine Sensors, December 2022. (in preparation)

causing viruses and bacteria such as Escherichia coli O157:H7, different species of salmonella, shigella, campylobacter jejuni, vibrio cholera, pseudomonas, and other microorganisms [4]. Chlorine disinfects water by destroying bacteria through oxidation reactions with the various cellular components, membranes and proteins which lead to the collapse of cell processes, and cell death [5], [6]. Free chlorine also has a slow decay rate in water systems. So free chlorine persists in water systems, continuing to kill bacteria ensuring that the water is safe to consume for long periods of time [2], [7]. With its relatively slow decay rate in water systems, it becomes a very desirable disinfectant compound in water treatment systems.

The World Health Organization (WHO) standards state that free chlorine levels in drinking water must be kept between 0.1 – 4 parts per million (ppm) for effective disinfection whilst maintaining acceptable standards for residual concentration [8], and in swimming pools between 1 – 3 ppm (**Figure 1-1**) [9]. Free chlorine is also used as an additive in water to wash fecal matter, bacteria, or other contaminants, and to clean food from incidental contaminants – an important factor in preserving the cleanliness of fruits and vegetables, and by extension their freshness by eliminating bacteria that would promote oxidation reactions [10]–[13]. However, according to WHO, the chicken, fish and leafy greens are recommended to be washed in water with concentrations of free chlorine up to 200 ppm, and for red meat with concentrations up to 50 ppm [14].

Not maintaining the free chlorine levels at high enough concentrations will result in the water not being properly disinfected and thus increase the risk of water-borne diseases. If the free chlorine concentration is above these limits in water or food, then their consumption increases the risk of bladder cancer and tumors, increases the likelihood of the formation of toxic trihalomethanes and halogenated acetic acids, or the food and water may acquire mutagenic

properties, foul odors, foul tastes, or accelerate the evolution of antibiotic-resistant bacteria [9], [14], [15]. Furthermore, 3,000 kWh of electricity for the production of 1 metric tonne of chlorine from brine or salt water is required, making it a costly chemical to produce. Given these conditions, free chlorine levels should be heavily monitored and routinely regulated.

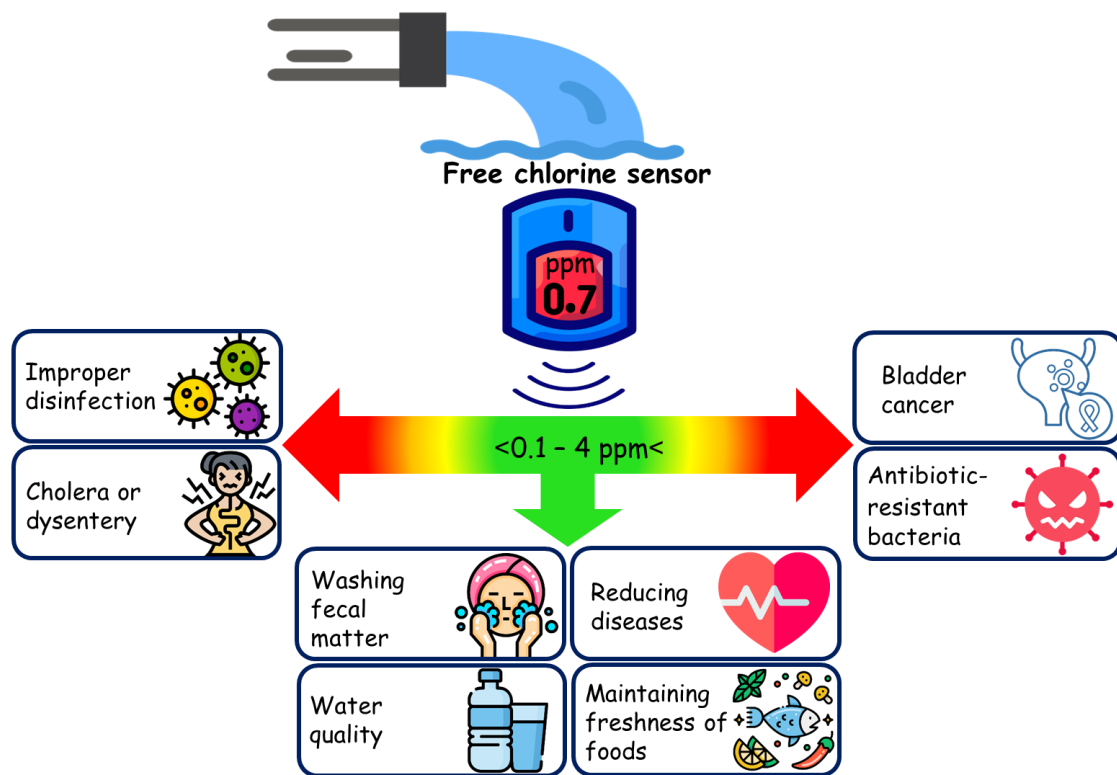
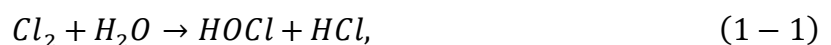


Figure 1-1: Graphic showing the effects of free chlorine concentrations that are too low or too high, and the uses of water properly disinfected within the acceptable limits.

1.2. Research Background

1.2.1. Sensing of Free Chlorine

When free chlorine is dissolved in water, it is present in solution as hypochlorous acid (HOCl) and hypochlorite ion (OCl⁻). Chlorine gas is bubbled into the water wherein it dissolves and eliminates the contaminants, producing HOCl according to the following chemical equation:



where HOCl is a weak acid and is partially dissociated into H⁺ and OCl⁻ in water:



For a given concentration, the percentage distribution of HOCl and OCl⁻ is a function of the concentration of H⁺ (H₃O⁺) and is usually expressed by:

$$\log \frac{[OCl^-]}{[HOCl]} = \log K_a - \log [H^+], \quad (1 - 3)$$

where [OCl⁻] and [HOCl] are the equilibrium concentrations of OCl⁻ and HOCl, respectively, and K_a is the dissociation constant of HOCl (3.0*10⁻⁸ at 25 °C), and [H⁺] is the concentration of H⁺ ions in the solution [16], [17].

Diverse methods of measuring free chlorine are available with varying levels of difficulty and accuracy for purposes such as industrial use, municipal use, and academic research. Due to the prevalent use of chlorinated water, its use has become known to the general public, and thus conventional measurement methods are standardized and published in handbooks and guidelines. Analytical methods to measure residual free chlorine with varying user difficulty and accuracy, and for uses in academia, industries, and municipalities are widely available [18]–[22]. Due to its wide-spread use, conventional measurement tools were standardized, but these methods can be used only with specific materials and devices, which limits the extent of the applications they can reach [8], [9], [18], [23].

The current standard for measuring free chlorine declared by the United States Environmental Protection Agency is a colorimetric method which requires the use of N,N'-diethyl-p-phenylenediamine (DPD) and is widely used because of its high sensitivity [13], [24]–[27]. The hypochlorite oxidizes DPD to form a compound which colors the solution magenta at a pH of ~7 as shown in **Figure 1-2**. The color is read through a photometric detector which determines the concentration of free chlorine based on the intensity of the magenta coloring. The detection range of DPD is roughly between 0 to 9 ppm with an accuracy of 0.04 ppm [4], but the

use of such a method is not user-friendly, toxic, prone to error, and expensive [25], [26]. There are other existing methods used to measure the concentration of free chlorine in a solution such as colorimetric sensing methods in which the intensity of the color change of a compound is compared to a set of standards. Some colorimetric sensors include luminescent quantum dots fabricated from ZnO [28] and others which make use of smartphones to identify free chlorine concentrations [29], [30]. There are also various types of fluorescent free chlorine sensors such as those made using carbon dots [31]–[33] and others such as the organic molecule, BODIPY, which glows green under ultra-violet light in the presence of free chlorine [34].

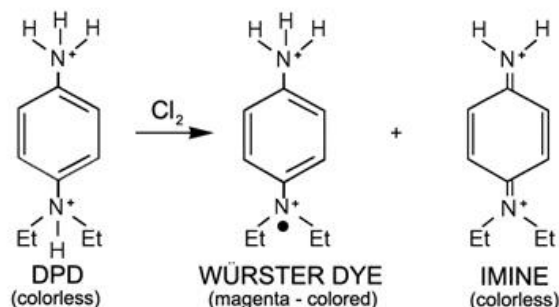
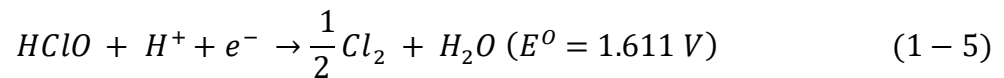
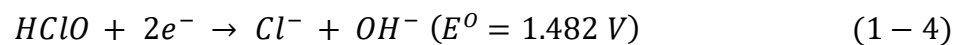


Figure 1-2: DPD-chlorine reaction product [35].

The above mentioned approaches to measuring free chlorine levels in water are either time consuming, or require expensive laboratory-based equipment [21]. As a result, alternative sensing technologies must be used to address these limitations. Recent developments in accurate and easy-to-use electrochemical free chlorine sensors enable the use of such sensors that are quick and simple to use outside of laboratory environments. Electrochemical sensors using electrochemical methods offer a way to measure free chlorine with high-sensitivity and excellent accuracy using various materials and systems that are already established for other water quality monitoring applications, and can often out-perform standard colorimetric methods [21], [36].

Electrochemical sensing technologies address some challenges presented by colorimetric or fluorometric sensing. These include accurate, easy-to-use methods that have small footprints using inexpensive sensors, making them attractive alternatives. Recent developments in fabrication technologies have significantly facilitated the realization of these sensors, and have enabled precise control of material morphologies (roughness, smoothness, grain size), properties (conductivity, resistivity, carrier mobility), and the quantities of materials used [21]. The free chlorine compound is detected at the surface of the electrode where it is broken down into its reduction products. Below is the equation for the electrochemical reduction of free chlorine used by many sensors. The irreversible reduction reaction of free chlorine is given by Eq (1-1) and Eq. (1-2) with their the reduction potential, E^0 [37], [38]:



The equations show that HClO reduces into two different products via two different reactions: at a reduction potential of 1.482 V, HOCl is reduced into Cl^- and OH^- , and at a reduction potential of 1.611 V, HOCl is reduced into Cl_2 and H_2O . This reduction creates a current that can be detected by a dedicated device or system. These chemical reactions shows the transfer of electrons which generates a current that is proportional to the concentration of free chlorine. Larger amounts of free chlorine will generate larger currents. This proportionality makes it useful for electrochemical analysis, but an accurate measurement of free chlorine also needs careful control and precise measurement of the pH, temperature, flow rate, and pressure of the solution [24]. Without precise control, the measurements will be subject to the consequences of the changing physical parameters, and this will appear as interference in the measured results.

The advantages that electrochemical sensors have over other types of sensors include wider sensing ranges and faster responses while maintaining competitive performance characteristics [21]. The sensors can easily be integrated with microelectronic components for automated operations, or they can be made compatible with cell-phones. They are also compatible with existing water distribution systems and with fabrication technologies such as additive fabrication [13], [21], [39]. They are also developed at a lower total cost to reach a wider variety of applications. Some electrochemical sensors include hand-drawn chemiresistive sensors made using PEDOT:PSS [12]. However, one of the challenges with PEDOT is that it is not safe to use near food and thus, an alternative approach is needed. Also, Ni metal nanoparticles were combined with graphene shells to fabricate electrochemical free chlorine sensors; however, this has the risk of heavy metal poisoning [40]. When using sensors near water systems and food products that will be used by people, it is extremely important that the sensor materials are safe and that they do not leach into and contaminate the food. When people consume this water or food, they will not have to worry about being exposed to toxic compounds. Therefore, the safety of free chlorine sensors is important because many free chlorine sensors, although they use electrochemical methods, are not safe enough to be used in drinking water environments or they are not suitable to be used near food products.

1.2.2. Machine Learning

The ethos of Machine Learning (ML) is to learn from previous experiences, or to provide a set of rules or an algorithm, for which the computer can find answers for a given problem [41], [42]. This is in contrast to classical programming applications where the program is designed to take inputs and perform tasks with explicit instructions. **Figure 1-3** shows this contrast between classical programming where in classical programming, the program is given data and creates an

output with explicit instructions [43]. On the other hand, ML consists of the process of making computers capable of performing functions or tasks without being explicitly programmed. The machine essentially learns what it must do using the data made available to it. This enables the automation of tasks that are generally easy for people to do themselves such as recognize photos, characters, speech, or build patterns and equations, but they may not be aware of the underlying mechanisms when carrying out these tasks. The main assumption for using ML is that data used previously will not be very different than data that will be seen. This allows the same rules to be used continuously.

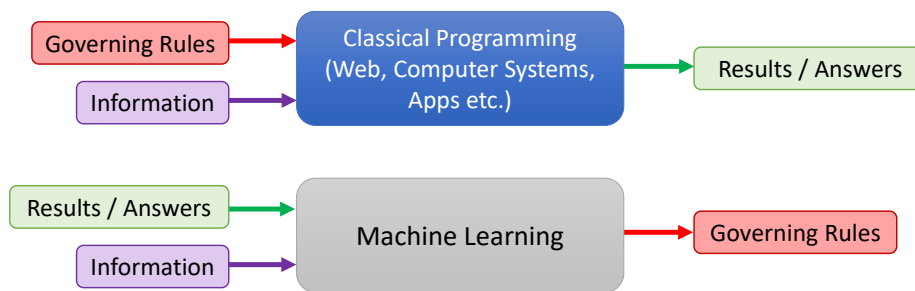


Figure 1-3: Comparing inputs and outputs between classical programming and machine learning [43].

In applications where the training data used has known inputs and outputs, such as sensor applications, the ML problems are known as supervised learning problems [41]. For a given task, the ML algorithm is given data where each item consists of a pair - an input and its corresponding correct output. For example, if a model is trying to detect the contents of an image, it can be considered a classification problem. This is where the goal is in trying to predict a discrete output from a set of discrete categories. The other type of problem is a regression problem which is designed to predict a continuous output by mapping a set of input variables to a continuous function over some range. For evaluating and predicting the performance of the free chlorine sensors, the nature of the problem is a regression problem. This is because to train a model for the sensors, it requires a set of inputs with parameters related to fabrication and testing

where the output is a continuous function for the free chlorine concentration in ppm over a range of 0 – 9 ppm.

There are many different types of methods and algorithms that can be used to create models for regression problems [41]–[45]. Some of the more popular algorithms include linear regression algorithms, polynomial regression algorithms, and neural network (NN) algorithms. For the free chlorine sensors, the algorithm to be used is the NN regression algorithm due to the simplicity in training and development [46]–[48]. **Figure 1-5(a)** shows a diagram of a NN with 1 input layer, 1 output layer, and 2 hidden layers [43]. The first input layer has five nodes, the first hidden layer has seven nodes, the second hidden layer has five nodes, and there is one node in the output layer [**Figure 1-5(b)**]. Each of the nodes in a layer are connected to all the nodes of the layer before it and after it, with the exceptions being the input and output layers as shown in the figure. During the training of the NN, the training data is fed through the input layer, and the output is used as a target for the inputs. Through repeated inputs and iterations, the weights and values for the nodes and connections are calculated. The end result is a model with values on each node and connection which would resemble a series of matrix equations where each layer's value depends on the one preceding it. Once the model is trained, the NN can be used to predict outputs.

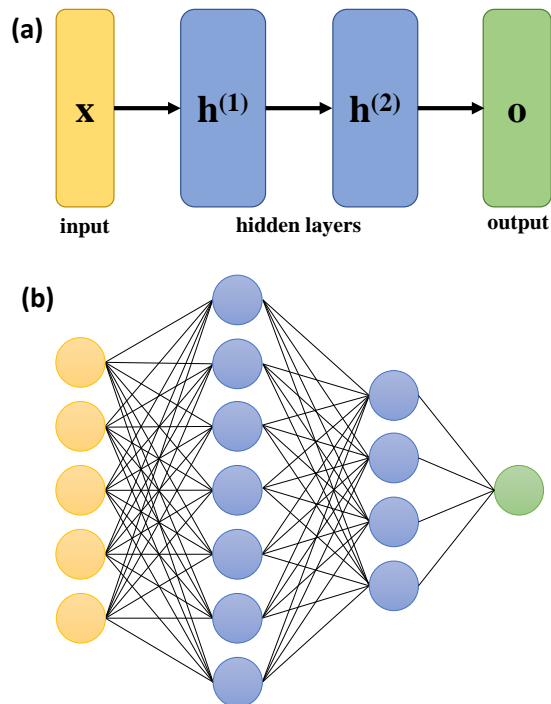


Figure 1-4: (a) NN diagram showing the direction of data flow from input layer, across hidden layers, to the output layer [43]; (b) Diagram of NN with 5 nodes in the input layer (\mathbf{x}), 7 nodes in the first hidden layer ($\mathbf{h}^{(1)}$), 4 nodes in the second hidden layer ($\mathbf{h}^{(2)}$), and 1 node in the output layer (\mathbf{o}).

1.2.3. Research Challenges

Electrochemical free chlorine sensors have been growing in popularity over the last five years, and will continue to grow due to increasing interests in water quality monitoring sensors [7], [18], [19], [21], [49]–[51]. While some free chlorine sensors have low limits of detection (LOD), high sensitivities, fast response times, and reversible measurements, others exhibit moderate performance characteristics and others show poor characteristics. One of the key issues in electrochemical free chlorine sensing is related to sensor stability and repeatability due to the oxidizing effect of free chlorine. These phenomena are likely related to:

- Physical degradation of the sensing materials: materials on sensor surface impacted by water flow causing them to break apart, reducing response characteristics
- Chemical degradation of the sensing materials: irreversible reactions between the sensing material and H_3O^+ alter its chemical composition

- Interference from the test solution: free chlorine oxidation/reduction sensing blocked due to adsorption of other ions or from bio-fouling
- Lack of reversible sensing materials for HOCl and OCl⁻

Another research challenge is in relation to the fabrication technologies which determine the sensor costs. The sensor fabrication costs should be minimized and should use as little material as possible. Thus, fabricating sensors at high temperatures or using vacuum environments should be avoided as much as possible as well as fabrication methods where only single sensors can be created at a time which creates a bottle-neck in the fabrication process. The alternative would be making solution-based sensors using low-cost processing where the sensitive material is an ink and can be printed in high volumes. However, the quality of materials used to make the sensors depends highly on post-treatment processing at high temperatures creating a trade-off between performance characteristics and sensor costs which is a stimulus for further research into this problem.

Given the number of published articles on free chlorine sensors, one can conclude that research and development on electrochemical free chlorine sensors is not as expansive compared to that of, for example, pH sensors which are a more popular water quality sensing device [36], [49], [52], [53]. The major drawback with free chlorine sensing is the lack of diversity in reversible electrochemical materials able to sense free chlorine. Ideally, the electrochemical sensing material will either react with free HOCl or OCl⁻ reversibly so it will return to its original state, or selectively transport free chlorine to the target electrode. Colorimetric methods like DPD-based sensing methods are examples of irreversible processes because the chemical undergoes an irreversible reaction, and the reacted material must be discarded after every use. The consequences are that waste is continuously generated so long as it remains a standard.

Furthermore, the chemical reactivity of free chlorine further reduces viable options. For example, cyclic voltammetry must be carried out to determine an optimal bias voltage for the amperometric measurements – this is also a factor which increases the complexity of the sensor. One of the most common challenges with free chlorine sensors is the interfering effects of dissolved O_2 which would affect the sensing accuracy as it is an electroactive compound between a voltage range of ± 1 V. Finally, as listed above, the need for a potentiostat for amperometric or voltammetric free chlorine sensors increases both sensor cost and sensor complexity. The potentiostat or readout system would have to be adjusted for every individual material. Addressing all these challenges can make free chlorine sensor configurations and conditions similar to those for pH sensors by improving performance characteristics while at the same time reducing fabrication costs.

1.3. Research Contributions

The focus of this research was on a biodegradable and solution-based free chlorine sensor with a dedicated readout system. This work targets the development of these sensors, and by extension water quality monitoring sensors. The aim is for the sensors to be more environmentally friendly and suited to mass-production while also maintaining competitive performance characteristics for drinking water, pool water, wastewater, and food processing applications. The main contributions of this work are the following:

- **Literature review on carbon-based electrochemical free chlorine sensors and their various implementation methods.** Through the process of this review, fundamental concepts, mechanisms, and fabrication methods were explored, and the results are presented for some of the most novel carbon-based electrochemical free chlorine sensors.
- **Material and fabrication design, and performance results of a biodegradable solution-based material for free chlorine sensing using chronoamperometry.** The

proposed free chlorine sensor aims to be biodegradable using environmentally-friendly materials and solution-based fabrication processes to facilitate printing methods whilst also maintain performance characteristics competitive with other free chlorine sensors in literature. Using chronoamperometry for the electrochemical sensing method, the measurement results of the sensor validate the performance characteristics and the successful approach in using solution-based processes, although future considerations should be to print the sensors with an inkjet printer.

- **Neural network modelling of sensor’s testing parameters for performance characterization.** A neural network model was trained and tested to evaluate the impact of various parameters during the testing of the sensor. The neural network model was used to characterize the longevity of the sensor, the effect of hysteresis on the sensors’ performance, and the effect of changing fabrication parameters. The model was also used to minimize the total amount of sensing time required and predict the sensor’s performance characteristics after repeated uses.
- **An integrated system was developed using an Arduino Uno microcontroller with Bluetooth connectivity to a smartphone application to sample, process, and display signals from the free chlorine sensor.** This design aimed to demonstrate the performance characteristics of the sensor when used in real applications with non-laboratory equipment such as a commercial potentiostat. The potentiostat uses circuit designs from the literature to create a potentiostat device limited to chronoamperometric measurements. The sensor is characterized to have moderate performance but is within an acceptable standard in measuring drinking water and pool water.

Publications:

1. J. Siddiqui, M. Taheri, A. U. Alam, and M. J. Deen, “Nanomaterials in Smart Packaging Applications: A Review,” *Small*, vol. 18, no. 1, p. 2101171, 2022, doi: 10.1002/sml.202101171.
2. J. Siddiqui and M. J. Deen, “Biodegradable asparagine-graphene oxide free chlorine sensors fabricated using solution-based processing,” *Analyst*, 2022, doi: 10.1039/D2AN00533F.

1.4. Thesis Organization

In Chapter 1, an introduction to the importance of water quality monitoring is presented. As a motivation for the following chapters, the mechanism through which free chlorine is sensed and measured is discussed. Next, various types of sensors that include the recent trends and activities in free chlorine sensing are discussed and then compared with the current standard. Then the challenges relevant to the existing modes of free chlorine are presented to introduce the motivation of developing solution-based biodegradable electrochemical free chlorine sensors. Finally, a summary of the major contributions of this research and the structure of the thesis are described.

In Chapter 2 an extensive literature review of carbon-based electrochemical free chlorine sensors is presented and discussed. The fundamental elements of electrochemical sensing that provide the basis for free chlorine sensing is described. Following this, the electrochemical methods used to measure various types of free chlorine sensors are presented and evaluated. Then, the fabrication methods for free chlorine sensors are presented and evaluated in comparison to one another.

In chapter 3 the material and design parameters for the solution-based biodegradable free chlorine sensors are presented. While many types of electrochemical free chlorine sensors were shown to produce repeatable and sustainable performances, it comes at the cost of not being environmentally friendly or not easily producible. We used common building block materials and methods to design a material that is biodegradable and has the potential to be manufactured in large quantities. Following this, the design parameters used to create a neural network machine learning model are described to demonstrate the uses of machine learning algorithms for sensors in electrochemical water quality monitoring systems.

In chapter 4, we discuss the procedures and setups used to fabricate and test the device. Described in this section are reagents, apparatus, fabrication process for the sensors using the proposed designs, and experimental set-ups for measurements. Then, the results for the various experiments are presented and analyzed, and discussed in the context of sensitivity, hysteresis, temperature dependence, interference, and drift. The performance of a neural network model is described to highlight the potential of neural networks with water quality monitoring.

In Chapter 5, a readout system for the free chlorine sensor is presented. The free chlorine sensor uses a standard amperometric sensor designed to be compatible with the asparagine-GO sensor. An Arduino Uno microcontroller with a compatible printed circuit board, and a smartphone application with Bluetooth wireless capabilities were programmed as the user interface to sample, process, and display the sensor signals.

Chapter 2 [†]

Review of Free Chlorine Sensors

2.1. Fundamental Concepts

An electrochemical sensor is a device that can detect the exchange of electrons between a transducing component and the analyte [54]. For free chlorine sensors, this is the electrode and the free chlorine, respectively. The sensor has two basic functional units [49]: a receptor and a transducer. The receptor takes the results of the chemical interaction between it and the free chlorine and transforms it into usable energy, then the transducer takes this energy and converts it into an electrical signal. This electrical signal is in response to the reduced free chlorine that oxidizes the surface of the electrode. In this redox reaction, the exchange of electrons as seen in Eq. (1) and (2) is what indicates the transfer of information, whether it is a current, voltage, resistance, or another change in a material's electrical properties.

The measurement is carried out by immersing the sensor into a solution of free chlorine with one or two additional electrodes, all together making up the electrochemical, or voltaic or galvanic cell, under the mechanisms of the electrical double layer (EDL) [55]. In a galvanic cell, reactions occur spontaneously at the electrodes where they are converting chemical energy into electrical energy. Focusing on carbon-based free chlorine sensors and the electrochemical methods used with these sensors, the main electrochemical methods that will be mentioned are voltammetry (cyclic voltammetry, linear sweep voltammetry); amperometry

[†] Part of this work will be submitted for consideration for publication in RSC Advances as: J. Siddiqui, M. Taheri, M. Nami, M. J. Deen, Carbon-Based Electrochemical Free Chlorine Sensors, December 2022. (in preparation)

(chronoamperometry, hydrodynamic amperometry); potentiometry; chemi-resistivity; and transistor-based methods.

The working electrode of electrochemical sensors are built on the electrical double layer (EDL) [49], [55]. The applied potential at the electrode forms what is effectively a capacitor between the solution and the electrode. In the solution, the double layer is made up of a few layers: the inner layer is made up of solvent molecules, ions, or other charged species in the solution [Figure 2-1(a)] and is known as the *Helmholtz* or *Stern layer*. The region of electrical charges is called the *Inner Helmholtz Plane* (IHP) which is represented by the first dashed line, has a total charge density σ^i from the adsorbed ions in this layer. Approaching this IHP are solvated ions at a distance represented by the second dashed line which is called the *Outer Helmholtz Plane* (OHP). Because of thermal diffusion and Brownian motion in the solution, the molecules/ions that are not adsorbed are distributed throughout the diffuse layer which begins at the end of the OHP into the bulk solution with the charge density σ^d . The charges at the surface of the electrode and the IHP form what is effectively a capacitor: two charged planes separated with a dielectric, and the IHP and OHP form another charged layer, or capacitance layer, with a charged plane and a second plane with a lower charge density. These layers combine to form the EDL.

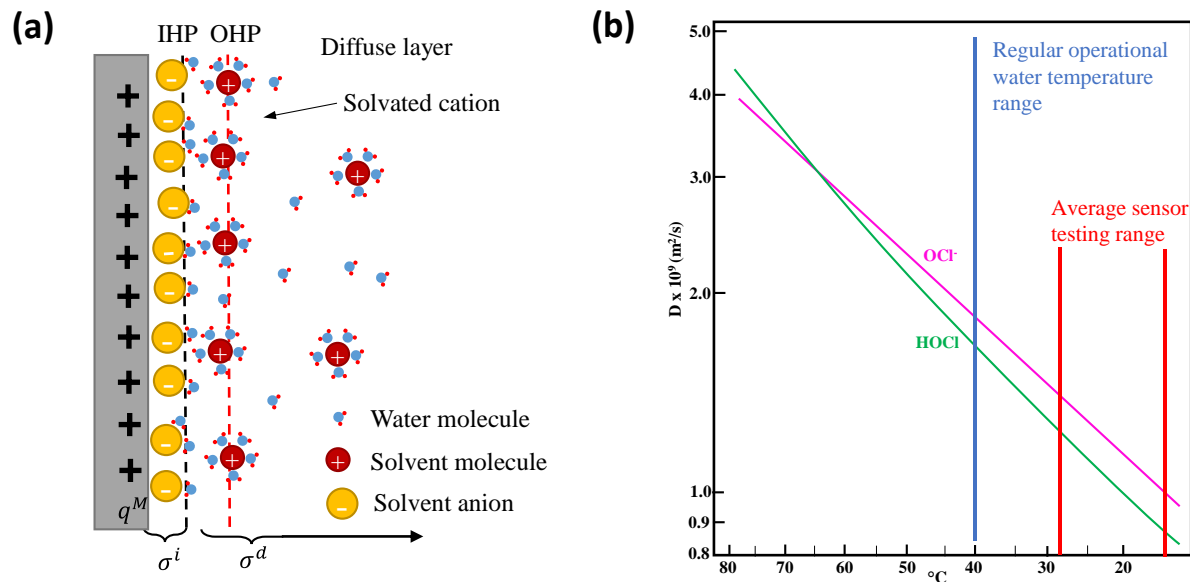


Figure 2-1: (a) Models of the electric double layer region where anions are adsorbed to the surface of the electrode [55]; (b) a plot of the diffusion coefficients of HOCl and OCl⁻ at different temperatures, the regular operational temperature range, and normal range measured with sensors [16].

The detection of free chlorine here depends on the reaction rate of HOCl, the dissociation ratio between HOCl and OCl⁻ and the mass transport as a result of the diffusion of the HOCl from the bulk solution to the electrode surface [16], [56], [57]. This is dependent on the pH level which influences the dissociation ratio between HOCl and OCl⁻, and the temperature which influences the rate of diffusion. **Figure 2-1(b)** shows the dependence of diffusion on temperature, as well as normal operating and testing ranges for various types of sensors. For example, a graphite pencil lead functionalized with ammonium carbamate was found to be dependent on pH and temperature. so the free chlorine values were compensated using empirically constructed relationships [24]. If the sensors are used over small pH ranges or small temperature ranges, the effects of temperature and pH changes can often be ignored. If the ranges and effects are substantial, then they would require the results being compensated through various methods, such as empirically deriving mathematical relationships between current, pH, temperature, and free chlorine concentrations [21], or through ML modelling [58]–[63]. If the

sensor is to be used in applications with small temperature ranges, then the mass transport effect is negligible as can be determined from **Figure 2-1(b)**, but if it is used in applications with a wider temperature range, then the free chlorine sensor should be used in tandem with a temperature sensor to compensate for the effect caused by the change in the diffusion constant.

2.2. Experimental Methods

2.2.1 Voltammetry

Voltammetric sensing methods require three electrodes submerged into a solution: working, counter and reference electrodes to obtain precise measurements, as shown in the schematic in **Figure 2-2(a)** [21], [64]. At the working electrode where the desired electrochemical reaction occurs, an electrical potential is applied that is varied linearly with time and the current that flows between the working electrode and counter electrodes is measured. The purpose of the reference electrode (often a silver/silver chloride electrode (Ag/AgCl)) is to control the potential between the working and counter electrodes (usually a platinum wire), and the counter electrode provides the current required to sustain the reaction [65]. This arrangement prevents large currents from passing through the reference electrode that could change the potential between the reference and working electrodes.

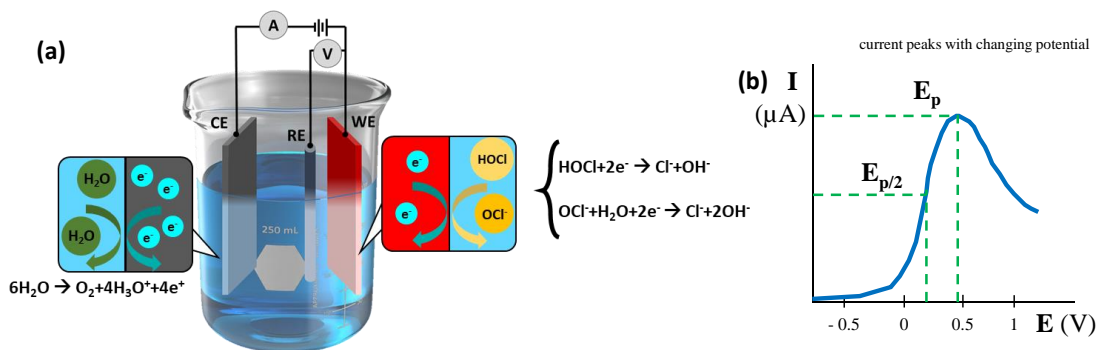


Figure 2-2: (a) 3-electrode setup used for voltammetry and amperometry, and (b) linear sweep voltammogram with $E_{p/2}$ and E_p showing the voltages at the half-peak and peak current responses [66].

Depending on the method used to apply the voltage, different types of voltammetry arise with the two most commonly used methods in carbon-based free chlorine sensors being linear sweep voltammetry (LSV) and cyclic voltammetry (CV) [54], [67]–[71]. The potential sweep from a small potential to a larger one can generate a current peak if an analyte is oxidized (or reduced) over the given potential range. This peak is a result of the flow of electrons from the analyte to the sensor in the oxidation reaction (or the reverse in a reduction reaction) where the number of electrons is governed by the chemical Eq. 1-3 and 1-4. After reaching the peak, the current declines because the analyte begins to deplete at the electrode surface. On the other hand, a potential varying from high to low will generate a reduction peak which appears as a negative current [21]. CV and LSV are very similar in that they both use a potential changing linearly with time, but CV also reverses the potential back to the starting potential.

Voltammetric measurements require specialized equipment which include a waveform generator to produce the excitation signal, a potentiostat to apply this signal to an electrochemical cell, a current-to-voltage converter to measure the resulting current and convert it to a voltage, and an XY recorder or oscilloscope to display the voltammogram (displays current as a function of the potential) as shown in **Figure 2(b)** [70], [71]. The first three items are normally incorporated into a single electronic device although modular instruments are also used. The potentiostat ensures that the working electrode potential will not be influenced by the reaction(s) which occur.

Linear Sweep Voltammetry

In both LSV and CV, a stationary working electrode is submerged in a solution that contains an excess number of electrolytes so that the transfer of free chlorine between the electrode and the solution occurs only through diffusive processes. In LSV, the working

electrode potential changes linearly with time where the potential starts at a lower limit when there is no reaction occurring, and then increases to an upper limit potential where the free chlorine is reduced or oxidized. The value at which free chlorine is reduced varies with the surface chemistry of the working electrode as various types of chemical reactions can occur [55], [66], [72]. The rate at which the potential changes is called the *voltage scan rate*. The characteristics of the linear sweep are given by a voltammogram displaying the current as a function of potential [**Figure 2-2(b)**]. The characteristics of the linear sweep voltammogram recorded depends on a number of factors that arise from the interaction between the electrode and the material such as: (i) the electron transfer reaction rate(s); (ii) the chemical reactivity of the electroactive species; and (iii) the voltage scan rate.

In the voltammogram in **Figure 2-2(b)**, the voltage E_p at the peak current value is related to the formal potential of the redox process and to the reversibility of the process, and provides information on the nature of the analyte in the reaction [66]. Similarly, the peak current at E_p provides information on the concentration of analyte, the number of electrons involved in the reaction, and may also indicate the presence of other chemical reactions. If the potential is scanned in a region where no charge transfer occurs, the electrode-solution interface behaves like a capacitor, and only a small capacitive current is measured as ions and molecules only modify their orientation at the electrode surface. When the potential reaches a region where there is an electrochemical reaction, a Faradaic current is measured which increases until it reaches a maximum [66]. After this maximum, the current decreases as the potential continues to increase. This peak occurs because of the increasing electron transfer rate as the potential reaches the analyte's reduction/oxidation potential while an increasing diffusion layer caused by the depleting or reacted free chlorine further and further away from the electrode surface. The peak

occurs when these two effects balance each other where the analyte concentration at the electrode's surface is still none-zero.

LSV measurements are shown in **Figure 2-3(a)**, and carried out on a crumpled graphene oxide (CGO)-decorated SnO₂ nanocolumns at six different concentrations of NaOCl (0, 0.1, 0.9, 4.01, 8.05, 10.08 ppm, increasing from i) to vi) [73]. The scan shows a well-defined reduction peak at -0.45 V for detecting free chlorine, and the intensity of the peak increases with the increased concentration of free chlorine. The inset shows the calibration curve from the LSV responses at the peaks which gives the electrode a sensitivity of 51.29 $\mu\text{A cm}^{-2} \text{ppm}^{-1}$. Another free chlorine sensor, a boron-doped diamond (BDD) electrode, was used with LSV to measure free chlorine in pH solutions over the pH range 4 –10, characterizing the relationship between current, pH and free chlorine [67]. In a solution of 96 ppm free chlorine and operating at 0.1 V s⁻¹, the results in **Figure 2-3(b)** show that as the solution pH decreases, the height of the peak also decrease, confirming that the concentration of OCl⁻ decreases with pH. The results demonstrated that the pH-dependent formation of OCl⁻ can be electrochemically tracked using a single BDD electrode, removing the need for extra sensors to measure both free chlorine and pH. Over a range of 0 – 100 ppm, the sensitivity of the sensors was found to be 2.2 $\mu\text{A ppm}^{-1}$ with an R² of 0.999 and high reproducibility using a very robust sensor.

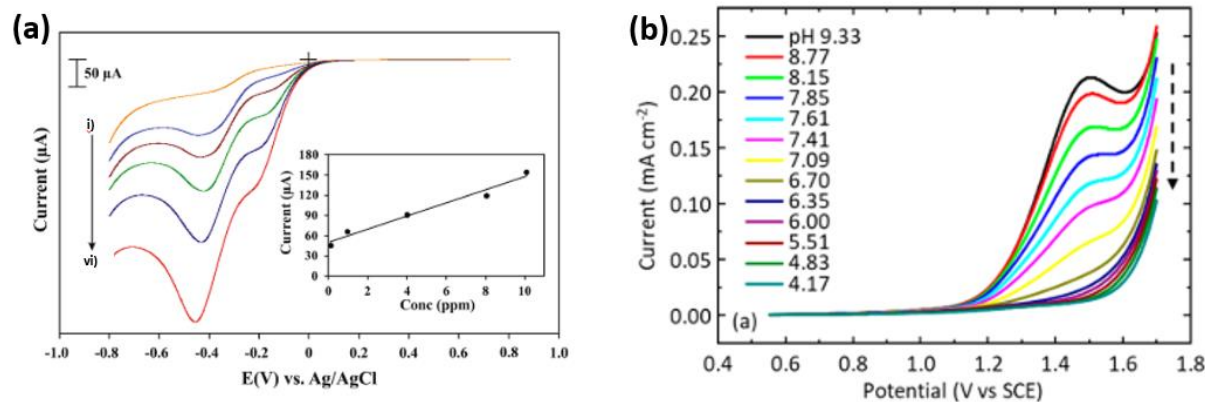


Figure 2-3: (a) LSV voltammogram of CGO-SnO₂ electrode reducing NaOCl (concentrations of **i** – **vi** 0, 0.1, 0.9, 4.01, 8.05, 10.08 ppm) [73]; (b) LSV voltammograms overlaid from the BDD electrode, across a pH 4–10 in 96.4 ppm free chlorine solutions; scan rate 0.1 V s⁻¹. Dashed arrow points to decreasing pH values [67].

Cyclic Voltammetry

Cyclic voltammetry (CV) is a versatile electroanalytical technique and is used in many different sensing applications [20], [65]. It is often the first experiment that is performed during electrochemical studies of a given compound or an electrode surface where its effectiveness lies in its ability to measure and observe reduction and oxidation behavior over a wide potential range. CV is similar to LSV, but the potential sweep is also reversed which results in a cycling of potential at the working electrode. The voltammogram for CV measurements is obtained by measuring the current at the working electrode during the potential scan, and the voltammogram displays the current as a function of potential. As shown in **Figure 2-3(a)**, the excitation signal for CV is a linear potential scan with a triangular waveform. This triangular signal sweeps the potential of the electrode between two values, a lower and a higher limit, and is sometimes called the switching potentials given by E_i and E_f [65]. **Figure 2-3(b)** shows the oxidation and reduction peaks, E_o and E_r , respectively, with the forward and backward current peaks, I_{pf} and I_{pb} , respectively. The formation and decay of these peaks is analogous to LSV, and was previously discussed.

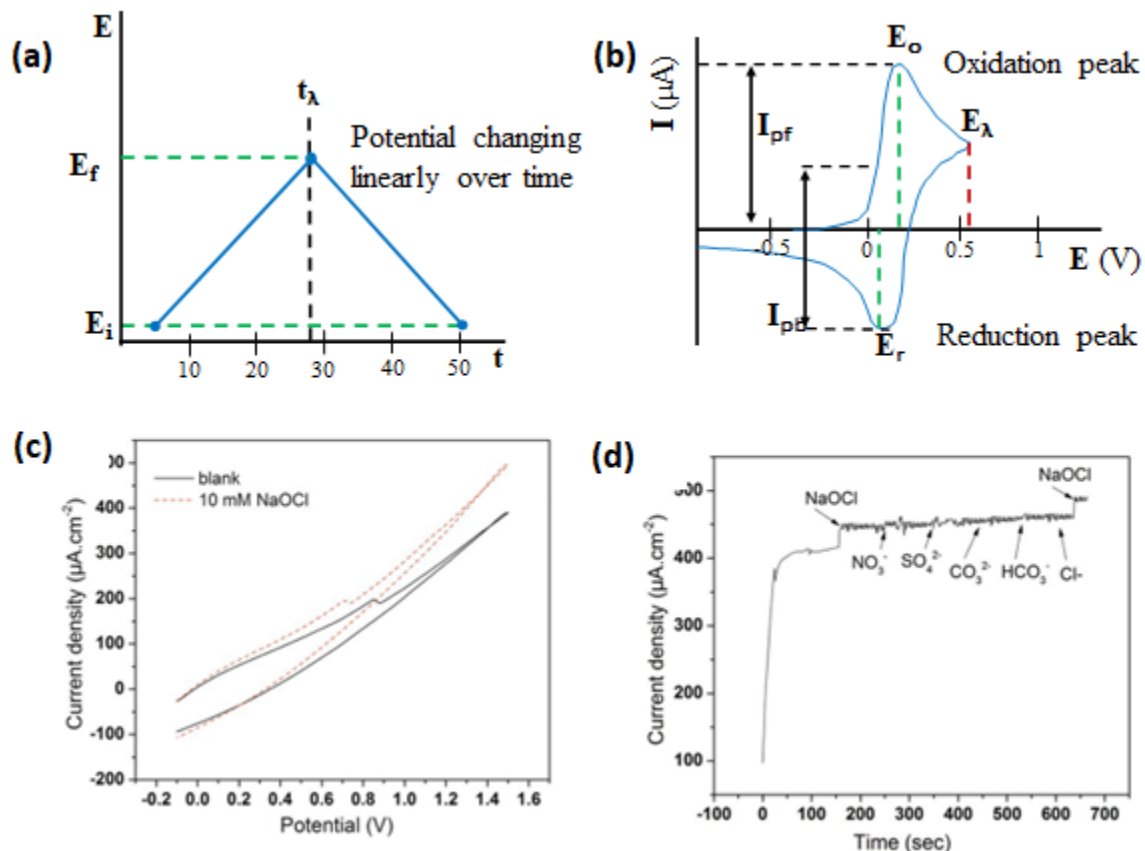


Figure 2-4: (a) CV Potential waveform plot with E_i and E_f showing the minimum and maximum potentials applied, respectively, and t_λ showing the midpoint of one cycle [66]; (b) CV voltammogram showing oxidation and reduction peaks and their potentials, E_o and E_r , respectively, and forward and backward peak currents, I_{pof} and I_{pob} , respectively [66]; (c) CV voltammogram of PDPE in 744 ppm NaOCl at a scan rate of 0.05 V s^{-1} [74]; (d) Selectivity measurements on PDPE in the presence of NO_3^- (7.3 ppm), SO_4^{2-} (13.5 ppm), CO_3^{2-} (11.3 ppm), HCO_3^- (14.5 ppm), Cl^- (1.8 ppm) ions at $V_{app} 1.5 \text{ V}$ [74].

A detailed understanding of CV can be gained by considering the Nernst equation and the changes in concentration that occur in the solution adjacent to the working electrode during electrolysis. The voltage excitation signal controls the ratio of HOCl to OH^-/Cl^- at the electrode surface described by the Nernst equation:

$$E = E_{\text{HOCl,Cl}^-/\text{OH}^-}^0 + \frac{RT}{nF} \ln \frac{\text{HOCl}}{\text{Cl}^-/\text{OH}^-} \quad (2-1)$$

where E_{HOCl} is the formal reduction potential of the coupled chemical reaction between from HOCl to OH^-/Cl^- [65]. An initial value of E which is sufficiently positive of E_{HOCl} maintains a

ratio wherein HOCl predominates, thus a higher potential creates a negligible current. Because this is an irreversible reaction the concentration of HOCl continues to decrease until the potential that remains in the solution is made up only of E°_{HOCl} [38].

One sensor that used CV to determine an operating potential was a low-cost and multifunctional graphite-pencil lead electrode. CV was performed at a scan rate of 50 mV s^{-1} as shown in **Figure 2-4(c)** [74]. The sensor obtained a sensitivity of about $0.515 \mu\text{A cm}^{-2} \text{ ppm}^{-1}$ where the free chlorine was reduced by the pencil-drawn graphite electrode into its reduction products shown in Eq. (1). The sensitivity obtained was $4.2 \mu\text{A cm}^{-2} \text{ ppm}^{-1}$ over a wide range between 0 – 262 ppm. **Figure 2-4(d)** shows the graphite electrode's selectivity measurements, respectively, where both of them show responses to free chlorine.

2.2.2. Amperometry

Similar to voltammetry, amperometry requires three electrodes submerged in a solution for precise measurements: the working electrode, the counter electrode, and the reference electrode [13], [21], [55], [64]. When a time-dependent electric potential is applied at the working electrode, a current flows between the working electrode and the counter electrode, and the reference electrode maintains a constant potential between the other two electrodes. The current is a result of either electrochemical oxidation or reduction of an electroactive species. If the electrons are flowing into the solution creating a negative current, then it is a sign that free chlorine is being reduced. On the other hand, if the current flow is positive, electrons are flowing into the electrode where the electrode is being reduced and may be a sign of reactions of involving compounds other than free chlorine. In this technique, the potential is often determined based on the position of redox peaks in the corresponding voltammogram [75], [76]. This potential is fixed on a what is usually a Pt, Au, or C-based working electrode, or an array of

electrodes with respect to a reference electrode [55]. The current as a result of this oxidation or reduction is directly correlated to one of two things: either the bulk concentration of the electroactive species, or the production/consumption rate of the electroactive species.

Amperometry provides the ability to distinguish between many electroactive species by carefully selecting a given electrode material and/or an applied potential which is determined through CV or LSV. However, since the number of oxidized species will likely increase as the applied potential is increasingly positive or the number of reduced species will likely increase as the applied potential is increasingly reduced, a suggested desirable range to avoid interfering ions is in the potential range between -0.2 to +0.2 V for analyte detection [77].

Amperometry sensing suffers from several limitations. For instance, the electrochemical reaction product may become adsorbed onto an electrode surface and interfere with the transfer of electrons [77]. This causes heterogenous electrochemical reactions to occur at the electrode-solution interface creating a gradual loss of sensitivity. One method for overcoming this adsorption is by using a pulsed potential instead of a continuously applied potential, however the experiment and desired results should also be modified to take this change into account. In the pulsed method, the amperometric detector measures current only for a short interval, which limits the duration of the sensor being oxidized and thus limits the amount of the sensor fouling. Another limitation with this method is the deterioration of the electrode surface which causes an increase in baseline noise. The deterioration altering the surface morphology or exposing the current collecting material may cause unwanted or random reactions and increase the sensor's baseline noise. Overcoming this limitation requires materials that are resistant to physical or chemical deterioration and requires further research.

Chronoamperometry

Chronoamperometric measurements use potential steps, a technique which can make use of only a few milliliters of solution when the solution that is being measured does not have to be stirred. The potential begins from a value where no Faradaic reaction occurs, and is stepped to a potential [Figure 2-5(a)] where the surface concentration (at the working electrode) of the electro-active species becomes effectively zero [Figure 2-5(b)] [77]. It is also used to investigate the various mechanisms of reactions and processes that occur on the electrode simultaneously with the movement of the electrons.

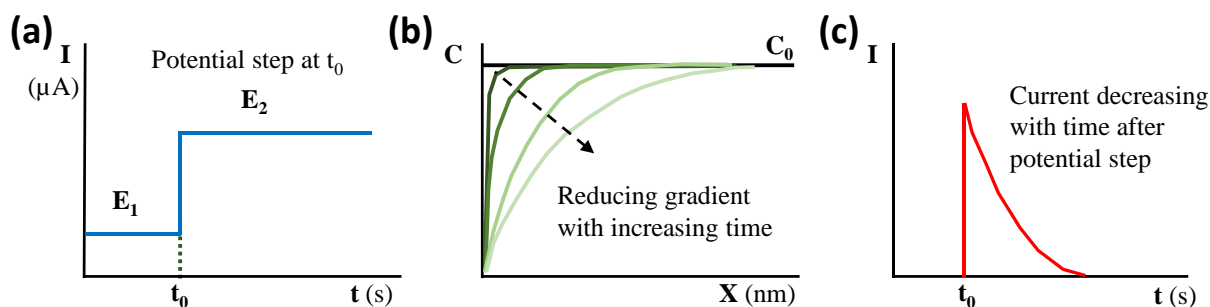


Figure 2-5: (a) A potential step at t_0 used in chronoamperometry measurements [77]; (b) The growth of the diffusion layer and its thickness over time [77]; (c) Resulting current as a function of time [77].

One of the advantages for a 3-electrode chronoamperometric system is that it allows researchers to determine the diffusion coefficient in reactions with a slow transfer of electrons. With slow electron transfer kinetics, the potential can be controlled and maintained at a value where the reaction itself is strictly diffusion controlled [78]. Since mass transport is diffusion-controlled, the resulting current as a function of time reflects the concentration gradient at the electrode's surface. The relationship between current and time is shown in **Figure 2-5(c)**, and is given by the Cottrell equation:

$$I(t) = \frac{nF\sqrt{D}C_{HOCl}^*A}{\sqrt{\pi t}}. \quad (2-2)$$

In the Cottrell equation for the reduction of $HOCl$, $n = 2$ gives the number of electrons in the reduction reaction, F is Faraday's Constant ($96485.33 \text{ C mol}^{-1}$), A is the sensor surface area, C_{HOCl}^* is the initial free chlorine concentration, and D is the diffusion constant of the $HOCl$ in the solution, often in the range of $10^{-3} - 10^{-4} \text{ mm}^2 \text{ s}^{-1}$ [24], [55]. The current decreases by $1/\sqrt{t}$, is proportional to \sqrt{D} , and is linearly proportional to the free chlorine concentration, C_{HOCl}^* . For solutions where C_{HOCl}^* is known, chronoamperometry can be used to determine the diffusion coefficients, or it can be used to determine the electrode surface area if the other variables are already known. Since the diffusion of a species is dependent on the temperature of the solution, an increased temperature would result in an increase in current and a lower temperature would result in a lower current [24], [39][16].

A unique property of chronoamperometry is that the chronoamperometric system may be simplified to having only two electrodes where the counter electrode is removed, and the reference electrode functions as both the reference and counter electrodes. This can occur when the applied potential at the working electrode is 0 V as was shown for a graphite and carbon paste electrode functionalized with ammonium carbamate, and another electrode made of sputtered gold [13], [24], [39]. A limitation for chronoamperometry, however, is that very short and very long experimental times should be avoided. This can be seen by the initial large current at low timescales, and a current approaching zero at high timescales, conforming to the Cottrell equation.

The physical process in chronoamperometric measurements in **Figure 2-5(a)-(c)** shows the formation of the electrical double layer and the diffusion from the start of the measurement until the system reaches a steady state. **Figure 2-5(b)** shows the free chlorine (green) dispersed in the solution. **Figure 2-5(c)** shows the initial formation of the products (yellow) just after the

potential step. The dashed lines show the EDL forming slowly. In **Figure 2-5(c)**, the EDL is formed, and the system has reached the steady state where there's a steady diffusion of free chlorine towards the electrode, and the products diffuse back towards the bulk solution with the diffusion layer evolving over time. At $t = 0$, the concentration of analyte (HOCl) at the surface of the electrode is the same as that in the bulk solution. As the analyte is consumed in the reduction reaction, the analyte concentration gradient begins to decrease if there is no convection in the solution to replenish the consumed analyte. With convection, the analyte at the electrode surface would be replenished, which would allow the current to reach a steady state and therefore allow for a constant measured current for a given free chlorine concentration.

The limitation of chronoamperometry in relation to temperature is due to the diffusion of the free chlorine species [**Figure 2-1(b)**]. An increase in temperature will cause the current to increase as well for a given free chlorine concentration and may give incorrect readings as result. This effect was reported and also compensated using a temperature sensor [21], [24]. The change in the sensitivity of the free chlorine sensor was monitored at different temperatures and compensated using an empirically-obtained relationship. A similar sensor was reported which compensated both temperature and pH where the effect that pH has on the measured current is shown in **Figure 2-6 (d)** [39].

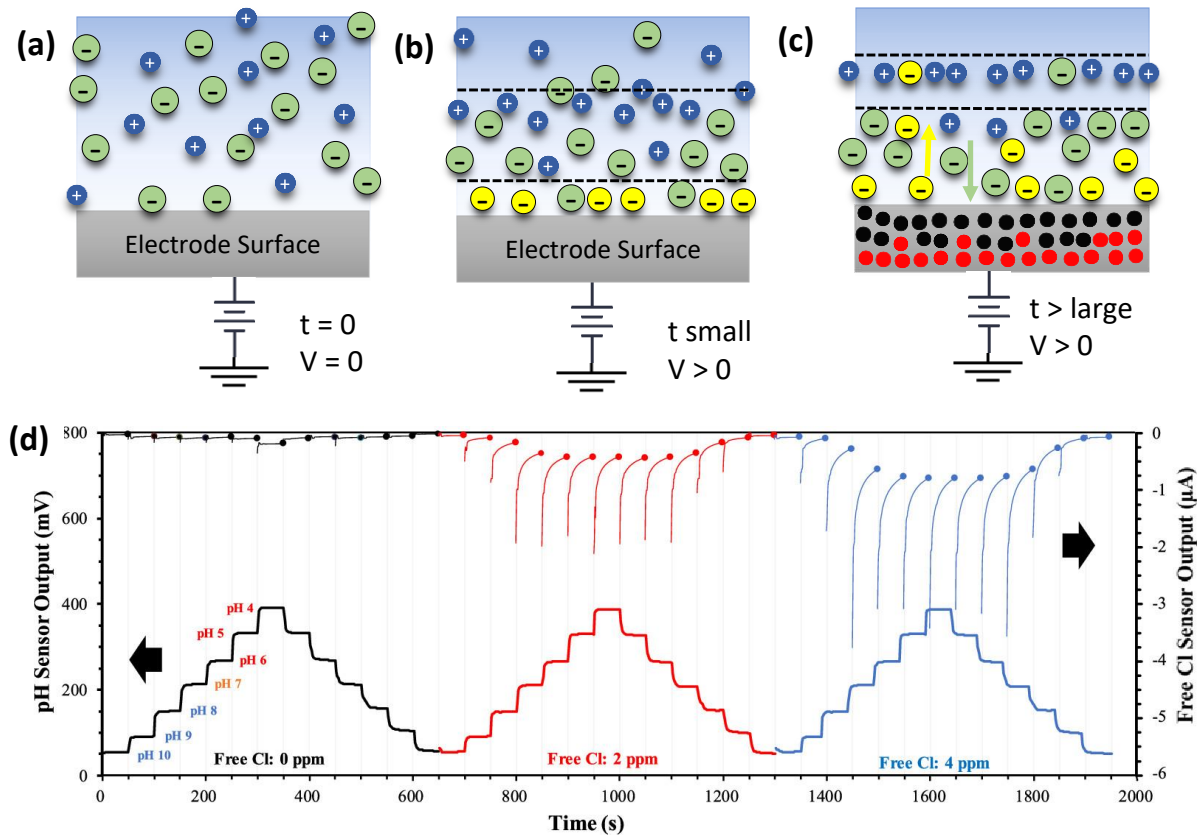


Figure 2-6: The chronoamperometry process for (a) $t = 0$ before the potential step where the free chlorine (green) is dispersed in the solution, (b) just after the potential step, there is a spike in current as the solute in contact with the surface of the electrode reacts immediately, forming the products of the reaction, and begins developing the electric double layer (dashed lines), and (c) at steady state shows the flow of the products (yellow) and free chlorine (green) and the electric double layer (dashed lines); (d) simultaneous pH and free chlorine measurement at varying pH (4 to 10) and free chlorine concentrations (0, 2, and 4 ppm) [39].

2.2.3. Potentiometry

Older types of potentiometric sensors that measured free chlorine concentrations used reduction reactions with ion buffer solutions called iodometric titration [79]–[82]. The chlorine would react with these ion buffers which would cause a potential change that would be measured by the sensor. This potential change, however, is only temporary. Due to the difficulty associated with the use of these ion buffers, its use did not become as wide-spread as colorimetric methods such as DPD or other electrochemical methods [26].

The standard potentiometric sensor systems are made of two electrodes: the working electrode which is made of the analyte-sensitive material, and the reference electrode which is commonly made with Ag/AgCl (**Figure 2-7**). When both electrodes are submerged in the solution, the open circuit potential between them is used to measure the free chlorine concentration in the solution [21], [83]. The measured potential was found to be linearly related to the log of the free chlorine concentration [83], [84]. One of the reported mechanisms for potentiometric free chlorine sensors is the use of an ion-selective membrane or material. One such effective membrane material was ferrocene used to measure various redox-active organic molecules is also shown to be effective in measuring free chlorine [84]–[86]. It was found that adding more ferrocene increases the current exchange density or increases the amount of free chlorine being reduced, and thus increases the current response of the sensor. However, too much ferrocene was also shown to affect the accuracy of the sensor such that the optimal composition of ferrocene was settled at 15%. The resulting sensitivity of the sensor was 52.9 mV/decade, close to the ideal Nernstein value of 59.16 mV/decade. This is because the transport of ClO^- anions into the material became easier at higher concentration gradients which increased the potential response at the working electrode; this is in accordance with Fick's first law of diffusion where higher concentration gradients diffuse faster across a given cross-sectional area [86].

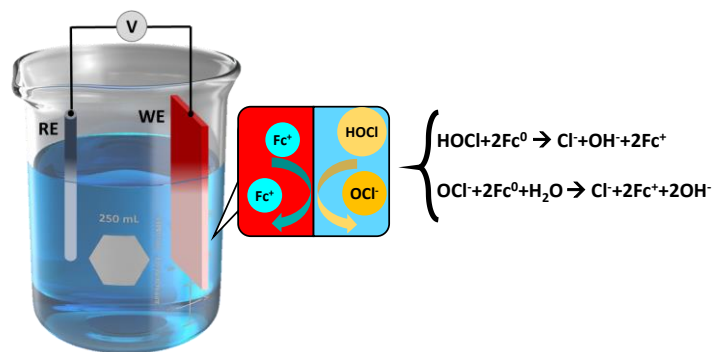


Figure 2-7: Two-electrode setup for potentiometric measurements; The chemical reaction shows the reduction of free chlorine using a ferrocene-based electrode [84].

One of the limitations of potentiometric sensors is that there is no internal signal amplification, so the measured signal is what the sensor detects. However, the advantage of using potentiometry for free chlorine sensing is that it only requires two electrodes without the need for a power source (as opposed to voltammetry or amperometry), the physical dimensions of the sensors can be reduced due to its structural resemblance to many types of potentiometric pH sensors [39], [87]–[89]. The potential difference measured between the working and reference electrodes is often hundreds of millivolts, and can be read by simple, inexpensive commercial voltmeters, and thus have the potential for greater use in laboratories and in the field for detecting free chlorine [21].

2.2.4. Chemiresistivity

Chemical sensors, also known as chemiresistors, are a type of sensor whose sensing mechanism is based on the change of electronic properties such as resistance or conductance due to interactions or contact with an electrochemical analyte such as free chlorine [54]. Chemiresistors are two-terminal devices made of source and drain contacts with the channel/transducing material as the sensitive material [Figure 2-8(a)] and has a constant applied potential (or current) between them when used to detect free chlorine [20], [90]–[93]. The sensing material has an intrinsic electrical resistance/conductance, which will change

accordingly upon exposure to solutions with different free chlorine concentrations. This can be irreversible such as the resistance of a nanohybrid chemiresistor [93] or it can be reversible such as carbon-based materials functionalized with phenyl-capped polyaniline tetramer (PCAT) [94] where the resulting current (or potential) signal is measured using a potentiostat or readout system [93].

One of the main advantages of the chemiresistor is that it has a simple physical structure, and this is a highly desirable characteristic for their miniaturization [21]. Moreover, since the sensing method is simple and straightforward, some more sophisticated designs to improve performance has been described such as the use of four terminal configurations or interdigitated electrodes [54], [95]. However, the dominant approach to functionalizing them has only been through non-covalent π - π bonds which may cause the sensors to suffer from poor durability and longevity; a limitation of the sensor's reversibility [20]. Another limitation regarding the non-covalent functionalization of graphene surfaces is that their characteristics have not been sufficiently studied [20]. For instance, a lack of uniformity in functionalizing the surface of the graphene may limit the sensor's selectivity as graphene exposed to free chlorine can carry out electrocatalytic reactions, making it difficult to understand the sensing mechanisms from reactions that occur between the functional material and the free chlorine. If these limitations can be overcome and the sensing mechanisms can be modelled, it will significantly facilitate development of chemiresistive free chlorine sensors.

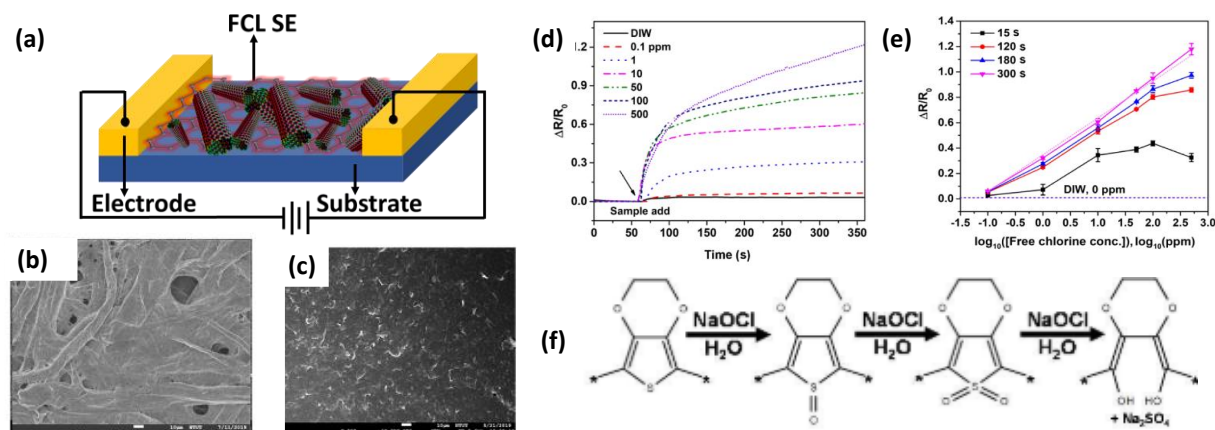


Figure 2-8: (a) Schematic of chemiresistive sensor with two electrodes and sensitive material deposited in between; (b) SEM images of Whatman no. 1 filter paper modified with PEDOT:PSS [93]; (c) SEM images of Whatman no. 1 filter paper modified with PEDOT:PSS/graphene nano hybrid ink [93]; (d) Nano hybrid ink-modified paper-based sensor signal responses in solutions with different concentrations of free chlorine [93]; (e) Linear relationships between the measured responses of the nano hybrid ink sensor material for different lengths of time, the normalized resistance and the logarithmic concentration of free chlorine [93]; (f) Overoxidation reaction scheme of PEDOT by NaClO showing the opening of conjugated double bonds and reducing its conductivity as a result [96].

The mechanisms mentioned that describe the change in resistance/conductance in chemiresistors are either that the chemical reactions between the analyte and the sensing material generates new materials with new electrical properties, or that the analyte induces changes in the charge depletion/accumulation layer in the sensing material [97]. However, the chemiresistive carbon-based free chlorine sensors are limited to just chemical reactions between free chlorine and the sensing material which generates a new material with new electrical properties. The chemical species can interact with the sensing film through various pathways such as physisorption, chemisorption, catalytic reactions, reactions at grain boundaries, and bulk reactions [95], [98]. The change in the electrical properties of the sensing material from the adsorbed chemical species can be caused by different processes such as oxidation/reduction of the surface or changes in the surface's work function.

One example of a chemiresistive free chlorine sensors is using a nanohybrid ink with PEDOT:PSS and graphene on a paper substrate [93]. **Figure 2-8(b)** and **Figure 2-8(c)** show SEM images of the filter paper modified with PEDOT:PSS and with PEDOT:PSS/graphene nanohybrid ink, respectively, showing the effect that graphene has on the morphology of the ink. The nanohybrid ink has a greater sensitivity than the plain PEDOT:PSS ink, making this a significant improvement over its predecessor [12]. **Figure 2-8(d)** shows the various lengths of time the chemiresistor is exposed to the free chlorine solution and the resulting normalized resistance. **Figure 2-8(e)** shows the relationship between the normalized resistance and the concentration of free chlorine. Although the sensor is made using simple methods, a limitation of the sensor is the length of time required for an accurate and repeatable reading, which may be a result of the necessary series of chemical reactions required to open up the 5-member ring to eliminate the ring's conductive properties [**Figure 2-8(f)**] [96].

2.2. Fabrication Methods

The main techniques used to fabricate free chlorine sensors include CVD processes [73], [99]–[102], electrochemical [24], [76], [103], [104] or chemical functionalization [68], [75], [91], [92], [94], [105] processes. Other techniques have also been used to fabricate electrochemical free chlorine sensors where the processes are very simple with low-cost materials [67], [74], [84], [93]. It was observed that the sensors with higher sensitivities and smaller LODs had more complex and more expensive fabrication methods such as CVD-fabricated monolayer layer graphene with an LOD of 10 ppb and high sensitivity of $1.9 \mu\text{A ppm}^{-1}$ [99], and pseudo-graphite with an LOD of 52 ppb and high sensitivity of $113.73 \mu\text{A cm}^{-2} \text{ppm}^{-1}$ [100]. For environmentally conscious and large-scale applications, these methods should be

modified to suit environmentally green standards to decrease both fabrication costs and impacts on the environment.

The classifications of the fabrication processes were based on the primary approach in fabricating the active material of the sensor. For CVD processes, pristine graphene or CNTs were deposited on a substrate through CVD. In the chemical and electrochemical functionalization processes, a chemical was functionalized onto a base material such as graphene, graphite, GO, rGO, and CNTs. The simple and cost-effective methods discuss how the active material was mixed in a composite or placed on the sensor substrate. A variety of techniques were employed in the characterization of graphene and its derivative materials with the most used among them being atomic force microscopy (AFM) [106], transmission electron microscopy (TEM) [107], scanning tunnelling microscopy (STM) [108], scanning electron microscopy (SEM) [109], and x-ray diffraction (XRD) [110]. These techniques can generally be used to characterize device morphology, intrinsic properties, crystal structure, chemical compositions, and morphology of graphene-based materials [50].

2.2.1. Chemical Functionalization

Functionalizing carbon-based materials is can be used to tailor the electrical properties and allow the hybrid materials to overcome some of the limitations of the intrinsic material as they acquire new and desirable properties [111]. Carbon-based materials are functionalized through a variety of chemical methods such as fluorination [112], chlorination [113], bromination [114], hydrogenation [115], addition of radicals [116], nucleophilic carbenes [117], and sidewall functionalization [54]. For free chlorine sensors, chemical functionalization of carbon-based substrates with various functional chemicals is a way to make the materials more selective or sensitive to free chlorine [54]. The schematic in **Figure 2-9** shows the different types

of compounds that were used to functionalize the carbon-based materials either through chemical or electrochemical methods, or other simpler methods. Furthermore, the fabrication methods that were implemented are limited to methods such as flowing molecules like PCAT through various apparatuses [91], [92], [94], the interfacial method [68], or in-situ functionalization methods [75], [105], [118], [119].

Surface functionalization can turn materials like graphene or graphite into more chemically sensitive and soluble materials, allowing for different deposition methods [111], [120], [121]. There are two main methods to functionalize graphene: (i) covalent functionalization by grafting molecules onto the sp^2 carbons of the graphene plane; and (ii) non-covalent functionalization through the adsorption of polycyclic aromatic compounds or hydrophobic interactions on the carbon plane [111]. For CNTs, like graphene, covalent functionalization is expected to make the material more sensitive, but the covalent functionalization may degrade their crystalline structure, affecting their conductivity and thus their transduction properties [54]. The covalent functionalization may end up destroying the CNTs themselves, limiting the applications of functionalizing CNTs.

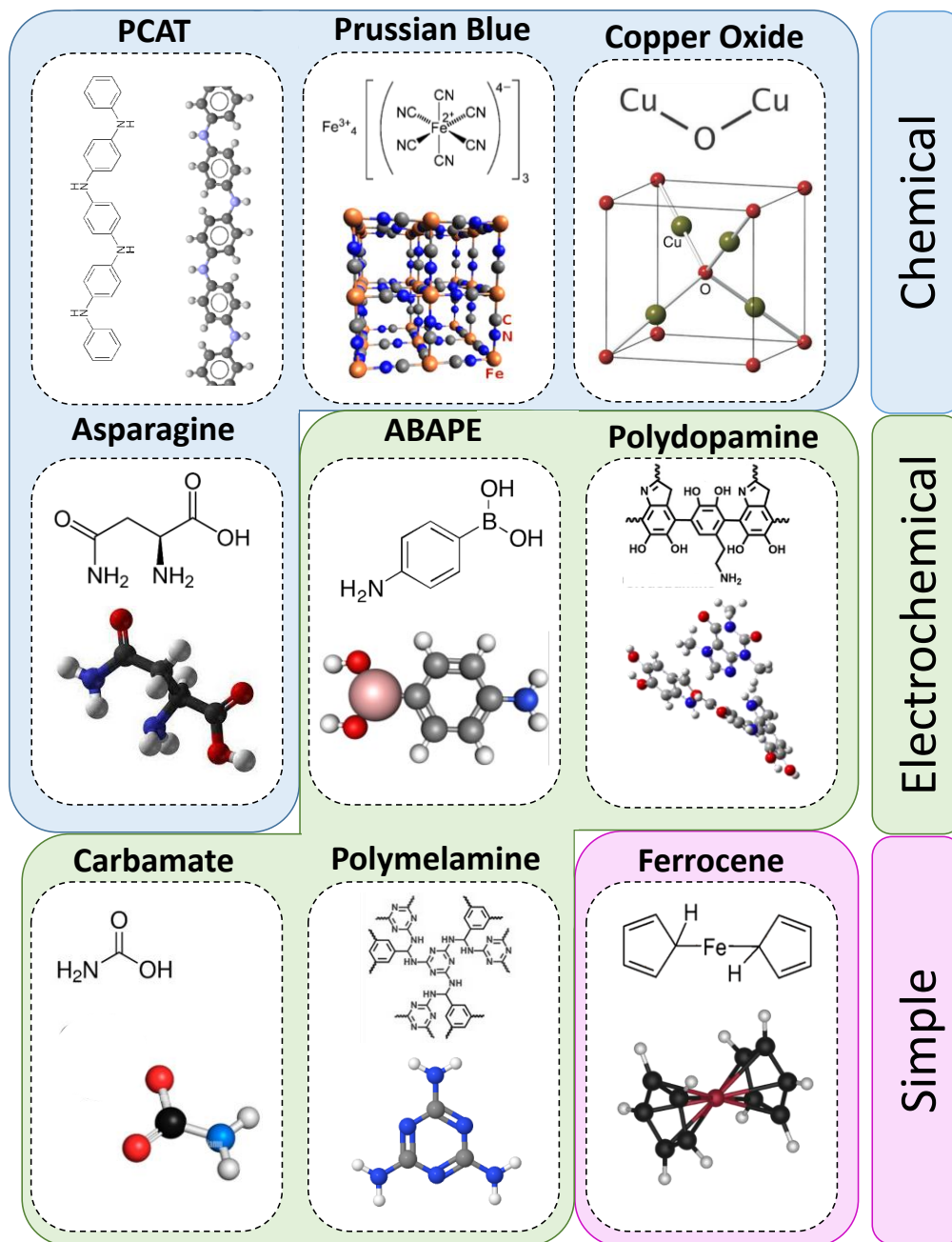


Figure 2-9: Chemical structures of functional groups used in functionalizing carbon-based materials for fabricating electrochemical free chlorine sensors. (PCAT: phenyl capped polyaniline tetramer; ABAPE: 4-Aminophenylboronic acid pinacol ester).

For graphene, covalent functionalization can be achieved through nucleophilic substitution, electrophilic addition, condensation, or addition reactions. The covalent functionalization ends up disrupting the cloud of delocalized electrons, forms a large density of

sp^3 hybridized carbon atoms in the graphene network, and leads to the scattering of charge carriers [111], [122]. If the graphene is bonded by acceptor functional groups, this give the graphene or p-type semiconductor properties, and if the functionalizing material is a donor group, this may give rise to n-type semiconductor properties. Although covalently functionalized graphene materials significantly decrease carrier mobility and scattering due to the change in the electron cloud, the properties imparted onto the materials include higher stability in the hybrid material, better solubility, and higher sensitivity [111].

2.2.2. Electrochemical Functionalization

Another approach to functionalizing the base materials is through electrochemical functionalization to achieve the same end results as chemical functionalization – creating a material with additional beneficial properties through the use of either voltametric or amperometric methods. This method was shown to reliably and effectively functionalize various types of amines such as polydopamine [76] and polymelamine [103] onto rGO and SPCE, respectively, through relatively simple means. **Figure 2-10** shows a visualization of an electrochemical reaction where an electrode is biased and the amines react with the substrate, and the remaining products are the H^+ ions and the functionalized substrate.

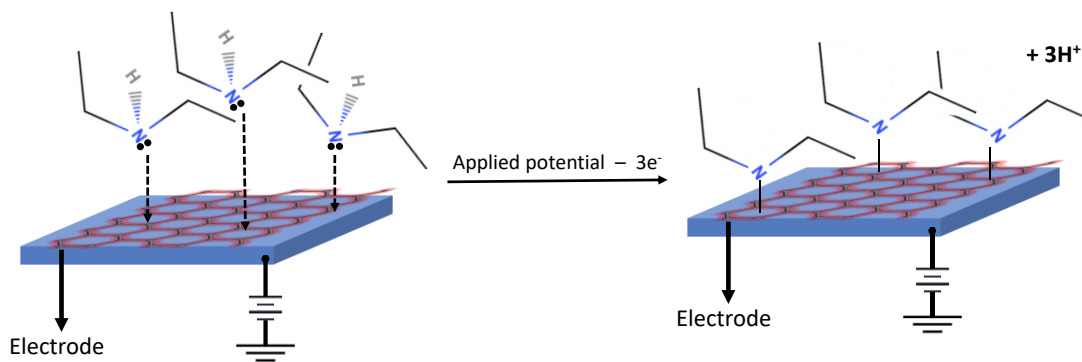


Figure 2-10: (a) Schematic of an amine compound undergoing an electrochemical reaction under an applied potential

For modifying the sensing electrode, the methods are experimentally simple, quick, and require only electrochemical equipment such as a potentiostat. With a variety of materials such as various alcohols and amines that can be grafted onto a substrate like graphene or CNTs, many types of monolayers can be formed from low-cost and widely-available reagents [123]. One of the processes in electrochemical functionalization is electrochemical oxidation of the carbon surface which is assumed to generate surface radicals with the functionalizing species in the solution [123], [124]. The final result is a functionalized carbon material.

The ready and wide availability of many types molecules that can be functionalized to the carbon-based substrates is a practical advantage of electrochemical functionalization compared to methods which require special chemical reactions [123]. One such example is the self-assembly and functionalization of PCAT on graphene [94] or CNTs [91]. The resulting covalently attached monolayers are more stable in harsh chemical environments, such as strong oxidative environments like free chlorine solutions, making for more robust electrode coatings. An example of a robust sensor is the pencil graphite electrode chemically functionalized with ammonium carbamate [104], [123], [125], [126]. With a competitive sensitivity of $0.302 \mu\text{A ppm}^{-1} \text{cm}^{-2}$, the sensor reported a very low hysteresis of 0.04 ppm and after being stored in DI water over a long period of 7 weeks, there was no deterioration in its performance.

2.2.3. Chemical Vapor Deposition

Chemical vapor deposition (CVD) is a vacuum deposition process that uses high-temperature environments and is a very expensive sensor fabrication method. This is due to the expensive and complex equipment required to use them, and the training required to operate vacuum-based equipment. The only method through which single-layer graphene was fabricated for the use of electrochemical free chlorine sensors is through CVD despite there being many different forms of fabricating graphene such as mechanical exfoliation [106], thermal decomposition of SiC (epitaxial growth) [127], electrical arc discharge [128], organic synthesis [129], and chemical method using dispersed graphite [130]. Although the cost of using CVD is higher than most of the other methods, the graphene is of very high quality where the materials are reversible reporting LODs of 0.1 ppm [73], 50 ppb [101], [111], 5.2 ppb [73] and 1 ppm, and linear ranges of 0-3 ppm [99], 0-262 ppm and 10-115 ppm [100]. However, because monolayer graphene is thin and can be broken easily, it is prone to physical degradation which would severely affect its performance [99], [101].

In the CVD process, gaseous or volatile gas chemical reactants/precursors are decomposed over metallic nanoparticles (e.g., Cu foil) which serve as catalysts or nucleation sites for products like single-layer graphene or CNTs. The precursors adsorb onto the substrate surface and then form islands that merge together or grow to form CNTs [**Figure 2-11**]. CVD processes require temperatures from 250 °C up to 900 °C for the deposition and reaction of these precursors. For CNTs, catalytic CVD is among the most widely used techniques for synthesizing CNTs [101], [105], [131], though many different synthesis methods were reported [50], [54], [111]. Variations of CVD used for manufacturing carbon-based free chlorine sensors are aerosol CVD [73], low-pressure CVD [99], and standard CVD methods [100]–[102]. Since there is no

single, perfect, way to synthesize CNTs or graphene, parameters such as temperature, catalyst purity, and the nature of the hydrocarbons were identified to affect the material quality [132]. Devices can be formed with nanometer precision and are often made on Cu foil as a catalytic substrate before being transferred onto another substrate [101], [131] or on quartz wafers [100].

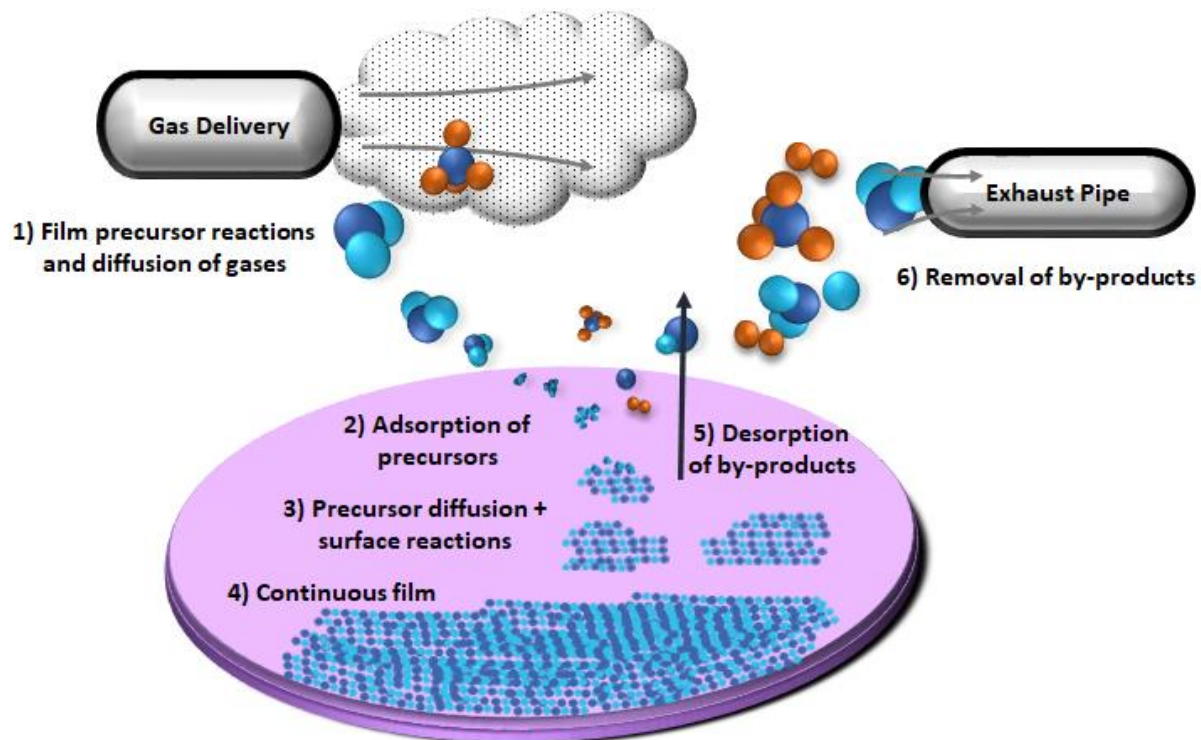


Figure 2-11: Fabrication schematic and mechanism of CVD process.

The advantages to using CVD are that the resulting sensors consistently have higher sensitivities and smaller (higher precision) LODs. The graphene and CNTs formed from the CVD process as a result have a very high carrier mobility and density, excellent electrical conductivity, large surface-to-volume ratio, high uniformity and high compatibility with other sensors [111]. An exception to the high performance characteristics is a sensor which used CVD-grown CNTs incorporated into a microfluidic analyzer [102]. The CNTs were mixed into an epoxy resin composite and the final sensor reported a sensitivity of $0.046 \mu\text{A ppm}^{-1}$ and an LOD of 0.05 ppm. Although the sensitivity is lower than other CVD-grown sensors, and this may be

due to the CNTs being in a composite and the electrode geometry which limits the surface area exposed to the free chlorine, the excellent LOD shows that CVD materials are still of a high quality.

2.2.4. Simple and Cost-Effective Fabrication methods

Several free chlorine sensors were fabricated through simpler fabrication methods as opposed to the previously mentioned methods [74], [84], [93], [133], [134]. Although the materials purchased were fabricated through CVD, thermal or mechanical processes, or with simpler methods such as the scotch-tape method, the fabrication of the sensors themselves were found to be very simple using minimal or no chemicals or dedicated equipment. There are no defined parameters on what simple and cost-effective fabrication methods are, so this section will discuss the fabrication of various sensors which do not fall under the previous sections.

A simple fabrication method for a free chlorine sensor using low-cost commercially available 6B pencil graphite that was insulated with an insulating polymer was reported [**Figure 2-12(a)-(f)**] [74]. The 6B pencil was used to draw on cellulose paper an electrode area of 1.25 cm² and then insulated with the insulating polymer [**Figure 2-12(g)-(l)**]. CV was used to find an optimal applied potential of 1.2 V and chronoamperometry was carried out using this potential. The pencil-drawn paper electrode reported a sensitivity of 0.52 $\mu\text{A cm}^{-2} \text{ppm}^{-1}$ and is selective to the standard suite of interfering anions (nitrate, sulfate, carbonate, bicarbonate, and chloride ion). The sensor possessed a very simple and bio-degradable design on a flexible substrate. Given that a graphite-based free chlorine sensor was made on paper, this creates the potential for other sensors to be made on biodegradable cellulose paper substrates as well.

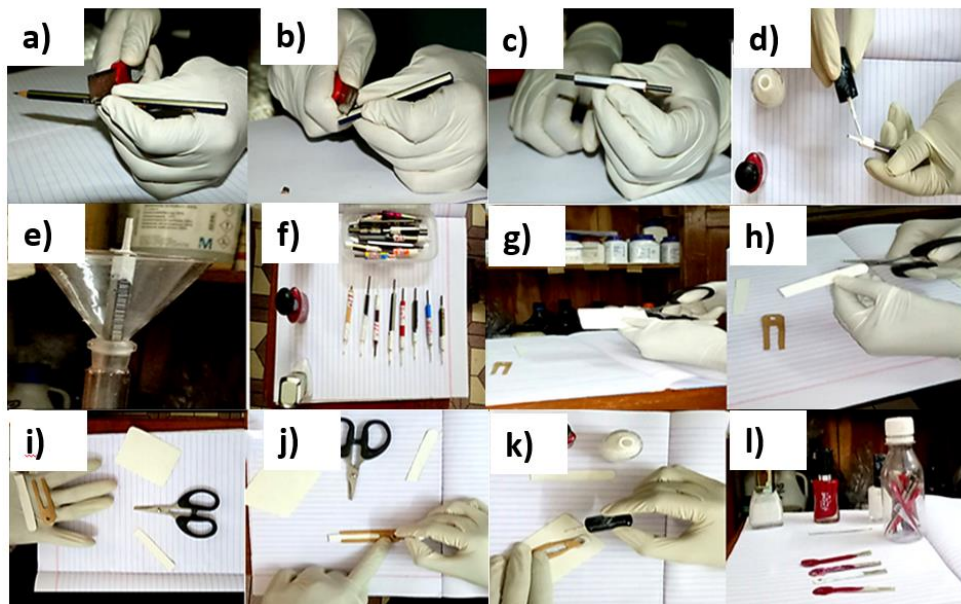


Figure 2-12: Stepwise fabrication of (a)-f) pencil graphite electrode and then g)-l) drawn on paper with an insulating polymer layer applied to define the desired surface area [74]. m) The preparation process of carbon paste electrode modified with ferrocene [84].

2.3. Conclusion

Over the past 5 years, research on electrochemical free chlorine sensors grew significantly. Many sensors were made using CVD, some through chemical and electrochemical functionalization, and others through simpler methods like mixing a material with an additive without chemical or electrochemical functionalization. Voltammetry, amperometry, potentiometry, and chemiresistivity are electrochemical methods used to measure free chlorine where all report their relative advantages and limitations. Among the challenges for making these sensors, many of which are made using graphene- or graphite materials, are the intrinsic challenges with large-scale fabrication. These include limitations such as low yields, poor material uniformity, and high costs [50]. In contrast, production methods with low material yields such as the CVD epitaxial growth of graphene develops high quality graphene with high uniformity. Although they can be expensive, these production methods are still at a lower cost

than the synthesis processes of other carbon-based materials like CNTs [111]. Electrochemical-based processes are lower cost than CVD processes, however they also require complex equipment such as a potentiostat, and harmful chemicals such as ammonium carbamate or PCAT are frequently used. Solution-based fabrication processes are ideal as a large quantity of sensing material can be fabricated and then printed using either inkjet or aerosol printers, but there is a limited number of available deposition methods. Although there is a general trade-off between fabrication complexity and sensor performance, many lower-cost sensors still show performance characteristics that are competitive with high-cost sensors and have the potential to exceed the performance characteristics of even complex and expensive sensors.

Chapter 3 ‡§

Design Parameters of Asparagine-Functionalized Graphene Oxide Free Chlorine Sensors & Predictive Modeling

3.1. Material Parameters

With the growing Internet of Things, the number of smart devices has increased to more than 30B in 2020 with many of them being printed using conductive, insulating, and semiconductive inks to produce electronic devices with a high throughput [135], [136]. These devices will be expected to improve human quality of life and will be deployed in as many places as possible such as packaged consumer goods or drinking recreational water sources to monitor water quality [137], [138]. This high throughput, low-cost of fabricating electronics, and the potential scale of delivering this project presents an environmental challenge. Sensors and substrates using heavy metals, plastics, semiconductors, other environmentally damaging materials will be expected to be fabricated at large scales. They will subsequently be a significant cause for electronic waste and waste created during production. The waste normally generated during the fabrication or disposal of electronics is toxic and dangerous, and is responsible for significant harm to human health such as what results from lead and cadmium poisoning [139],

‡ Adapted with permission from J. Siddiqui, M. J. Deen, Biodegradable asparagine-graphene oxide free chlorine sensors fabricated using solution-based processing, *The Analyst*, 144, 2022: 3643-3651. Copyright (2022) Royal Society of Chemistry (Appendix A)

§ Part of this work will be submitted for consideration for publication *RSC Advances* as: J. Siddiqui, M. Taheri, M. Nami, M. J. Deen, Carbon-Based Electrochemical Free Chlorine Sensors, December 2022. (in preparation)

various plastics such as polyphenylene oxide and polyvinyl chloride which contaminate the soil, leading to plants showing toxic compounds in their leaves [140]–[142]. For this reason, the materials with the sensors being fabricated must be restricted such that minimal harmful electronic waste, producing functional sensing devices with environmentally-benign materials, and developing innovative solutions to environmental problems.

The main requirements for the environmental compatibility of the materials is that they are bio-degradable, sustainable, and the use of toxic materials during fabrication is minimized. A biodegradable material is one such that through a natural process, the chemicals and materials are converted to simpler compounds through oxidation, hydrolysis, or degradation by microorganisms, then turned into minerals, and finally redistributed through elemental cycles such as the carbon or nitrogen cycles [143]. A key consideration is the central role of enzymes or various organisms within the biosphere required in the biodegradation process [144]. The biodegradability of a material depends greatly on the origin of the material and its chemical structure. If the source of the material or its chemical structure is not a part of the degradation cycles or receptive to enzymatic decomposition, then the material will remain in the environment and potentially harm its surroundings. As for sustainability, the material should be easily and widely available without impacting the environment either through harvesting the material or through its use. This is to ensure long-term and stable development of both electronics and electrochemical sensors that perform well and do not harm the environment in the process.

For free chlorine sensors, given the widespread use of free chlorine in both drinking water and its use in washing foods, the sensors must be fabricated by biodegradable materials under conditions such that the materials are safe to incorporate near food and drinking water. They must also be scalable to meet the demands of both these industries. Many of the

amperometric sensors reported in literature have good sensitivities and limits of detection. However they are often fabricated using toxic materials such as polymelamine [103], polyaniline [91], or ammonium carbamate [104] – materials which are unsafe to use near food. When tested in drinking water systems, there is a risk of the toxic materials leaching into the water and being consumed. When using the sensors in these systems, leaching is difficult to avoid. To minimize the harmful effects of this leaching, the materials must be environmentally friendly and biodegradable, and also maintain an ability to electrochemically detect free chlorine.

3.1.1. Graphene Oxide

Graphene oxide is well-known and widely used for its biodegradable properties, but it is mainly used for its unique electrical properties [64], [145]–[150]. Graphite, graphene and its derivatives, carbon nanotubes [Figure 3-1(a)-(c)] and similar materials were incorporated into many types of electrochemical free chlorine sensors via functionalization, conjugation, or tuning methods. These materials were proven to be resilient in the presence of harsh chemicals which is a significant advantage in the presence of a strong oxidizers like free chlorine [98], [151]. The sensors' diverse fabrication methods include chemical vapor deposition (CVD), drop-casting, solution processing, and electrochemical synthesis processes, which make them excellent choices for widespread applications. Graphene is able to detect small changes in free chlorine concentrations due to having very low noise. Also, its high surface area ($>2000 \text{ m}^2 \text{ g}^{-1}$) and few defects makes it an excellent base material for sensors [98]. Its high conductivity due to its symmetrical honeycomb-lattice arrangement comprised of sp^2 hybridized orbitals allow for high charge carrier concentrations [20]. With the high surface areas for graphene and carbon nanotubes ($\sim 1600 \text{ m}^2 \text{ g}^{-1}$), and high carrier mobilities, these properties allow for graphene, graphite, CNTs and similar materials to detect small changes in free chlorine concentrations

[150]. Their ability to be doped (n- or p-doped), high electron transfer rates and carrier mobilities, high surface-to-volume ratio, and robustness makes them excellent materials for a variety of sensing applications, including free chlorine sensing [Figure 3-1(d)] [111].

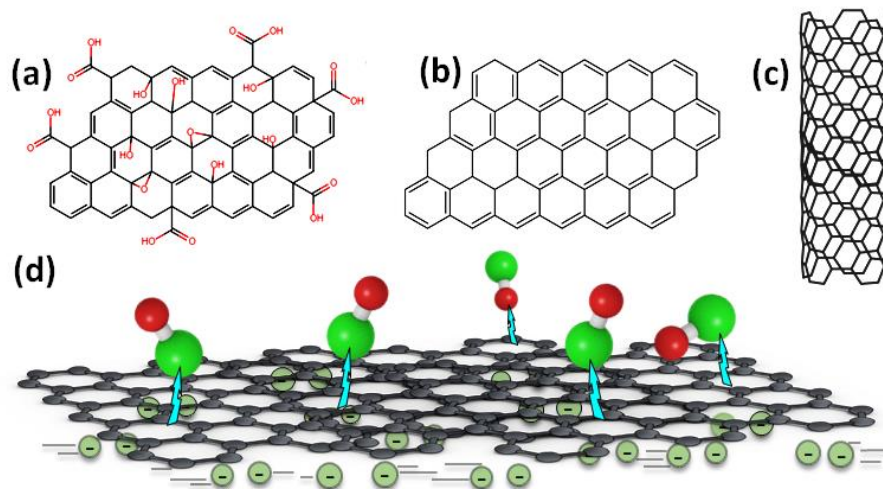


Figure 3-1: Schematic diagram of a (a) graphene oxide sheet, (b) graphene sheet, (c) CNT, and (d) diagram of graphene sheets reducing free chlorine molecules.

3.1.2. Asparagine

Amino acids are organic molecules with two essential functional groups: amines and carboxylic acids. A carboxylic acid is an acidic organic molecule (tends to donate protons in solution) with a carboxyl group or a COOH group attached to another R- group, where its general formula is R-COOH and the R- can be any sort of carbon chain or carbon ring [Figure 3-2(a)]. Though the carboxylic acid is usually drawn with a double bond from the carbon to one of the oxygens (C=O), and a single bond to the other (C-O), the bond structure is in-between a single bond and double bond between the two oxygens because the electron probability distribution is equal between the two. The oxygen groups make the organic molecule very polar which makes a molecule with a carboxylic functional group an excellent polar solvent or capable of making acidic or basic buffer solutions. The second functional group is the amine which is an organic material derived from ammonia by replacing one or more of the hydrogen groups with a

carbon. This causes the nitrogen to be bonded to at least one carbon atom, two hydrogen atoms, and be left with a lone electron pair to give it a trigonal pyramidal molecular geometry. This functional ammonia group imparts a high degree of polarity on the organic molecule and gives it unique functionality as a solvent or a reagent in chemical reactions. With the two functional groups in a particular composition, amines and carboxylic acids create the foundation for an amino acid. The primary carbon attached to the amine is termed the alpha-carbon (α -carbon) and this α -carbon is the aforementioned R- group [152]. This thesis discusses the use of asparagine which contains an amide, or an NH_2COCH_2 -, group attached to the α -carbon shown in **Figure 3-2(b)**.

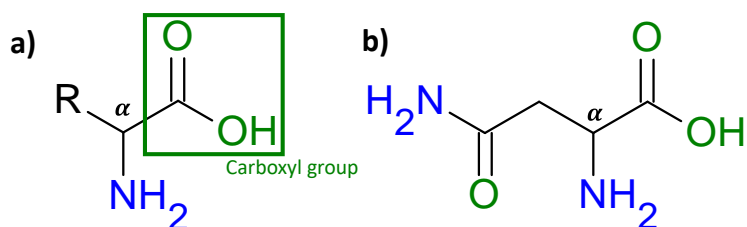
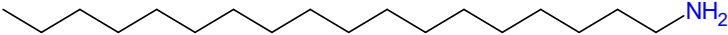
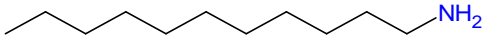

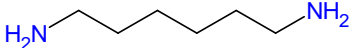
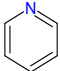
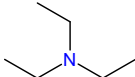
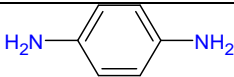


Figure 3-2: Chemical diagram of (a) amino-acid base form and (b) asparagine.

For free chlorine sensors, amino acids can be functionalized onto graphene oxide sheets to create a functional material [153], [154]. It has been reported that many free chlorine sensors have already used the reaction between hypochlorite and the amine groups on macrocyclic molecules in both colorimetric [26] and electrochemical sensors [104] for the detection of free chlorine. Also, since graphene oxide has locally conductive regions due to delocalized electrons, it was successfully hypothesized that an amine-modified GO would be a suitable material for free chlorine sensing [104]. Functionalizing amines to GO was carried out by many different intermediary materials, many of which are toxic or corrosive such as different types of amines, diamines, and pyridine as shown in **Table 3-1**, or the methods used complex processing equipment during fabrication such as reflux condensers, vacuum ovens, and potentiostats [76],

[103], [104], [155]–[157]. As a result, amino acids became the remaining material with a functional amine group that could be functionalized to GO [154].

Table 3-1: Amines used to functionalize to GO, their chemical structures, and hazards

Amine Name	Chemical Structure	Hazards
n-octadecyl-amine		Corrosive, Environmental and Health Hazard, Irritant
dodecyl-amine		Corrosive, Environmental and Health Hazard, Irritant
ethylene-diamine		Oxidizer, Corrosive, Health Hazard, Irritant
hexa-methylene-diamine		Corrosive, Irritant
Pyridine		Oxidizer, Irritant
Triethyl-amine		Oxidizer, Corrosive, Irritant
P- phenylene-diamine		Toxic, Environmental and Health Hazard, Irritant

3.2. Fabrication

The main techniques used to fabricate free chlorine sensors include CVD [73], [99]–[102], or electrochemical [24], [76], [103], [104] or chemical functionalization processes [68], [75], [91], [92], [94], [105]. For environmentally conscious and large-scale applications, these methods should be modified to suit environmentally green standards to decrease both fabrication costs and impacts on the environment. During the fabrication process, the materials, intermediate chemicals, and solvents must limit their toxicity and wastage, and also eliminate the complexity of the manufacturing process. This is to ensure a safe, stream-lined, and efficient process. Eliminating the toxic materials would limit the potential hazards that result from accidental chemical spills, or reducing the amount of hazardous chemical waste generated during the

fabrication process so all the materials used throughout the fabrication process are environmentally friendly and safe. The materials used in the fabrication processes must be biodegradable to eliminate a lasting or permanent presence in the environment. As the end of the sensors' lifetimes are reached, the sensing materials should not require material separation like standard electronics which minimizes the end-of-life sorting process and reduces material pollution. The goal, from fabrication to end-of-life management, is to minimize both toxicity and the lasting presence of the materials in the environment, thereby creating, sustainable, and effective sensors.

3.2.1. Solution-Based Processing

In solution-based processing, the key materials are soluble in solution and the steps in the fabrication process are in solution. As it can be made compatible with roll-to-roll additive manufacturing or printing-based deposition methods, solution-based processing can be scaled to volumes much higher than the current fabrication throughput of electrochemical free chlorine sensors. To stay within the parameters of being environmentally benign, a process was developed through 1-step chemical reaction using a NaOH solution as the solvent. After dispersing GO in DI water, a separate NaOH solvent was prepared with the asparagine which, due to the high pH, dissolves the amino acid in solution [154]. The chemical reaction occurs in a single step wherein the GO solution and asparagine solution are mixed together using a magnetic stir bar for 24 h. The purpose of the high pH is to prevent the formation of amides by neutralizing carboxylic acid groups on the GO, and to promote the reaction between asparagine and GO [153]. Once the reaction is completed, the solution is separated from the NaOH and the unreacted solute from the GO, and then mixed in an approximately 1:1 deionized (DI) water and

ethanol solution. The purpose of the ethanol and water solution is to prepare it for a printing process during the deposition.

Proposed Fabrication Mechanism

Figure 3-3 shows the proposed reaction products and reactants of asparagine functionalized to GO. In **Figure 3-3(a)** is the asparagine molecule in its base form where the COOH group forms a covalent bond with the GO sheet. This extends the delocalisation of the electrons from the GO sheet into the oxygen pair. Another possible reaction mechanism is shown in **Figure 3-3(b)** that shows the α -amino group with a positive charge from an additional hydrogen atom. This amino will covalently bond to one of the -COOH groups on GO in the presence of harsh reaction condition such as a high pH environment due to the presence of a strong base like NaOH. These two structures are possible reaction products, however other structures are possible as is the commonly found in organic reactions [158].

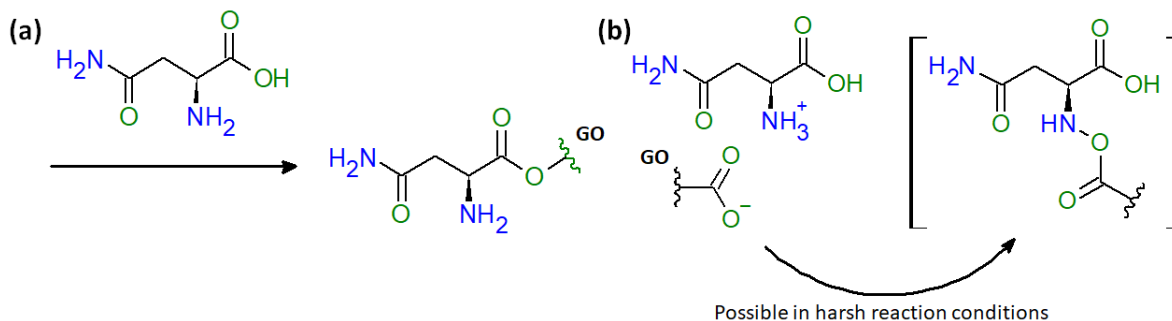


Figure 3-3: Proposed reaction products of asparagine with GO where (a) the COOH group is covalently bonded to the GO sheet, and (b) the α -amino is covalently bonded to one of the carboxylic acid groups on the GO sheet.

Proposed Reaction Mechanism

Figure 3-4 shows two possible reaction mechanisms based on the products shown in **Figure 3-3**. For the products shown in **Figure 3-4(a)-(b)**, if the compound is in a neutral or high pH environment, such as a tap water environment with a pH close to 7, the reactions indicated by the green arrows will occur. Since NaOCl has a high pH of 11, the amino group can react to form

-NHCl or even NCl_2 depending on the concentration of OCl^- present in solution [159], [160]. However, this group is not very stable, and can undergo other reactions such as a base-catalyzed hydrolysis, returning it back to the original compound. An applied positive potential would create a charge gradient increasing the localized concentration of the electron donor OH^- group which may facilitate the base-catalysis hydrolysis reaction. Higher concentrations of the OCl^- would push the reaction toward the formation of -NHCl groups and result in an increased detection of free chlorine, but the steady flow of OH^- would shift the reaction back towards the initial asparagine-GO product. With -NHCl in **Figure 3-4(b)**, the bonding of the electron-withdrawing Cl would change the electron distribution due to the delocalisation of electrons through the -COOH group and through to the -NHCl group and potentially create a significant change in current, as measured using chronoamperometry in Chapter 4. Over time, the forward and reverse reactions may reach a relationship with a steady current flow that can be described by the Cottrell equation.

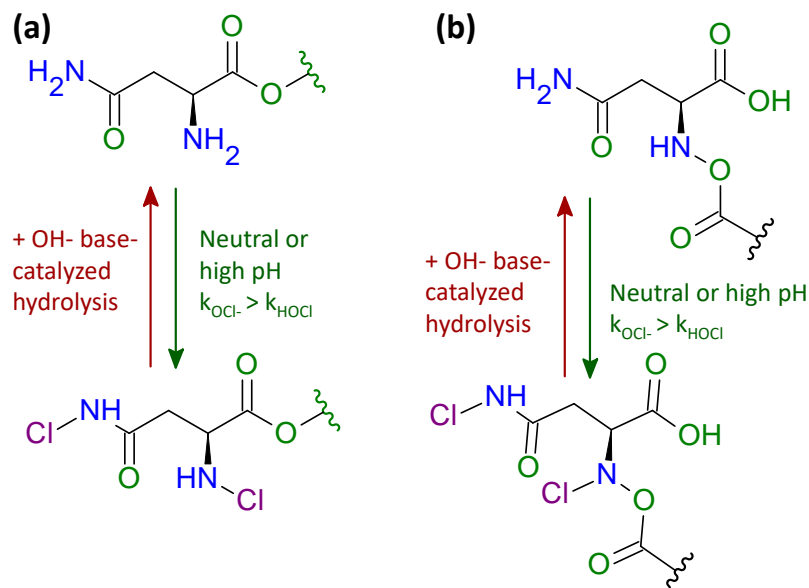


Figure 3-4: Proposed forward and backward reaction products of asparagine-GO in the presence of OCl^- where (a)-(b) the -NHCl group is formed at α -amino group and the amide group due to the presence of high pH, and the reversible reaction due to the presence of OH^- being the catalyst for base-catalyzed hydrolysis.

3.2.2. Ink Deposition

Using a printer would minimize the amount of material wasted, which would also minimize the costs associated with wasted material. This would create a uniform surface morphology and provide a consistent surface area for the sensor to measure free chlorine consistently and reliably. Due to the lack of availability of an inkjet or aerosol printer, the remaining options were drop-casting and spin-coating. Both deposition methods were used, however, spin-coating was given preference as it showed better and more consistent results when compared to drop-casting. **Figure 3-5** shows a diagram of the spin-coater and an SPCE. The SPCE is taped to the rotating chuck using double sided tape such that the conductive area of the electrode is directly above the center of chuck to ensure a uniform spread. For spin coating, normally the rotation speed and rotation time are controlled to specify the thickness of the deposited material when depositing polymeric materials, especially in the photolithography processes. Although the deposition area is very small, the spin coater manages to create surfaces with sufficient uniformity.

The limitations in the process concern repeatedly handling the sensor and the limited precision in using the spin coater. First, aligning the center of the SPCE directly on top of center of the rotating chuck without supports or guides restricting the movement of the sensor may introduce errors in fabrication. If the SPCE is off-centre, the spinning will cause the sensing material to be spread unevenly and potentially affect the sensor performance. Furthermore, there is a limit to the quantity of sensing material that can be placed on the SPCE after which, the material must be dried and then repositioned on top of the rotating chuck which creates more potential fabrication errors. This can introduce variation between sensors, limiting reproducibility. To overcome this limitation would require building fixed rails on the rotating

chuck which would prevent the SPCE from being positioned anywhere else, and limiting the volume of sensing material deposited on the SPCE.

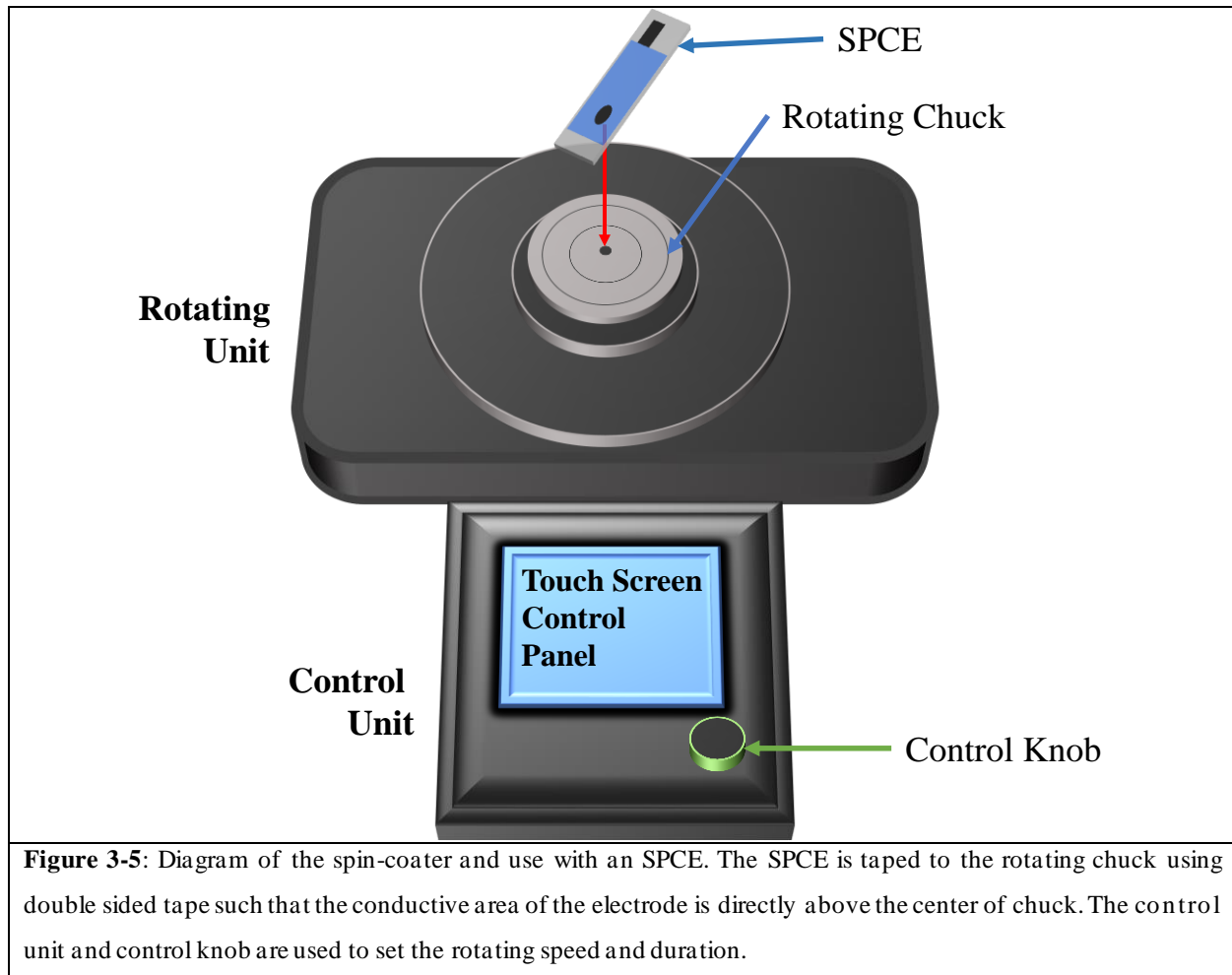


Figure 3-5: Diagram of the spin-coater and use with an SPCE. The SPCE is taped to the rotating chuck using double sided tape such that the conductive area of the electrode is directly above the center of chuck. The control unit and control knob are used to set the rotating speed and duration.

3.3. Neural Networks Design for Predictive Modelling

Neural networks (NN) are a type of machine learning (ML) algorithm made by a series of interconnected nodes using a set of data points to build a model to predict outputs with new and unique inputs. The NN consists of a group of neuron-like nodes where each node (**Figure 3-6**) is grouped with other nodes in layers. The nodes in each layer are connected to the nodes in the previous and subsequent layers. The weights (w_1, w_2, w_3) control the influence of each input on the subsequent layer such that a higher weight would give an input node (x_1, x_2, x_3) a higher

influence over a specific node of the following layer (y) and a lower weight would minimize its influence. The biases (b) are to minimize the overfitting of the model, so it is accurate on the training, test, and validation sets. Using the information provided in **Figure 3-6**, the output for each subsequent node is given by:

$$y = g(z), \quad z = \sum_{i=1}^3 w_i x_i + b, \quad (3 - 1)$$

where y is the output of either the node in the following hidden layer or the output of the entire neural network after applying the activation function, $g(z)$, and z is the sum of the products of the weights, w_i , inputs, x_i , and the bias, b .

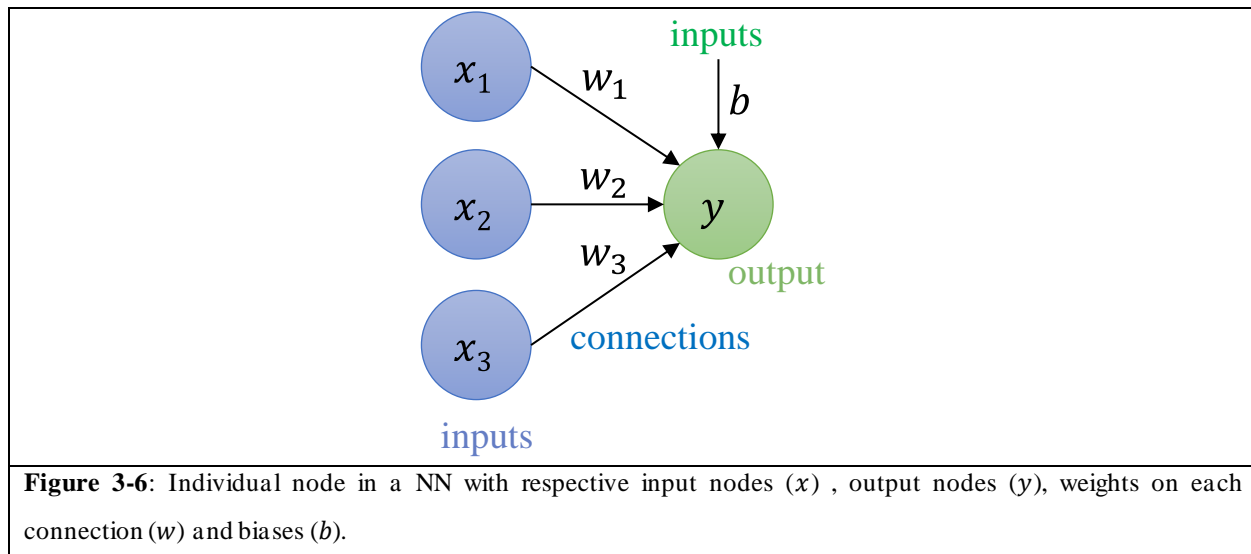


Figure 3-6: Individual node in a NN with respective input nodes (x), output nodes (y), weights on each connection (w) and biases (b).

3.3.1. Neural Network Inputs

The input parameters for the neural network (NN) model in total are ten. They include the time ('Time'), current ('Current'), temperature ('Temperature'), whether the sensor was spin-coated or not ('Spin Coated'), and if the measurements were while the free chlorine concentration was in an increasing cycle ('Increasing ppm'). The parameters that offer detailed information includes the cycle number for each sensor ('Sensor Cycle') wherein each cycle consists of a phase when the free chlorine concentration was increasing and then decreasing (or

only increasing, limiting the sensor cycle number to 1), the days elapsed since a batch of the sensitive material was fabricated ('Days Elapsed'), and three parameters that identify which batch each measurement came from ('A', 'B', 'C') (3 batches of sensitive material were fabricated). The resulting inputs designed for the NN were the 10 input variables, and the output was the free chlorine concentration. In total, 9385 data points were recorded and used to train, validate, and test the NNs.

One of the uses of the parameters is to quantify and differentiate the impacts of the testing parameters and conditions on the sensors' performance. The sensors were fabricated using spin coating as a substitute for printing with the aim to achieve uniformity and optimize performance as opposed to drop-casting the ink onto the SPCE. By keeping track of whether the sensor performance varied either when the free chlorine concentrations were increasing during each cycle or decreasing, the expectation is to identify the impact of the hysteresis of the sensor and the impact of sensor fouling during each cycle. 'Increasing ppm' quantifies the impact of hysteresis on sensor performance where a 1 is assigned if the measurements were carried out when the free chlorine concentration was being increased, and 0 if the free chlorine concentrations were being reduced. 'Sensor Cycle', quantifies the degree to which the sensor fouls up to three cycles, after which the sensor was discarded due to observable performance degradation. The parameters 'A', 'B', and 'C' are used to keep track of the variation of the sensors between the batches of sensing material that were made. Each column is assigned a 0 or a 1 where a 1 indicates the sample came from a given batch, and the values are mutually exclusive so if Batch A is assigned a 1, Batch B and C are assigned a 0.

3.3.2. Datasets

The data sets were partitioned into 60%, 20%, and 20% for the training, validation, and test sets, respectively. The input values were standardized to improve model accuracy according to the normalization formula in Scikitlearn, a python library, which uses the following formula to normalize the values of each of the different parameters given by:

$$z = \frac{x - \mu}{s}, \quad (3 - 3)$$

with,

$$\mu = \frac{1}{N} \sum_{i=1}^N x_i, \quad s = \sqrt{\frac{1}{N-1} \sum_{i=1}^N (x_i - \mu)^2}, \quad (3 - 4)$$

and where, μ is the mean of the training samples and is unique to each feature, s is the standard deviation of the training samples calculated independently for each feature, and the final results is z which gives the scaled feature values prepared to be input into the neural network, trained, and evaluated. This equation allows a balanced distribution between the different parameters and facilitates the convergence to an optimal model.

The training set is the set of examples wherein the output values, or the free chlorine concentration ppm values, are known for each data entry. The training set is used to build the NN model with all the biases and weights and update them through training-specific iterations. The validation set is data split from the training data and measured against the trained model to evaluate the amount of overfitting or underfitting of the model. For instance, if the model performs very well on the training data but poorly on the validation data, the model is overfitting, and if the model performs poorly on both, it is underfitting [41]. Solutions to overfitting is to include more data or reduce the complexity of the model (fewer nodes). Solutions to underfitting

is by increasing the complexity of the model or increasing the number of parameters (also increase input nodes). The test set is another set of examples for which the labels are also known to evaluate how close the predicted values are to the real values and is used to test the final NN model. The NN takes an input from the test set, uses the current model to evaluate the output, and then the real output with the predicted output are compared to determine the performance of the model.

3.3.3. Validation Process

Keras, an open-source software, was used to build and test the NN architecture. Keras is an industry standard deep learning API which was developed for enabling fast experimentation and is written in the python programming language on top of the machine learning engine *TensorFlow* [42], [43]. *TensorFlow* is also an open-source platform specialized for machine learning with a comprehensive and flexible environment with various tools, libraries, and communities to optimize and excel in machine learning applications [42]. Keras is simple to use as it reduces the complexity in designing neural networks for each application with simple customizability, flexible in facilitating stream-lined workflows and is scalable to many applications.

Using Keras for training neural network requires preprocessing to facilitate end-to-end training and model performance evaluation. After extracting the raw data, it is formatted into a dataset where the columns are the input parameters, and the data is shuffled to avoid the presence of unintended biasing of the NN's weights and biases. The target labels column, 'Concentration', is removed from the dataset to be used train the NN and the remaining data is scaled using Eq. (3-3) and (3-4). After normalization, the basic architecture of the model is initialized. The model is designed to have 10 input nodes and 1 output node. The NN had two hidden layers where the

number of nodes in the hidden layers would vary to evaluate both underfit and overfit models. The hidden layers were a minimum of 8 nodes to limit the computation time and avoid small networks with very significant underfitting. The maximum size of the network would have 32 nodes among the two hidden layers to limit the complexity of the network which would lead to very long and resource-intensive run-times.

The goal for varying the number of nodes in the hidden layers is to identify the optimal model over a range of possible models. **Figure 3-7(a)** shows the ranges where the first hidden layer has only 8 nodes, and the second hidden layer has 24 nodes to sum together to 32 nodes. **Figure 3-7(b)** has 16 nodes in each hidden layer which sums to 32 nodes as well. The range of architecture should be expected to account for both underfitting and overfitting models, with the optimal model to be somewhere in between these two architectures. The nodes between the NNs are made of layers that are all fully-connected layers because all the units of previous layers are connected to all units of the subsequent layer. At each output node is an algorithm or an output function used to determine the output that will be used for the subsequent calculations. For hidden layers, the output function is called ReLu (rectify linear unit) shown in **Figure 3-7(c)**, which is given by:

$$g(z) = \max(0, z), \quad (3 - 5)$$

where, only positive values are accepted by the function, and if the value is less than 0, then the function will output a 0. Combined, the architecture and activation functions for the NN make up its hyperparameters in relation to the architecture of a NN.

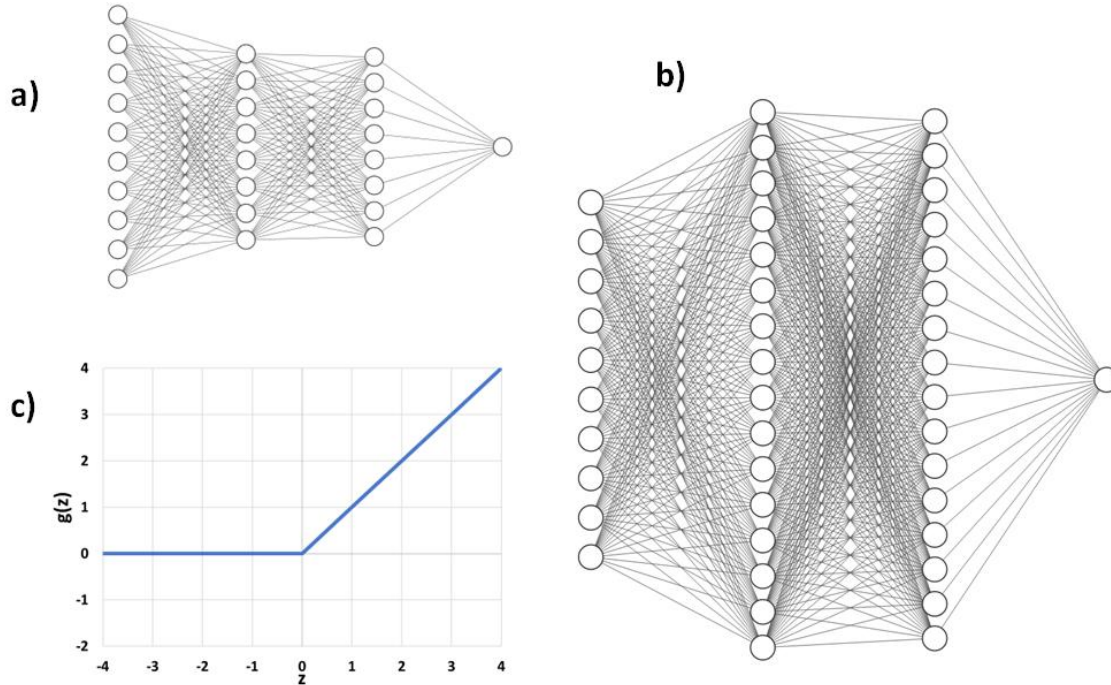


Figure 3-7: NN architecture with 10 nodes in the input layer, 1 node in the output layer, (a) 8 nodes in both hidden layers, and (b) 16 nodes in both hidden layers; (c) ReLU activation function used in the nodes of the hidden layer.

After a blank model is created with the specified architecture, it is trained and evaluated using another built-in Keras function which allows the customization of several training hyperparameters. The hyperparameters include the number of epochs used to train the model, where each epoch is one iteration through the entire dataset during training of the model. Using the inputs for the datapoints and the corresponding targets/labels, the models are trained using the training data, validated using the validation data, then tested using the test data. The results of the evaluation of the model used from Keras' built-in evaluation functions outputs is the mean absolute error which is given by [43]:

$$MAE = \frac{\sum_{i=1}^n |t_i - y_i|}{n}, \quad (3 - 6)$$

where t_i is the real value measured, y_i is the predicted value from the NN, and n is the number of data points. The MAE will measure the average accuracy of the outputs, or the difference

between the predictions and targets (in ppm). The second metric used to evaluate the optimal model is the Pearson Correlation Coefficient (PCC) given by:

$$R = \frac{\sum_{i=1}^n (t_i - \bar{t})(y_i - \bar{y})}{\sqrt{\sum_{i=1}^n (t_i - \bar{t})^2} \sqrt{\sum_{i=1}^n (y_i - \bar{y})^2}}. \quad (3 - 7)$$

The PCC is determined between t_i , the true label of a data point and y_i , the predicted value using the inputs of the same data point, and n is the number of datapoints. The correlation is high if $R = 1$ and low if $R = 0$ where a higher PCC shows that the model can accurately predict the real values of a data point from a set of inputs. The optimal NN is obtained using the lowest MAE value to determine which NN would give the smallest error in predicting the free chlorine concentration in the test set. Using each model, the test parameters are isolated and evaluated on this model to determine their impacts and influence.

K-Fold Cross Validation

K-Fold Cross Validation (KCV) is a method to reliably evaluate models with varying architecture of design parameters, and this is usually carried out when there is not sufficient data. In this case, KCV is being used to balance out the distribution of values in each parameter so that once the optimal models are selected, the relevant parameters will be isolated and its impact on the performance characteristics of the sensors will be quantified. KCV operates by first splitting up the training data into K partitions or folds (J_1, J_2, J_3, J_4), and create K identical blank NNs with an identical number of nodes and network parameters. As shown in **Figure 3-8**, each NN will be trained on one of the $K - 1$ partitions (blue) and the model parameter (w) will be recorded. Then, on each model, the remaining partition (black) is evaluated from which the error ($\epsilon_1, \epsilon_2, \epsilon_3, \epsilon_4$) is recorded. The averages of all these errors are then calculated over all the folds using the following equation which gives the error for the model with the given architecture:

$$\hat{\varepsilon} = \frac{\varepsilon_1 + \varepsilon_2 + \varepsilon_3 + \varepsilon_4}{4}, \quad (3 - 7)$$

where $\hat{\varepsilon}$ is the average error across each of the four folds. Both the MAE and PCC are calculated using this method where the PCC is averaged across the four folds as well.

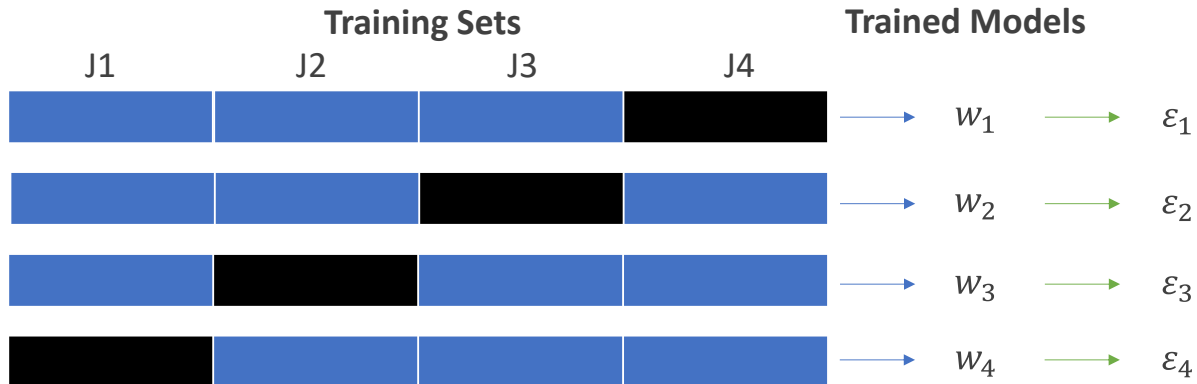


Figure 3-8: K-fold Cross Validation method where four identical blank NNs are created. The training data is divided into four equal parts or folds, and used to train and test the models such that three folds (blue) are used to train the model and the last fold (black) is used to test the model. The weights, biases, and other NN parameters are given by w , and the test errors are given by ε . The final error is given by calculating the average of the errors of all four tested models.

Flowchart

The sequence of tasks carried out for the NN from pre-processing, training, validation, and model selection is shown in the flowchart in **Figure 3-9**. The data is first preprocessed according to Keras' requirements (purple) and is split into training and test data. Once the data is prepared, the details for the NNs including the number of nodes in each hidden layer, the number of folds for K-fold cross validation, the number of epochs used to train a model, and the batch size are all evaluated. The algorithm initializes the first NN, splits the training data into K folds, and trains K different NN models on K different folds, then obtains the average MAE using the K-fold cross validation method (blue). After looping through all possible architecture combinations constrained by the aforementioned limits (orange), the model with the lowest MAE is selected as the optimal model, then the PCC is calculated on the model. The model is then

used to evaluate the parameters isolated and ordered according to the values under a given column (yellow).

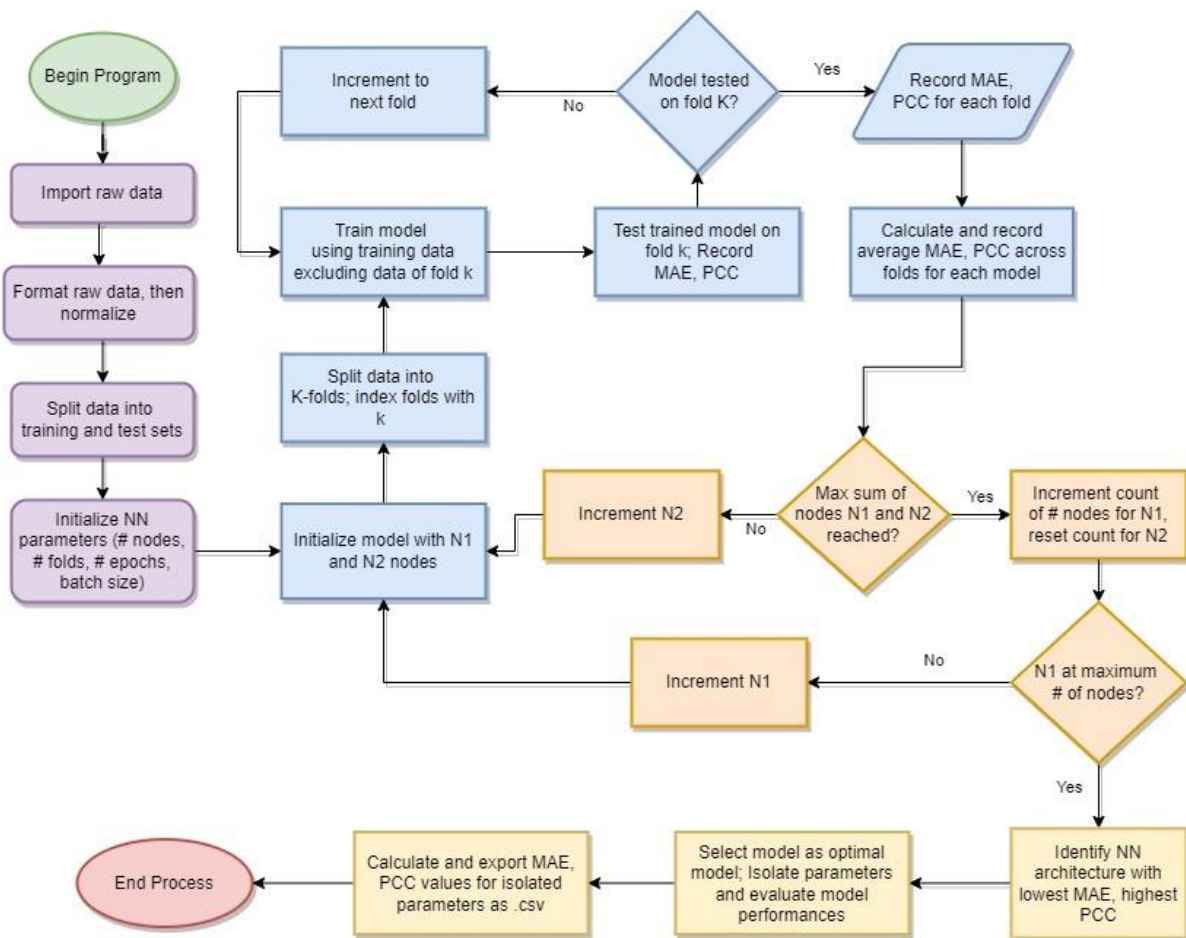


Figure 3-9: Flowchart that details each step and task carried out from importing and formatting the raw sensor data (purple), evaluating, and testing (blue) various different NN architectures (orange), then isolating the parameters and evaluating the MAE and PCC of each parameter to quantify their impact on the sensors' performances (yellow).

3.4. Conclusion

In this chapter, we presented and discussed the design parameters and design of both the free chlorine sensors and the NN for evaluating the optimal test parameters for the asparagine-GO free chlorine sensors. The substrate material is made using GO and it is functionalized with the amino acid, asparagine, both of which are biodegradable and intended to be broken down

under environmental conditions and this may be a limitation in its performance longevity. Furthermore, fouling is a well-documented limitation of free chlorine sensors due to the strong oxidizing properties of OCl^- and this would limit the lifetime of the sensor. However, by measuring large amounts of sensor data, the measurements can be used to train NNs that can develop statistically generated models of the sensors, quantify the degradation of the sensors, and therefore limit its impact. These models were trained using industry-standard software and K-fold cross validation, and can be consistently improved with additional parameters, but requires computational power and datasets that scale alongside the increase in parameters.

The solution-based fabrication process for the sensor was designed to facilitate the sensors being printed onto a plastic or biodegradable substrate. As a proof of concept, a spin-coater was used in place of a printer which minimized both the cost and time associated with developing a printable ink formulation. While this development is expected to add uniformity to the surface morphology and thus consistency in the sensor performance, the proposed design requires tuning to make the ink compatible with both the printer and any potential substrates. Another challenge with printers is the technical skill required to operate, tune, and repair them, as well as making modifications to the ink when a new substrate is being used.

An approach in improving the sensor performance involves varying the materials used in fabricating the sensor. Varying the substrate, GO to other forms of graphene, or other types of GO may change the degree of functionalization. Varying the species of amino acid for measuring free chlorine may also affect its performance characteristics such as sensitivity, LOD, and longevity. Other testing parameters such as temperature, concentration, rotation speed, and reaction time can also be varied to create the optimal fabrication process, and evaluate comprehensive performance characteristics of multiple sensors under multiple fabrication

parameters. However, this was not implemented in this work due to the computation time and power required to test this large quantity of parameters. As the number of fabrication and test parameters increases, the number of samples required to build a suitable and accurate model increases exponentially with it. More parameters requires more data which requires more nodes, and that means a larger architecture, and thus a significantly larger computation and processing time. The number of parameters and the scope of tested architectures were limited to eliminate excessively long computational times, and to prove the use of NN as a proof-of-concept for electrochemical water quality monitoring sensors.

Chapter 4 **

Experimental Results of Asparagine-Functionalized Graphene Oxide Free Chlorine Sensors & Predictive Modeling

4.1. Experimental Setup

4.1.1. Chemicals and Reagents

Graphene oxide (GO) (796034-1G), sodium hydroxide pellets (S8045), asparagine (A0884), and sodium hypochlorite (NaOCl, 425044-250 ML) were purchased from Sigma Aldrich and used as received. Deionized (DI) water ($>18\text{ M}\Omega$) was used to prepare all solutions used in the reaction. A single-electrode screen printed carbon electrode (SPCE) was purchased from CH Instruments and used as received. Hamilton (Ontario, Canada) municipal tap water was used to make all the free chlorine solutions used for testing the sensor.

4.1.2. Apparatus

All chemical solutions were made using a standard magnetic stirrer and centrifuge (Benchmark MC-24 Touch Microcentrifuge) to remove the reacted GO from the precursor solution. A conventional three-electrode electrochemical cell was used to measure the free chlorine solutions with an EmStat potentiostat (PalmSense BV, Utrecht, The Netherlands), a

** Adapted with permission from J. Siddiqui, M. J. Deen, Biodegradable asparagine-graphene oxide free chlorine sensors fabricated using solution-based processing, *The Analyst*, 144, 2022: 3643-3651. Copyright (2022) Royal Society of Chemistry (Appendix A)

reference electrode (CHI111) and a counter electrode (CHI115), all connected to a laptop with the software necessary to operate the potentiostat (**Figure 4-1**).

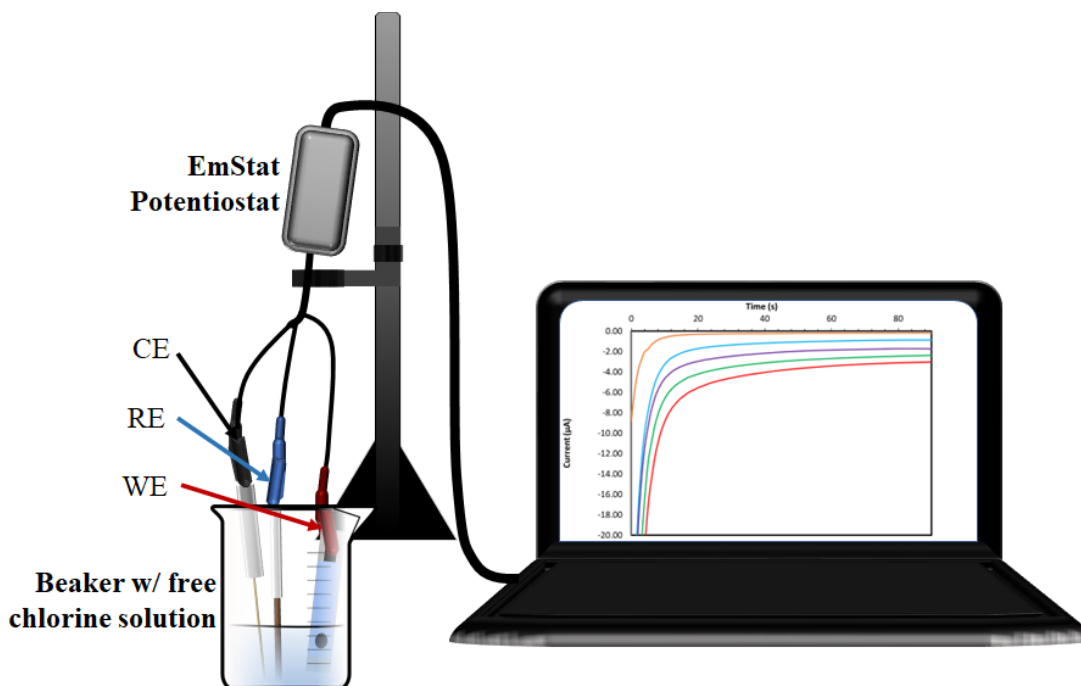


Figure 4-1: Experimental setup including laptop with potentiostat software, EmStat potentiostat, 3-electrode configuration with counter electrode (CE), reference electrode (RE), working electrode (WE), and a beaker with the free chlorine solution.

4.1.3. Preparation of the Electrode

Figure 4-2 shows a schematic of the fabrication process of the free chlorine sensors. A 10 mL solution of 10 mg mL⁻¹ of GO in DI water was sonicated until the GO was dispersed homogeneously according to the fabrication process in functionalizing GO with amino acids [153], [154], [161]. Another 10 mL solution of 1 M Asparagine and 1.5 M NaOH which was prepared to dissolve the asparagine, prevent the formation of amides by neutralizing carboxylic acid groups on the GO, and promote the reaction between asparagine and GO [153]. The two solutions were mixed together and then stirred for 24 hours at 1500 RPM under ambient conditions using a magnetic stirrer. After that, the dispersion was centrifuged at 7600 RPM for 45 min, and then washed a total of 3 times with a mixture of DI water and ethanol at

approximately a 1:1 ratio. The remaining material was suspended in a 15 mL solution of the same DI water and ethanol ratio. From this final dispersion, 12 μL was drop-casted onto an SPCE and spin-coated at 600 RPM for 10 s, and then dried on a hotplate for 10 min at 60°C.

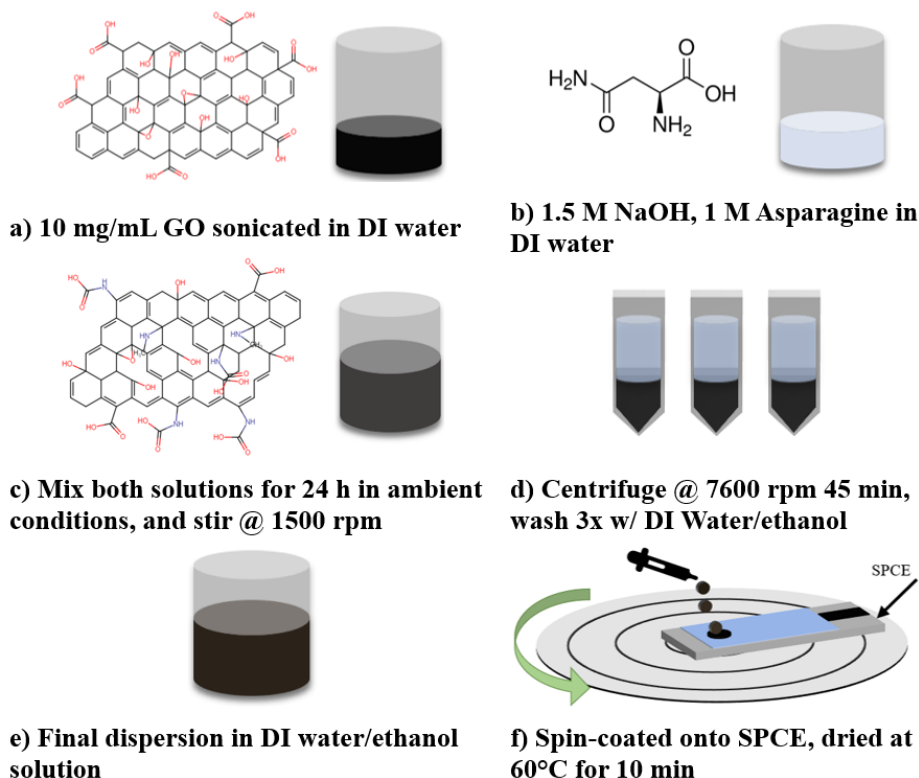


Figure 4-2: Fabrication steps of the asparagine-GO free chlorine sensor

4.1.4. Preparation of Samples

The free chlorine stock solution was used to prepare different concentrations of free chlorine (NaOCl) by diluting the as-received NaOCl using only tap water. The free chlorine solutions in tap water were calibrated using the LaMotte 2056 ColorQ PRO 7 Hand-Held Photometer which is a commercial DPD-based colorimetric test kit (**Figure 4-3**). The free chlorine sensors were characterized using an amperometric test set-up where the asparagine-GO on SPCE was the working electrode, Ag/AgCl was used for the reference electrode, and platinum for the counter electrode. Current was measured at a sampling rate of 1 Hz for 50 s with the electrodes dipped into free chlorine solution. Interference measurements were carried out by

adding 2*0.1 mL of interfering ion solution where each solution was made separately with 400 ppm of Na₂SO₄, KNO₃, NaCl, K₂CO₃, NaHCO₃, (NH₄)₂SO₄, CaCl₂, Al₂(SO₄)₃, MgCl₂, CuCl₂, ZnNO₃, (NH₄)₂SO₄ each. The individual ion solutions were added sequentially and measured in real time. All free chlorine measurements were performed at (23 ± 2 °C).

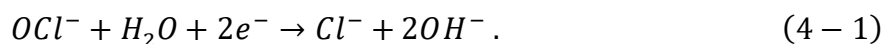


Figure 4-3: ColorQ PRO 7 Hand-Held Photometer commercial DPD-based colorimetric test kit with accompanying test tubes and chlorine reagents.

4.2. Results and Discussions

4.2.1. Mechanism

The free chlorine concentration was monitored by an amperometric sensor with an asparagine-functionalized GO as the working electrode, Ag/AgCl reference electrode and a platinum counter electrode at a applied potential of 0.1 V. This much lower than the theoretical reduction voltage range for dissolved oxygen which begins at 0.4 V [21], [49] is to avoid the reduction potentials of interfering ions [37], [104]. At the working electrode, OCl⁻ undergoes electrochemical reduction according to the chemical equation:



The output current stabilizes after the initial potential step, characteristic of chronoamperometric curves, to a level that is linearly dependent on the concentration of free chlorine [55]. As shown in **Figure 4-4(a)**, the total response time was 50 s. This allows the system to reach less than 5% of its initial value and is sufficient time to allow the system to reach a steady state. The output current at the 50th second was used for the calibration measurements. The reproducibility of the sensors was measured using 3 different free chlorine sensors that were fabricated in the same batch and their response characteristics are shown in **Figure 4-4(b)**. The average sensitivity was $\sim 0.30 \mu\text{A ppm}^{-1}$ ($0.43 \mu\text{A cm}^{-2} \text{ppm}^{-1}$ for the sensors with an electrode area of 0.7 cm^2). The maximum recorded variation in the sensor's sensitivity is 15 nA ppm^{-1} ($21 \text{ nA cm}^{-2} \text{ppm}^{-1}$; $\sim 5\%$ of the sensitivity) which corresponds to an accuracy of $\pm 0.05 \text{ ppm}$. Therefore, the sensors show high reproducibility with a low variation of output current between sensors [13], [24].

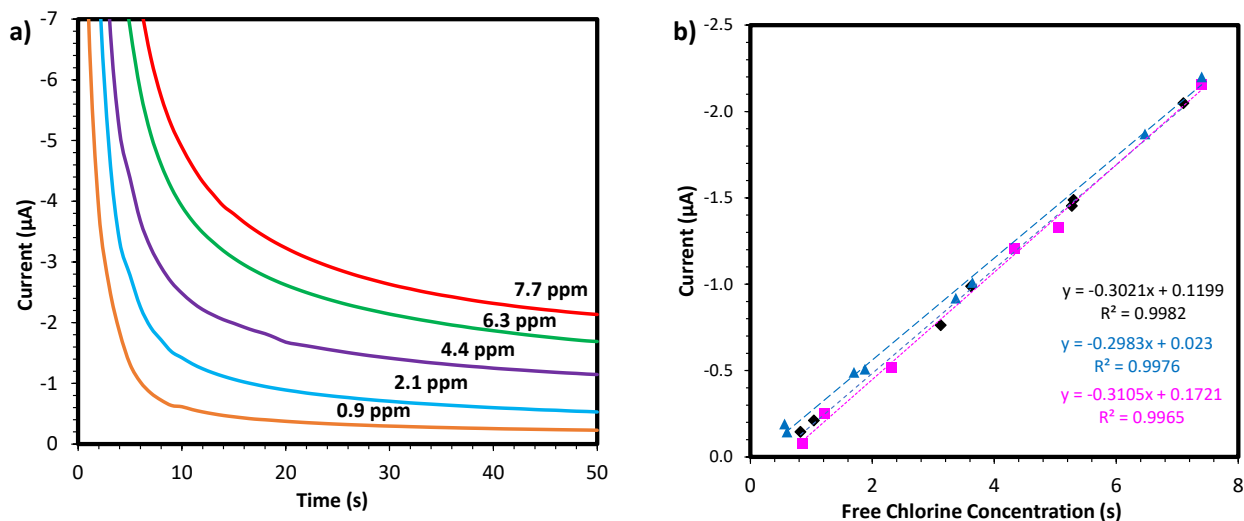


Figure 4-4: (a) Varying free chlorine measurements measured using chronoamperometry, from low to high concentrations of free chlorine; (b) The current response of 3 different free chlorine sensors measured at 50 s to show the reproducibility of the sensors.

In **Figure 4-5(a) – (c)**, we compare the use of the asparagine sensors with the use of plain GO and the plain SPCE that show that the use of GO is not suitable for use as a free chlorine

sensor given its very large hysteresis, possibly due to the breakdown of the sensor at higher free chlorine concentrations, and the SPCE is shown to be not responsive enough to free chlorine to be used as a free chlorine sensor. Furthermore, **Figure 4-5(d)** shows the cyclic voltammetry response of the SPCE, plain GO, and GO-asparagine where the dashed lines represent the absence of free chlorine and solid lines represent the addition of ~220 ppm free chlorine. The reduction potential of 0.1 V provided the sensor with optimal stability and is within an established and often used potential range for measuring free chlorine using sensors with similar functionalizing chemicals.

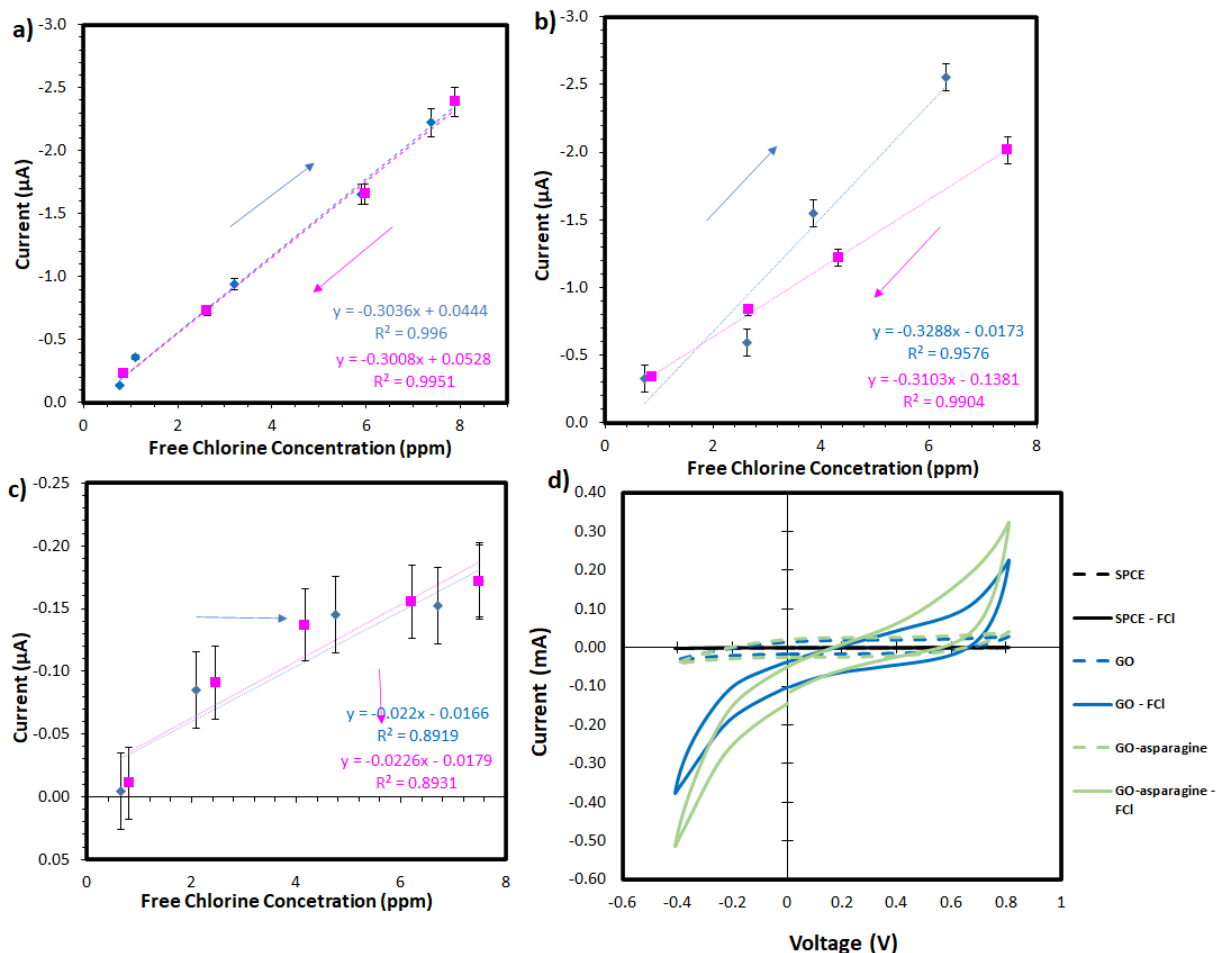


Figure 4-5: (a) Response current of chronoamperometry measurements at 50 s to show hysteresis behavior of sensor with free chlorine measurement cycling from low to high (blue) then high to low (orange) for (a) asparagine-GO (b) GO (c) SPCE; (d) Cyclic voltammetry response of the SPCE, plain GO, and GO-asparagine (FCI = free chlorine).

4.2.2. Hysteresis

The resolution of the free chlorine can be determined from its hysteresis. **Figure 4-6(a)** shows 3 cycles of chronoamperometry responses recorded at 50 s where free chlorine concentrations were cycled from 0.9 ppm to 8 ppm (solid blue circles) then back to 0.9 ppm (hollow black circles). This resulted in an average hysteresis of 51 μA which corresponded to a resolution of 0.2 ppm. This resolution is high enough for the safe monitoring of drinking and pool water given that the smallest amount of free chlorine currently present in drinking water is 0.2 ppm [8].

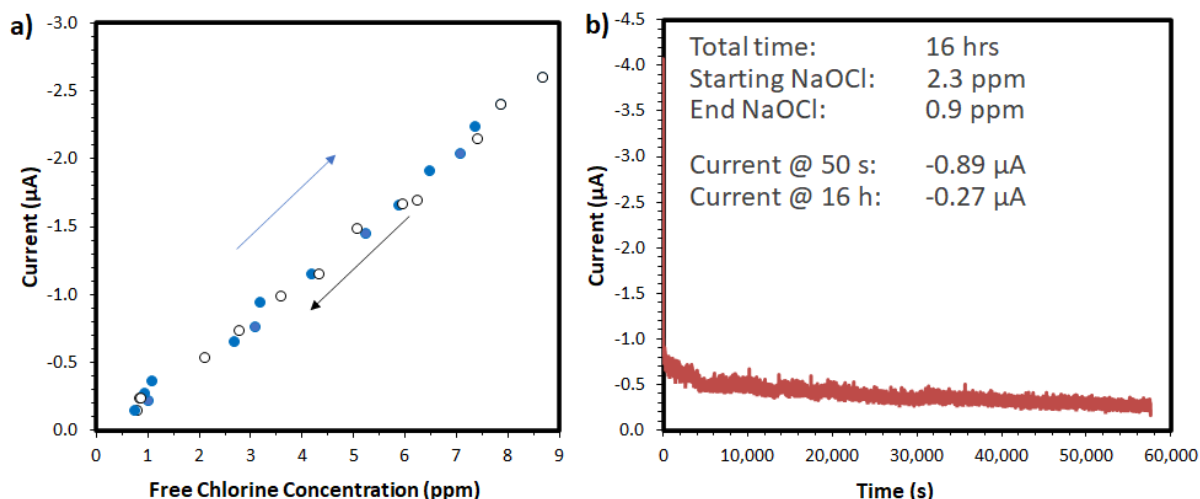


Figure 4-6: (a) Current response at 50 s vs. free chlorine concentration to show the hysteresis behavior of the sensor from 3 increasing and decreasing concentrations, and (b) drift measured with asparagine-GO free chlorine sensor in tap water over 16 h

4.2.3. Drift

The drift behaviour of the sensor was measured using chronoamperometry, shown in **Figure 4-6(b)**, by creating a 2.3 ppm solution of free chlorine with the sensor submerged in the solution for a period of 16 h, a value and duration comparable to measurements performed in literature [24]. The solution was placed in the dark to prevent free chlorine decay due to exposure to light. The drift rate was measured to be 0.039 $\mu\text{A h}^{-1}$ equivalent to 0.013 ppm h^{-1}

which is significantly lower than the resolution of the sensor. The free chlorine concentration at the end of the 16 h was measured at 0.9 ppm such that free chlorine decayed at a rate of 0.088 ppm h⁻¹. Since free chlorine decays intrinsically in water and is consumed during the course of amperometric sensing, this may be a major contributor in the measured drift of the free chlorine sensor.

4.2.4. Interference

The selectivity of the sensor was measured by adding 0.2 mL of interfering ion solution into 25 mL of 3.28 ppm NaOCl solution as shown in **Figure 4-7**. Each arrow represents 0.1 mL added of 400 ppm solutions, with the ion solutions made up of Na₂SO₄, KNO₃, NaCl, K₂CO₃, NaHCO₃, (NH₄)SO₄ and CaCl₂. The ions were being added sequentially in real time and the solution was being stirred at 750 rpm so that the ions can disperse in the solution quickly, providing a faster response from the free chlorine sensor. The concentrations are much larger than in real water samples which range between 7 and 15 ppm for most of the ions, and between 2 – 3 ppm for Al³⁺ [8]. Also, Al₂(SO₄)₃ at very high concentrations, 100x more than what is found in tap water, is shown to have an observable effect on the sensor, but this effect is expected to be negligible at the much lower concentrations found in tap water. The immediate responses from most of the ions normalizes within a few seconds showing that the sensor is not responsive to them. Thus, besides (NH₄)₂SO₄ and Al₂(SO₄)₃, all the interfering solutions had negligible effects on the sensor response. After the selectivity test, the sensor was still able to show a reliable response to 0.1 mL additions of 600 ppm NaOCl to the original solution.

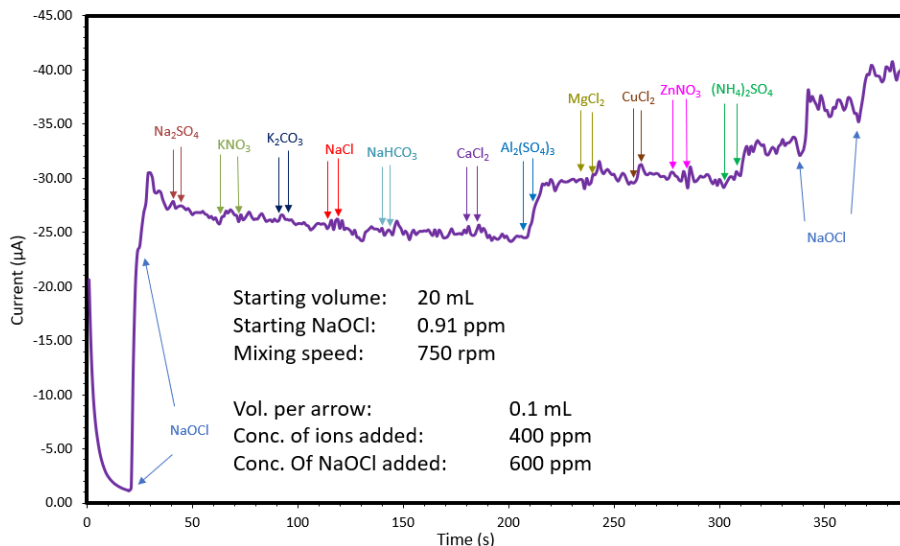


Figure 4-7: Insensitivity to commonly interfering ions and sensor response to an equal volume of free chlorine after introducing ions. Details for ion addition are shown in the graph

4.2.5. Temperature

To study the temperature dependence of the sensor, a large batch of water was chilled to 10 °C, then warmed up to room temperature over a hot plate. Once the water in the flask reached the desired T, the free chlorine concentrations were measured. Chronoamperometric responses were measured between 10 °C and 45 °C in intervals of 5 °C at a constant free chlorine concentration of 1.0 ppm from tap water. The detection of free chlorine depends on the reaction rate of HOCl, the dissociation ratio between HOCl and OCl⁻ and the mass transport diffusion of the HOCl from the bulk solution to the surface of the electrode [16]. With the increased reaction rate and increased mass transport, the free chlorine sensor responses are expected to be temperature dependent. The current responses in **Figure 4-8** show that at 50 s, the output current is dependent on temperature, and this linear relationship is given by $0.0025 \mu\text{A } ^\circ\text{C}^{-1}$ which is equivalent to $0.008 \text{ ppm } ^\circ\text{C}^{-1}$. This variation comes mainly from the diffusion of free chlorine [16]. For example, the diffusion coefficient of NaOCl is $\sim 0.94 \times 10^5 \text{ cm}^2 \text{ s}^{-1}$ and $2.1 \times 10^5 \text{ cm}^2 \text{ s}^{-1}$ at 10 and 45 °C respectively. The ratio between the diffusion rates is ~ 2.2 and the ratio between the

current at 10 °C and 45 °C is 2.4. The change in diffusion rate is responsible for more than 90% of the change in current over this wide range. If the sensor is to be used in applications with a small temperature range, then the mass transport effect is negligible, but if used in applications with a wider temperature range, then the free chlorine sensor should be used in tandem with a temperature sensor to compensate for the effect of the change in current due to diffusion.

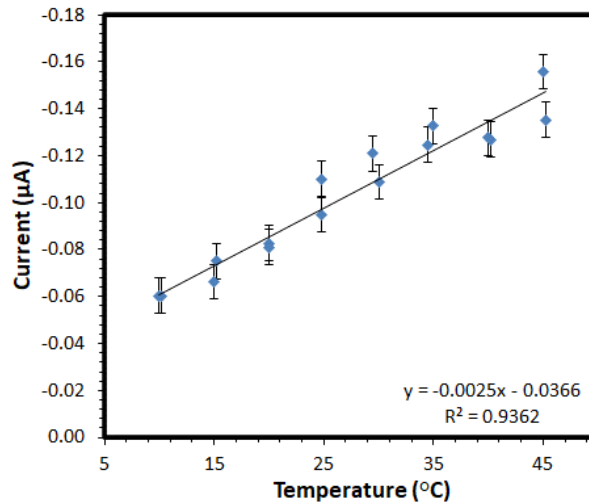


Figure 4-8: Change in current due to change in temperature with constant source of tap water.

4.2.6. Figure of Merit

In **Table 4-1**, a summary of the performance characteristics of the asparagine-GO sensor with other amperometric sensors made using graphene or graphene derivatives as a base, is provided.

Eq. (4-1) was used to calculate the sensors' figure-of-merit (FoM):

$$FoM = \frac{Sensitivity \left(\frac{\mu A}{ppm \times cm^2} \right)}{Hysteresis(ppm) \times Response\ time\ (s)}. \quad (4 - 1)$$

The performance characteristics of the sensor that quantify high precision and repeatable measurements are sensitivity, hysteresis, response time as well as the sensor's drift and temperature dependence. Apart from Alam [13] and Qin [24], in no other publications were numerical values for hysteresis or drift reported, limiting the parameters that can be compared

between the sensors. Instead, qualitative terms were used based on observing the figures for the sensors' selectivity and hysteresis. Sensitivity and response time are important metrics that were included in the FoM of a free chlorine sensor and were reported in the literature for each of the amperometric sensors. For the asparagine-GO sensors, the response time was determined using the time it took for the current to reach 95% of its maximum response, as shown in **Figure 4-4(a)**, as it shows the response of the sensor to free chlorine rather than having its response be restricted by the diffusion-limited chronoamperometry process. Also, included in the FoM is hysteresis because it is a fundamental metric that presents the repeatability of the sensor. No other metrics were included as they are not reported for other free chlorine sensors. The calculated FoMs shows that the gold electrode has the best performance characteristics followed by the graphite pencil lead electrode functionalized with ammonium carbamate. The lowest FOM was obtained for the asparagine-GO sensor as the focus for the sensor was the biodegradable and solution-based fabrication process. However, the FoM is competitive with the other sensors in **Table 4-1**.

Table 4-1: Comparison of fabrication, sensitivity, range, hysteresis, selectivity, and response time of amperometric sensors made with graphene-based or carbon-based substrates

Year, Ref	Material	Fabrication	Sensitivity ($\mu\text{A ppm}^{-1} \text{cm}^{-2}$)	Range (ppm)	Hysteresis (ppm)	Selectivity	Response time (s)	Figure of Merit
2021, [74]	Pencil graphite	Pencil-drawn on paper	0.515	4.618 – 32.3	Moderate-low	High	3	-
2017, [76]	rGO + polydopamine	Electrochemical reduction, electro-polymerization	1.839	0.52 – 11.3	Moderate-low	Moderate-low	25	-
2017, [24] (our group)	Graphite pencil lead + ammonium carbamate	Electrochemical reduction	0.302	0.8 – 8	0.04	High	< 3	2.517
2021, [13] (our group)	Gold	PVD	11.6	0 – 6	0.06	High	50	4.64
2017, [73]	SnO ₂ -GO	Aerosol CVD	51.289 111.725 (tap water)	0.1-10.08	High	Very High	< 10	-
2014, [103]	Polymelamine-SPCE	Electro-polymerization	5.642	0.52 – 366.8	-	High	25	-
2019, [100]	Pseudo-graphite	CVD	1.05	10.48 – 115.3	-	Very High	120	-
This work	Asparagine-GO	Chemical functionalization	4.29	0 – 8	0.2	Very High	< 10	2.15

4.3. Neural Network Modelling

4.3.1. Optimal Model Selection

The operation for the neural network models generated 153 models with unique architectures. Recorded in **Table 4-2** are the MAE and PCC for each of the different models averaged across the different folds for each architecture design (PCC on top; MAE below). There were several aims for designing the NN. Among them was to accurately measure the concentration of free chlorine faster than 50 s and to evaluate its performance characteristics over time, repeated use, and under different testing conditions. From the table, we can see that the

model with 21 nodes in N1 and 10 nodes in N2 obtained the lowest MAE at 0.3395 with a PCC of 0.9727.

Table 4-2: Validation MAE and PCC of NNs (PCC on top; MAE below).

		N1																
		8	9	10	11	12	13	14	15	16	17	18	19	20	21	22	23	24
N2	8	0.9541 0.4562	0.9576 0.4161	0.9646 0.4024	0.9660 0.3954	0.9647 0.4409	0.9696 0.3841	0.9673 0.3963	0.9665 0.4215	0.9674 0.3957	0.9710 0.3586	0.9653 0.4013	0.9701 0.3723	0.9719 0.3584	0.9701 0.3663	0.9717 0.3563	0.9696 0.3748	0.9725 0.3619
	9	0.9637 0.4122	0.9525 0.4590	0.9606 0.4369	0.9659 0.3910	0.9659 0.3975	0.9652 0.4545	0.9686 0.3821	0.9634 0.4210	0.9711 0.3730	0.9706 0.3996	0.9681 0.3746	0.9719 0.3701	0.9705 0.3857	0.9728 0.3438	0.9693 0.4371	0.9717 0.3579	
	10	0.9583 0.4362	0.9575 0.4428	0.9669 0.3947	0.9640 0.4034	0.9672 0.3981	0.9684 0.3876	0.9679 0.3907	0.9722 0.3562	0.9700 0.3880	0.9684 0.3853	0.9704 0.3710	0.9693 0.3747	0.9682 0.3692	0.9727 0.3395	0.9700 0.3795		
	11	0.9547 0.4523	0.9589 0.4339	0.9616 0.4059	0.9659 0.4321	0.9645 0.4077	0.9674 0.4177	0.9663 0.4072	0.9668 0.4161	0.9723 0.3554	0.9675 0.4211	0.9704 0.3777	0.9725 0.3605	0.9683 0.4049	0.9691 0.3769			
	12	0.9634 0.4014	0.9631 0.4019	0.9690 0.3874	0.9641 0.4252	0.9638 0.4026	0.9678 0.3905	0.9692 0.3743	0.9687 0.3867	0.9702 0.3759	0.9711 0.3922	0.9679 0.401	0.9734 0.3517	0.9703 0.3706				
	13	0.9626 0.4124	0.9657 0.4054	0.9680 0.3971	0.9669 0.3969	0.9683 0.3926	0.9696 0.3836	0.9693 0.3855	0.9674 0.3929	0.9722 0.3674	0.9710 0.3812	0.9717 0.3674	0.9688 0.3672					
	14	0.9612 0.4326	0.9607 0.4317	0.9640 0.4225	0.9673 0.3855	0.9688 0.3846	0.9649 0.3917	0.9650 0.4106	0.9691 0.3901	0.9720 0.3813	0.9724 0.3616	0.9682 0.3859						
	15	0.9566 0.4660	0.9678 0.3847	0.9680 0.4027	0.9672 0.4141	0.9686 0.3943	0.9695 0.3992	0.9672 0.3860	0.9696 0.3763	0.9682 0.3961	0.9737 0.3663							
	16	0.9657 0.4074	0.9635 0.4065	0.9653 0.4060	0.9697 0.4084	0.9677 0.3837	0.9670 0.3931	0.9726 0.3641	0.9707 0.3851	0.9720 0.3627								
	17	0.9664 0.4088	0.9656 0.4197	0.9671 0.3898	0.9682 0.4005	0.9685 0.3687	0.9700 0.3742	0.9712 0.3839	0.9714 0.3516									
	18	0.9638 0.4048	0.9640 0.4229	0.9661 0.3949	0.9709 0.3697	0.9709 0.4021	0.9704 0.3685	0.9710 0.3728										
	19	0.9624 0.4294	0.9601 0.4613	0.9688 0.3828	0.9688 0.3808	0.9707 0.3712	0.9686 0.3900											
	20	0.9624 0.4171	0.9621 0.4142	0.9613 0.4282	0.9709 0.3720	0.9707 0.3773												
	21	0.9637 0.4060	0.9650 0.4086	0.9699 0.3791	0.9634 0.4135													
	22	0.9651 0.4154	0.9680 0.4149	0.9676 0.3886														
	23	0.9578 0.4301	0.9639 0.3995															
	24	0.9662 0.4011																

4.3.2. NN Training

Using the training data, 153 different unique models were created, and with one model for each fold, which would make a total of 612 models trained using the training data and evaluated using the validation data. For each model the validation dataset was used to calculate the MAE and PCC and the model with the lowest MAE was chosen as the optimal model.

Figure 4-9(a) shows the evolution of the MAE averaged from the K folds across 400 epochs, and **Figure 4-9(b)** shows a close-up of the evolution of the MAE between 200 epochs and 400

epochs. The figures show a plot with the peaks and valleys smoothed to 70% of their amplitude. After ~300 epochs, the model's rate of improvement diminishes and there is an increased amount of noise generated during the training stage. The final obtained MAE and PCC, as shown in **Table 4-2**, are 0.3395 and 0.9727, respectively.

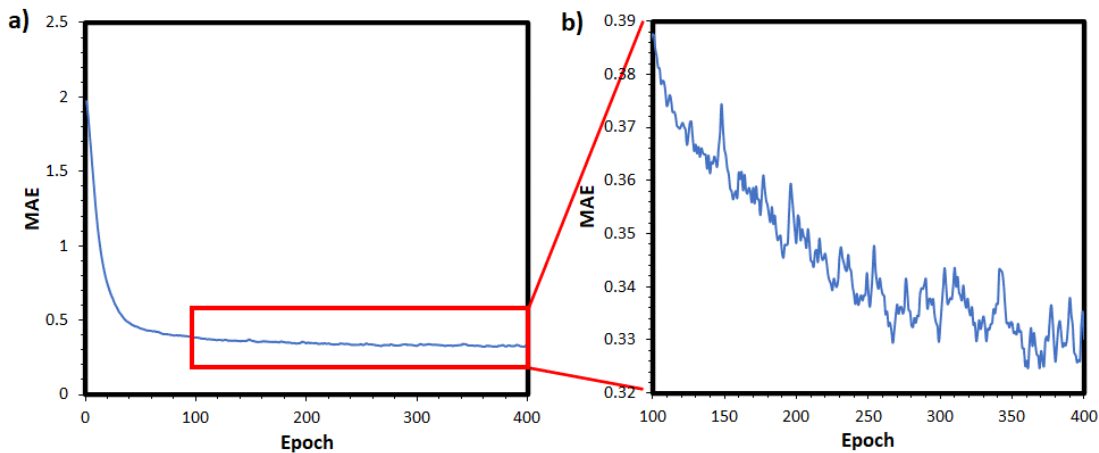


Figure 4-9: (a) MAE of validation curve of the optimal model and (b) a zoomed in image showing its evolution after 100 epochs

4.3.3. Input Parameter Performance

The following 4 parameters were isolated to investigate their influence on the sensor performance characteristics: ‘Time’, ‘Spin Coating’, ‘Increasing ppm’, ‘Sensor Cycle’. The models were tested on both the entire dataset and the test set. The entire dataset and test set contain 9385 and 1877 data points, respectively. When building constraints on the parameter values to test the model and parameters, the small number of values is a limitation in the dataset which creates large fluctuations in the resulting MAE and PCC values even with small variances between the datapoints. This resulted in statistically insignificant information when analyzing the results for several parameters, and as result, to maintain consistency, only the results from the entire dataset were investigated and discussed.

Time

Time was isolated to quantify the evolution of the performance of the model over time and the effect the changing time has on the MAE and PCC. This would also identify a more optimal range in which the sensor reaches a steady current flow when measuring free chlorine. **Figure 4-10** shows the evolution of the MAE and the PCC which shows the sensor performance stabilizing after 30 s, but this performance diminishes after 45 s; this can be attributed to evolution of the EDL at the surface of the sensor where the reaction rate is controlled by the diffusion of the analyte. At lower time scales near the potential step, the surface morphology caused by the irregularity of the graphene flakes creates a non-uniform concentration gradient. As the EDL moves further away from the electrode surface, the effects of the small irregularities diminish and normalize across the face of the electrode, and this allows the current flow to be more consistent across multiple sensors. **Figure 4-10(b)-(e)** show the correlation plots of the model at $t = 0$, $t = 10$, $t = 25$, $t = 50$ s, respectively, and the evolution of its performance. As time increases, the correlation plots converge to the $x = y$ relationship where the predicted value matches the real value. With **Figure 4-12(a)**, it was found that the window of time with the most consistent and reliable sensor performance is approximately between 30 and 45 s.

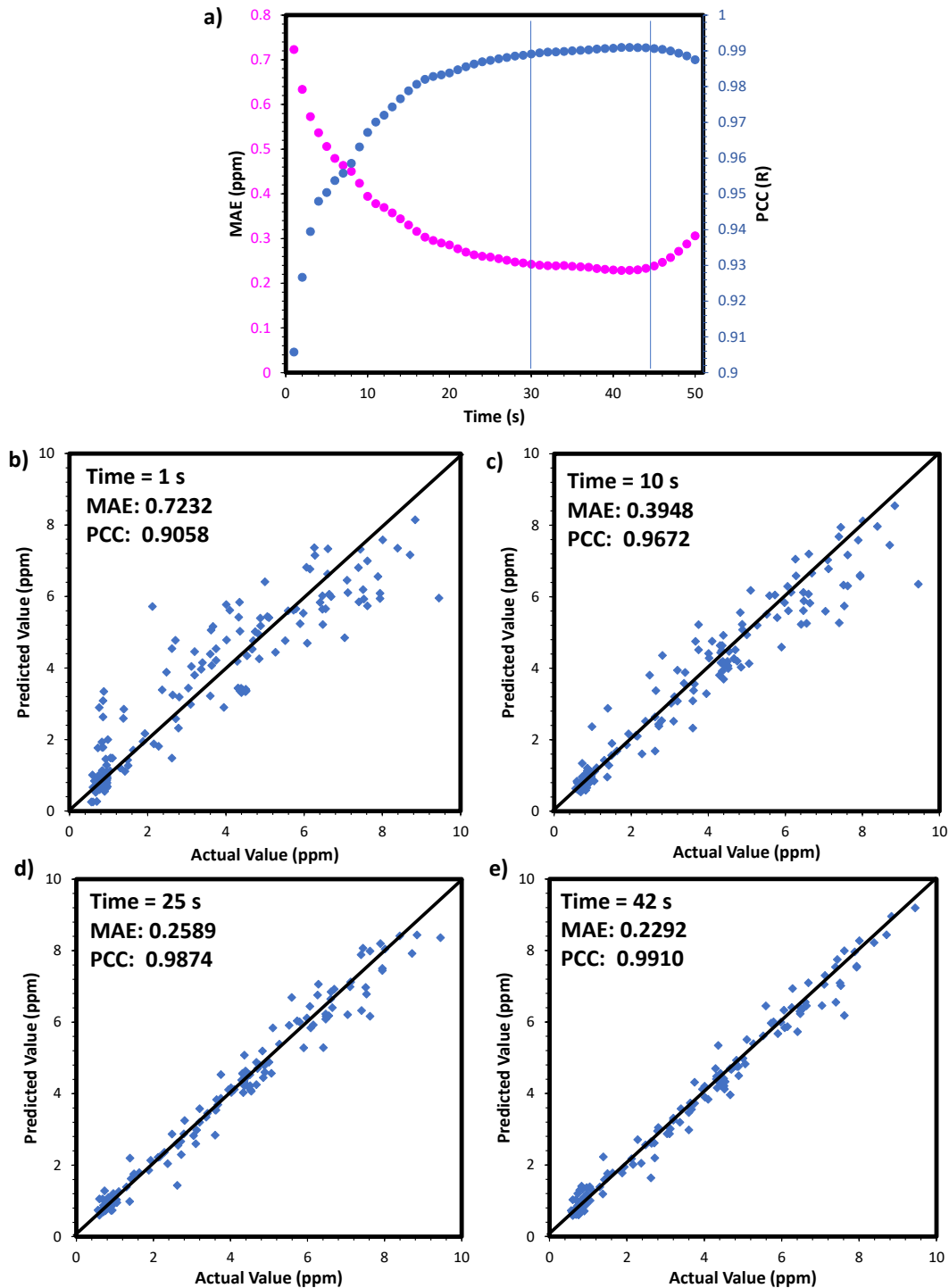


Figure 4-10: (a) Evolution of MAE and PCC on full dataset over duration of free chlorine measurement; Correlation plots of the model's performance on all the sensors at (b) $t = 1$ s, c) $t = 10$ s, (d) $t = 25$ s, e) $t = 42$ s to show the evolution of spread and the accuracy of the model at different points in time.

Spin Coating

Isolating the model's performance on the spin-coating parameter is to quantitatively determine the reliability and consistent performance of the sensors fabricated using spin coating, and how its performance compares over sensors fabricated using only drop-casting. **Figure 4-11(a)** shows the correlation plot of the non-spin coated and **Figure 4-11(b)** shows the correlation plot of the spin coated sensors, showing the impact of spin coating. The MAE for the spin coated sensors and non-spin coated sensors is 0.1958 and 0.4132, respectively. When only isolating the spin coating of the sensors there is a noticeable decrease in the MAE and increase in the PCC which indicates that the sensor performance is more consistent when spin coated as opposed to when it is not spin coated. Furthermore, when calculating the average sensitivity across the measurements for drop-casted sensors, the average sensitivity was $\sim 0.22 \mu\text{A ppm}^{-1}$ ($0.31 \mu\text{A cm}^{-2} \text{ ppm}^{-1}$ for the sensors with an electrode area of 0.7 cm^2) with an R^2 of 0.906. The low repeatability can be attributed to inconsistencies across sensors when drop casting the sensitive material. However, when compared to the results from spin coating, it is clear that spin coating significantly improves the performance characteristics of the sensors.

A factor to consider is the discrepancy in the number of data points between the two cases. The number of data points for drop casted sensor data and spin coated sensor data are 5814 and 3570, respectively. Since the results measured from spin coated sensors were found to be more consistent and provided competitive results across a smaller range of sensors, fewer sensors needed to be fabricated and tested which is why there are fewer data points. More trial, error, variations in the performance of the non-spin coated sensors is reflected in the large spread in Figure 4-11(a). To account for possible variation across the different batches and the days in which the sensors were fabricated, the parameters 'A', 'B', and 'Days Elapsed' were included in the model. However, from spread of the correlation plots in Figures 4-11(a)-(b), it shows that

these parameters did not account for this variation because if they did, the spread in the correlation plot would be much smaller. Overall, the correlation plots show that the sensor data from the spin coated sensors is more repeatable and can be modelled with higher accuracy than the sensor data from drop casted sensors.

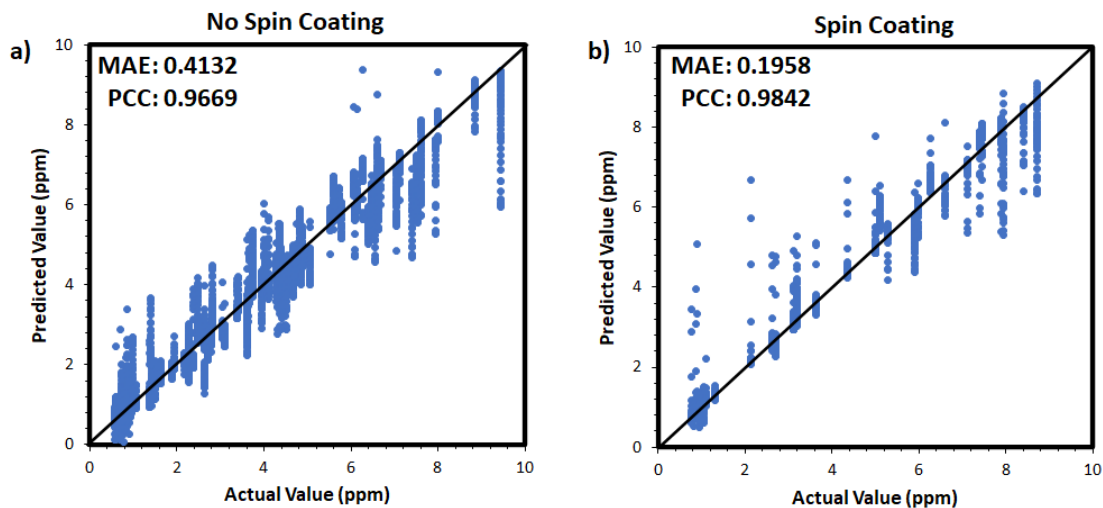


Figure 4-11: Correlation plot comparing the model performance on predicted free chlorine concentration of sensors fabricated (a) without and (b) with spin coating.

Increasing ppm

‘Increasing ppm’ is the parameter that accounts for each part in the measurement cycle. Its value is 1 when the free chlorine concentration is increasing, and a 0 when it is decreasing. Isolating the sensor performance based the parameter was used to quantify the hysteresis of the sensor. The dataset was first divided into two datasets according to whether or not the measurements were during an increasing or decreasing cycle. **Figure 4-12(a)** shows the correlation plot of data points when the free chlorine concentration is increasing from low to high, and **Figure 4-12(b)** shows the correlation plot of data points when the concentration is decreasing from high to low. With comparatively similar PCC values, the MAE shows that there is a difference of 0.0673 where the model highlights potential hysteresis in the model. The results when also isolating the datasets according to if the sensors were spin coated or not is

shown in **Table 4-**. When spin coated, the PCCs are comparable and the difference in MAE is 0.0062 whereas the difference in MAE is 0.0273 for sensors when they were drop-casted. Although there is a variation in the sensor data which can be seen from the correlation plots and MAEs, the NNs can model the sensor performance both in increasing and decreasing cycles consistently such that the impact of the hysteresis can be reduced. In both cases, the model results are comparable showing that the sensor performance can be modelled even when the data shows signs of hysteresis and degrading performance.

Table 4-3: PCC and MAE values of sensor data when isolating the ‘Increasing ppm’ parameter and again according to ‘Spin Coating’. (PCC top, bold; MAE bottom)

		Spin Coating	
		0	1
Increasing ppm	0	0.9693 0.3510	0.9752 0.3245
	1	0.9756 0.3237	0.9757 0.3307

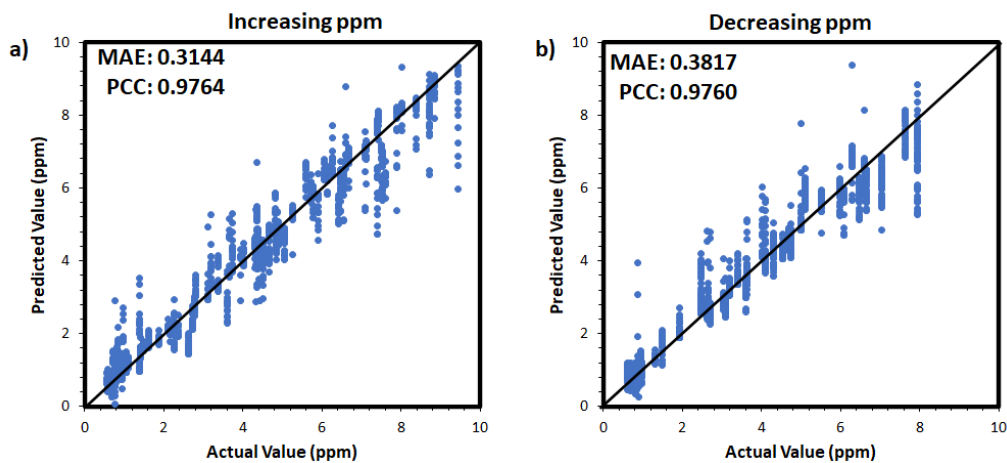
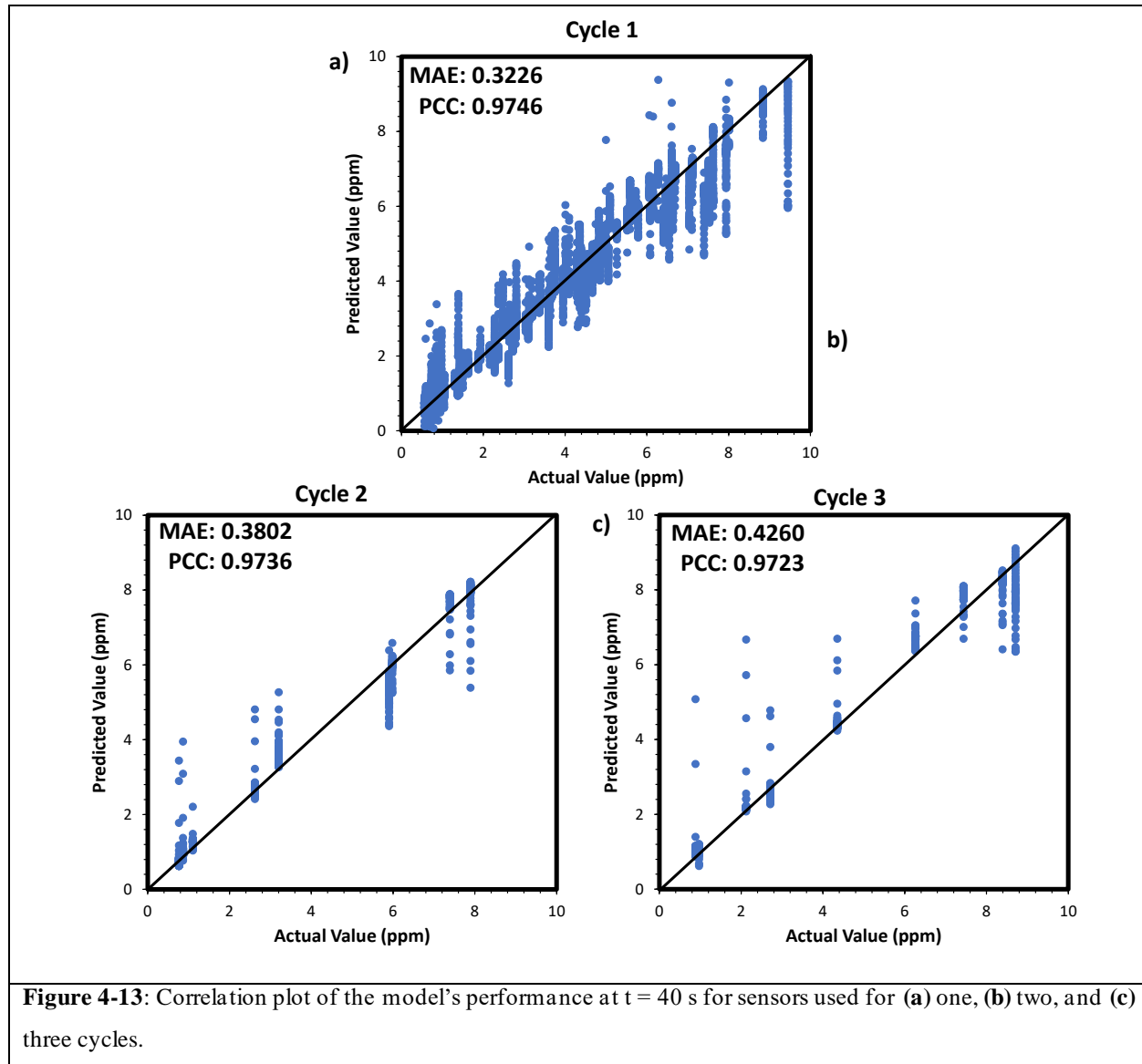


Figure 4-12: Correlation plot comparing the model performance on predicted free chlorine concentration of sensors fabricated (a) with decreasing and (b) increasing free chlorine concentrations during the measuring cycles.

Sensor Cycles

A cycle consists of a series of measurements of increasing free chlorine concentration, then after reaching between 9 – 10 ppm, decreasing the concentration. Isolating the model's performance on the sensor data for different cycles was carried out to evaluate the degradation of the sensor over time. On the fourth cycle, the sensor displayed noticeable signs of degradation, hence being limited to three cycles. **Figure 4-13(a)-(c)** shows the correlation plots for one, two and three cycles, respectively. With comparative PCCs for each of the three cycles indicating that the NN's ability to predict the free chlorine concentration values is similar across each cycle, the MAE values increase over time. This shows that the sensor performance consistency after repeated cycle decreases indicated towards the sensor's degradation.

The large difference in the number of data points, 8466, 459, and 459 for cycles one, two, and three, respectively, is due circumstances similar to measuring the difference between spin-coated and drop-cast sensors. The sensor data for every other testing condition and parameter is included under cycle one. On the other side, the number of data points for cycles two and three is relatively small because the number of tests required to evaluate the performance of the sensors did not require more than 10 measurements each. This can also be attributed to the consistent and reliable performance characteristics from spin coated sensor data.



To characterize the sensor's performance and evolution over time, the data set was further divided according to time. **Figure 4-14(a)** shows the MAE and PCC values for each sensor cycle for each second. Due to the large amounts of measurements carried out for one cycle, the model results are steady when compared to the results for cycles two and three. The large fluctuation for these cases is likely due to the small number of data points when compared to the large number of data points recorded for just one cycle. The correlation plot in **Figure 4-14(b)** shows the correlation plot for many data points including drop-cast sensor data which reflects the large MAE of 0.3481 and the large spread. **Figures 4-14(c)-(d)** show the correlation

plots for cycles two and three where the reported lowest recorded MAE is 0.157 and 0.184, respectively, but for a much smaller number of data points. These errors show that the predicted performance of the sensors is within the hysteresis-limited accuracy reported in Section 4.2, but also that the sensor performance begins to degrade after repeated measurements. Upon inspection of the sensor data, all the sensors tested in two and three cycles were only fabricated using spin coating, demonstrating the consistent performance of sensors fabricated with a spin coater.

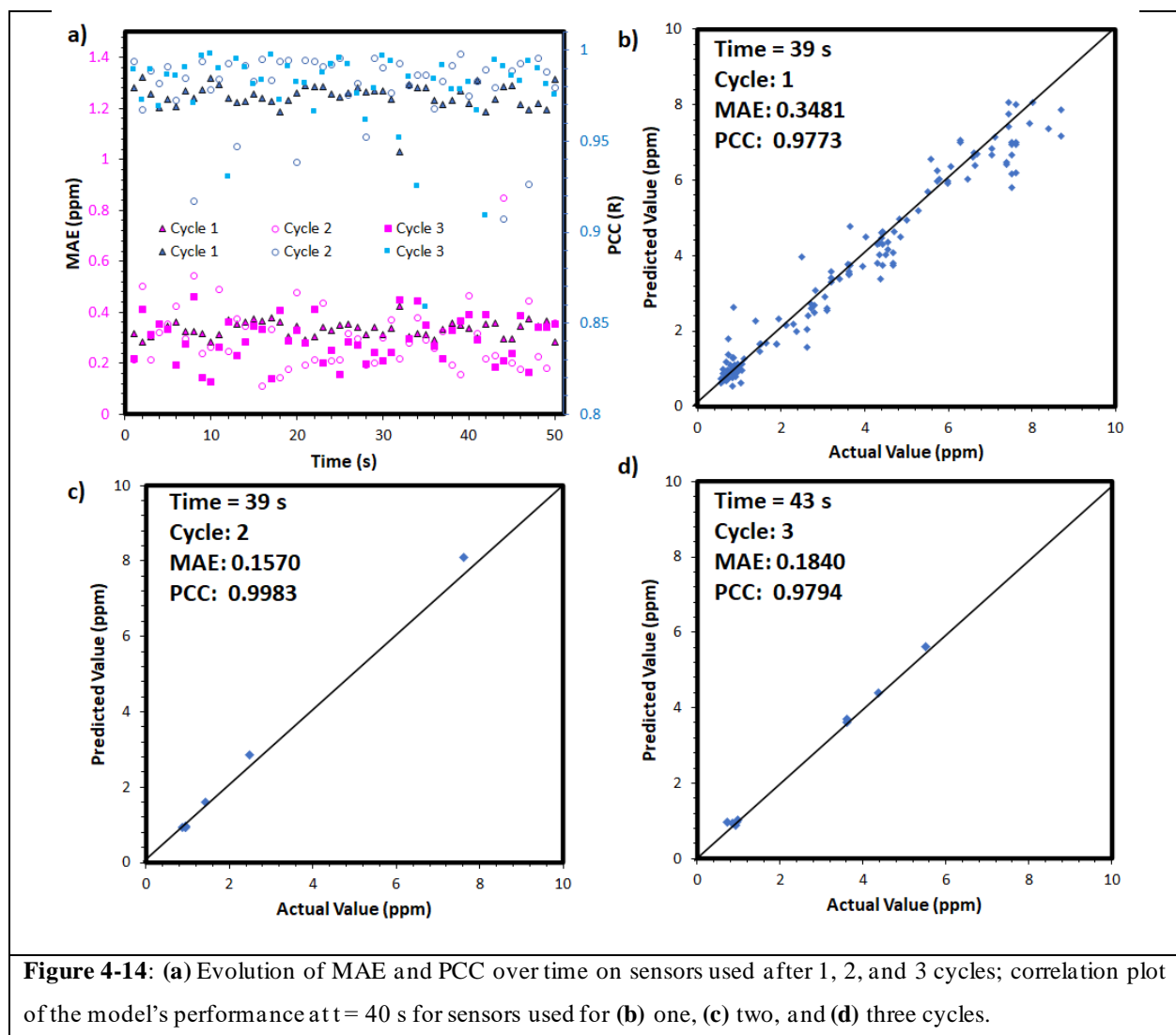


Figure 4-14: (a) Evolution of MAE and PCC over time on sensors used after 1, 2, and 3 cycles; correlation plot of the model's performance at $t = 40$ s for sensors used for (b) one, (c) two, and (d) three cycles.

4.4. Conclusion

Biodegradable free chlorine sensors were fabricated using graphene oxide functionalized with asparagine in a solution-based process and were used to measure free chlorine in real water samples. The sensor showed a high sensitivity with an acceptable resolution, good reproducibility, and excellent selectivity in the presence of a complex matrix of interfering ions. Using chronoamperometry, the sensitivity of the sensor to free chlorine is $0.30 \mu\text{A ppm}^{-1}$ at 50 s, with hysteresis of 0.2 ppm in the range between 0 – 8 ppm. The sensor showed stability to drift and an independence to temperature in narrow ranges but requires a temperature sensor to offset the temperature effect at wider ranges. Finally, the FoM showed competitive performances with other free chlorine sensors despite its focus being biodegradable and fabricated through solution-based processing. For future considerations, using an aerosol printer to create more sensors with more uniform surface morphology would serve to increase the sensitivity and decrease the hysteresis of the sensor, thus improving its important performance characteristics.

The sensors performance using the NN was corroborated by what was observed from the sensors. After training, testing, then comparing 153 NNs, the optimal NN architecture had 21 and 10 nodes in the first and second hidden layers, respectively, with a MAE of 0.3395 and a Pearson correlation coefficient of 0.9727. Several parameters were isolated and used to measure and analyze the sensor's performance characteristics, degradation, and hysteresis. The sensor was found to have an optimal measurement after 42 s and this number can be further reduced. Spin coating was found to significantly improve the sensor's performance and consistency. Although the hysteresis characteristics of the sensor affect its performance, it was found that the degradation behavior and hysteresis is repeatable and can therefore be modelled. The final parameter isolated was 'Sensor Cycles' which shows the degradation caused by fouling. To

potentially improve the performance of the sensor, it is recommended to vary the different fabrication parameters and experiment with the type of amino acids evaluate its performance, and extend the testing parameters from 3 cycles to 6 or 10 to quantify the extent of the sensors' degradation.

Machine learning models working in tandem with free chlorine sensors have great potential to optimize fabrication parameters, improve sensor performances, and response times. This is done by tabulating parameters and their outputs, testing various different NN models, then evaluating them based on key metrics. The challenges, however, continue to be the number of data points required. When increasing the number of parameters, the number of data points increases exponentially, increasing the waste and costs associated with sensor fabrication, thus defeating the purpose of making biodegradable sensors. As a result, parameters should be carefully selected which would also minimize both fabrication costs and computation costs.

Chapter 5 ^{††}

Conclusions and Future Work

5.1. Conclusions

This thesis focused on the design, fabrication, and characterization of solution-based biodegradable free chlorine sensors using standard experimental techniques and NN modelling. Using GO and asparagine, an amino acid, and a one-step chemical functionalization process, an environmentally friendly free chlorine sensor was able to detect standard levels of free chlorine in tap water with performance characteristics competitive with other electrochemical free chlorine sensors. Using a one-step chemical synthesis process in solution, the fabrication process can potentially be scaled up for mass-production and the sensing material in the form of an ink is also compatible with printing processes such as inkjet or aerosol printing. The sensors were tested under various testing conditions to find an optimal performance condition, and from the data collected, a NN model was trained and developed to quantify the sensor's response to various fabrication parameters, hysteresis, and longevity. By combining the results from standard experimental techniques and the results from the NN models, a clearer and more robust view of the sensor's performance characteristics can be quantified using both analytical and statistical methods.

Prior to creating the sensor designs, our thesis provided a detailed review of electrochemical techniques and fabrication methods of recently published carbon-based electrochemical free

^{††} Part of this work will be submitted for consideration for RSC Advances publication as: J. Siddiqui, M. Taheri, M. Nami, M. J. Deen, Carbon-Based Electrochemical Free Chlorine Sensors, December 2022. (in preparation)

chlorine sensors in Chapter 2. It was found that some of the intrinsic challenges of large-scale fabrication include low yields, poor material uniformity, and high costs yields. However, complex fabrication methods that generate smaller yields develop higher quality materials such as single layer graphene with high uniformity and few defects. Although there is a general trade-off between fabrication complexity and sensor performance, the performance characteristics of many lower-cost sensors can still be made competitive with complex and expensive sensors.

The free chlorine sensor design presented in Chapter 3 aimed to develop an electrochemical free chlorine sensor fabricated in a solution-based chemical functionalization process using only environmentally friendly materials and processes. GO was chosen as the substrate material due to its base material, graphene, being widely used in free chlorine sensors as a substrate material and because it is widely known to be biodegradable. The functionalizing material is asparagine, a well-known and biodegradable amino acid. Asparagine was chemically functionalized to GO in a simple and environmentally friendly chemical process to minimize the amount of waste generated during the fabrication processes and ensure that the waste generated from the fabrication process was non-toxic and easily disposable. These goals were achieved by using only GO, asparagine, NaOH, water, and ethanol for the entire fabrication process. However, one of the limitations of these materials is their longevity and resilience to free chlorine. The materials are biodegradable and free chlorine is a very strong oxidizer which limits how long the materials can be used under these conditions. To quantify the effects of this degradation, a NN model was training and developed using K-Fold Cross Validation that would be trained and tested on over 9000 data points and 10 parameters.

Following this, the experimental results for the free chlorine sensor and the NN are presented in Chapter 4. The free chlorine sensor reported a sensitivity of $\sim 0.30 \mu\text{A ppm}^{-1}$ (0.43

$\mu\text{A cm}^{-2} \text{ ppm}^{-1}$ for the sensors with an electrode area of 0.7 cm^2) and a hysteresis-limited resolution of 0.2 ppm . The sensor reported a low drift of $0.039 \mu\text{A h}^{-1}$ equivalent to 0.013 ppm h^{-1} , most of which can be attributed to intrinsic free chlorine decay and free chlorine consumption from the electrochemical reaction. The sensor also showed negligible responses to all interfering ions but a small response to Al^{3+} at very high concentrations which can be negligible at low concentrations. Finally, the sensor showed a low temperature dependence of $0.0025 \mu\text{A } ^\circ\text{C}^{-1}$ which is equivalent to $0.008 \text{ ppm } ^\circ\text{C}^{-1}$, most of which comes from the diffusion of free chlorine. Over small temperature ranges, this temperature effect can be ignored. The NN model was trained using 9385 data points, achieving a final MAE of 0.3395 with a PCC of 0.9727 with an architecture of 21 and 10 nodes in the first and hidden layers, respectively. By monitoring the evolution of the model's performance across the time range for measuring the free chlorine concentration, the NN was used to obtain a shorter sensing time with a more consistent performance. It was also used to quantify the degree to which spin coating improves the sensor's performance characteristics, as well as the amount of hysteresis. It was found that although there the sensor experiences hysteresis, its effect on the sensor is consistent as seen when measuring the differences in the MAE between increasing and decreasing free chlorine concentrations. The final parameter quantified was the degradation of the sensor where the MAE increases from 0.15 to 0.18 from cycle two to three, after which the sensor degrades beyond acceptable use. Based on these results, the combined use of experimental and statistical analytical techniques can be used to provide a wider and clearer picture of sensor parameters and performance characteristics.

5.2. Future Work

This work focused on developed a low-cost biodegradable electrochemical free chlorine sensor for water quality monitoring. However, we have identified several research challenges for this sensor and in general, electrochemical free chlorine sensors so that in the coming years, environmentally friendly water monitor quality sensing can be optimized with better and more reliable performance characteristics.

Sensor repeatability and reliability

One of the difficulties in using the sensor is in fabricating new sensors through spin coating each time. This requires a lengthy and sensitive process of placing the SPCE in the center of the rotating chuck on the spin coater, placing a drop of sensitive material on the electrode, spin coating it, drying the material, then again placing the SPCE in the center of the rotating chuck. Although this process has been shown to develop repeatable sensors, it is still a process done by hand with many steps which is prone to human error creating inaccuracies in the measurements. Therefore, there are two possibilities in developing a more accurate deposition process. The first is reduce the number of steps required for fabricating the sensors by reducing the volume used for fabricating the sensors or implement an inkjet printer for consistent and automated fabrication.

Linearity and sensitivity

The sensing range and sensitivity of the asparagine-modified GO free chlorine sensor should be increased. Although the sensor can accurately measure tap water free chlorine concentrations over a range of 0 – 8 ppm, the sensing range is not wide enough to measure the water used to wash meats and vegetables which ranges between 50 – 200 ppm. A wider sensing range may be obtained by increasing the concentration of asparagine for a higher degree of

functionalization, or vary the type of GO used with a higher concentration of oxides. To increase the sensitivity of the sensors, varying the ratios of the materials used in the fabrication process can increase the sensitivity by increasing the degree of functionalization of asparagine onto GO. This can also be done either by increasing the temperature or increasing the reaction time. Since there was a reduction in hysteresis after the GO was functionalized with asparagine, increasing the degree of functionalization may also decrease the hysteresis as well, making an overall better performing sensor.

Modelling

Incorporating machine learning models into the free chlorine sensors, and more generally, electrochemical sensors can facilitate fabrication [47], [162], [163], improve sensor performances, reduce response times, and reduce drift [61], [164]. This can be done by tabulating fabrication parameters, performance parameters and outputs, and training machine learning models such that the different models are used to optimize different aspects of the device performance or design. One of the greatest challenges for this, is the time and data required to train machine learning models. As the number of parameters increase, the number of training points to train a suitable model increases exponentially [162], [165]. Although one can space apart intervals for fabrication parameters such as temperature, chemical concentrations, reaction times, or mixing speed to minimize the number of data points needed, this task quickly becomes costly and time-consuming [166]. Therefore, parameters should be reduced as much as possible to limit the costs associated with maximizing sensor performances, and time should be spent in evaluating advantages of the performance of the sensor and the costs associated with optimizing its performance.

Temperature and pH

Electrochemical sensing methods are physically intertwined and affected by the interfering effects caused by temperature and pH, affecting diffusion and dissociation constants respectively [18]. Accounting for these changes requires empirical approaches that must be managed for every electrochemical free chlorine sensor. The most robust approach in mitigating the effects of interference caused by pH/temperature is either by measuring samples within a desired pH/temperature range or by identifying the relationship between them and free chlorine. Once a sufficient amount of data is collected, the interference effects can be compensated accordingly either through coding mathematical relationships in software [24] or via machine learning models which requires a less rigorous understanding of the physical relationships between free chlorine, temperature, and pH [162]. To compensate between free chlorine and pH/temperature, the sensor system requires the use of additional sensors and a dedicated sensor readout system. However, a simpler alternative is to ensure that pH and temperature are controlled over small ranges as the effects of these interfering parameters becomes noticeable over wide ranges.

Degradation and fouling

Carbon-based free chlorine sensors will degrade either physically or chemically, a property that may be amplified due to their intrinsic biodegradable properties [7], [21]. There are two types: the physical degradation is when the sensing material itself leaves the substrate's surface and becomes part of the solution, or voids, pinholes, flakes, or other mechanical products form; and chemical degradation which occurs when irreversible reactions take place on the surface of the sensitive material or when a reaction takes place in the material that is not completely reversible. Since free chlorine is a strong oxidizing agent, there may be reactions that

alter the chemical composition of the sensing material, modifying the sensitivity, increasing hysteresis or response time. Since the degradation can affect the lifetime of the sensors, new materials must be developed to lengthen their lifetime and maximize performance.

The free chlorine sensors are also susceptible to fouling caused by accumulated minerals, called mineral fouling or mineralization [7]. Mineral fouling usually occurs as deposited calcium carbonate which occurs in water systems inside pipes, taps and sensors caused by high pH environments, and it can interfere with the reduction reaction. For instance, the reduction of free chlorine forming an oxide film on the surface of a carbon electrode can inhibit the reduction in the electrochemical reaction and may likely have effects on the performance similar to the chemical degradation of the sensor. The consequences are significantly degraded performances for measuring free chlorine with an increase in hysteresis and a reduced sensor lifetime. Therefore, fouling should be considered from the sensor design where the ideal chlorine sensor is both simple and robust.

References

- [1] World Health Organization (WHO), “Progress on Household Drinking Water, Sanitation and Hygiene,” 2020. Accessed: Aug. 12, 2022. [Online]. Available: <https://www.who.int/publications/i/item/9789240030848>.
- [2] G. Connel, *The chlorination/chloramination handbook*. American Water Works Association, 1996.
- [3] J. W. Harrison and R. E. Hand, “The effect of dilution and organic matter on the antibacterial property of 5.25% sodium hypochlorite,” *J. Endod.*, vol. 7, no. 3, pp. 128–132, 1981, doi: 10.1016/S0099-2399(81)80127-6.
- [4] A. U. Alam, “Towards an integrated water quality monitoring system using low cost electrochemical sensors,” McMaster University, 2019.
- [5] A. K. Camper and G. A. McFeters, “Chlorine Injury and the Enumeration of Waterborne Coliform Bacteria,” *Appl. Environ. Microbiol.*, vol. 37, no. 3, pp. 633–641, 1979.
- [6] C. Venkobach, L. Iyengar, and A. V. S. P. Rao, “Mechanism of Disinfection: Effect of Chlorine on Cell Membrane Functions,” *Water Res.*, vol. 11, no. 8, pp. 727–729, 1951, doi: doi.org/10.1016/0043-1354(77)90114-2.
- [7] R. E. Wilson, I. Stoianov, and D. O’Hare, “Continuous chlorine detection in drinking water and a review of new detection methods,” *Johnson Matthey Technol. Rev.*, vol. 63, no. 2, pp. 103–118, 2019, doi: 10.1595/205651318X15367593796080.
- [8] WHO, *Guidelines for drinking water quality: Health criteria and other supporting information*, 2nd ed., vol. 2. Geneva, 1996.
- [9] Health Canada (HC), “Guidelines for Canadian drinking water quality: guideline technical document - Chlorine,” 2006. [Online]. Available: http://www.hc-sc.gc.ca/ewh-semt/alt_formats/hecs-sesc/pdf/pubs/water-eau/sum_guide-res_recom/summary-sommaire-eng.pdf.
- [10] H. Beshai, G. K. Sarabha, P. Rathi, A. U. Alam, and M. Jamal Deen, “Freshness monitoring of packaged vegetables,” *Appl. Sci.*, vol. 10, no. 21, pp. 1–41, 2020, doi: 10.3390/app10217937.

- [11] A. U. Alam, P. Rathi, H. Beshai, G. K. Sarabha, and M. Jamal Deen, “Fruit quality monitoring with smart packaging,” *Sensors*, vol. 21, no. 4, pp. 1–30, 2021, doi: 10.3390/s21041509.
- [12] Y. Qin, S. Pan, M. M. R. Howlader, R. Ghosh, N. X. Hu, and M. J. Deen, “Paper-Based, Hand-Drawn Free Chlorine Sensor with Poly(3,4-ethylenedioxythiophene):Poly(styrenesulfonate),” *Anal. Chem.*, vol. 88, no. 21, pp. 10384–10389, 2016, doi: 10.1021/acs.analchem.6b03211.
- [13] A. U. Alam, D. Clyne, W. Lush, and M. J. Deen, “A reusable, reagent-less free chlorine sensor using gold thin film electrode,” *Analyst*, vol. 146, pp. 2626–2631, 2021, doi: 10.1039/d1an00038a.
- [14] Food and Agriculture Organization of the United Nations and World Health Organization (WHO), “Benefits and Risks of the Use of Chlorine-containing Disinfectants in Food Production and Food Processing,” Ann Arbor, 2008.
- [15] W. Benjamin, “Chlorine, is there a better alternative?,” *Sci. Total Environ.*, vol. 1981, no. 18, pp. 235–243, 1981.
- [16] M. S. Chao, “The Diffusion Coefficients of Hypochlorite, Hypochlorous Acid, and Chlorine in Aqueous Media by Chronopotentiometry,” *J. Electrochem. Soc.*, vol. 115, no. 11, pp. 9–10, 1968, [Online]. Available: doi:10.1149/1.2410933.
- [17] J. Carrell Morris, “The acid ionization constant of HOCl from 5 to 35°,” *J. Phys. Chem.*, vol. 70, no. 12, pp. 3798–3805, 1966, doi: 10.1021/j100884a007.
- [18] P. Li, “Concise review on residual chlorine measurement: Interferences and possible solutions,” *J. Clean. Prod.*, vol. 323, p. 129119, 2021, doi: 10.1016/j.jclepro.2021.129119.
- [19] P. Kruse, “Review on Water Quality Sensors,” vol. 51, p. 203002, 2018, doi: doi.org/10.1088/1361-6463/aabb93.
- [20] A. Zubiarrain-laserna and P. Kruse, “Review — Graphene-Based Water Quality Sensors,” *Electrochem. Soc.*, vol. 167, p. 037539, 2020, doi: 10.1149/1945-7111/ab67a5.
- [21] Y. Qin, H. J. Kwon, M. M. R. Howlader, and M. J. Deen, “Microfabricated electrochemical pH and free chlorine sensors for water quality monitoring: Recent advances and research challenges,” *RSC Adv.*, vol. 5, no. 85, pp. 69086–69109, 2015, doi: 10.1039/c5ra11291e.
- [22] M. H. Banna *et al.*, “Online drinking water quality monitoring: Review on available and

- emerging technologies,” *Crit. Rev. Environ. Sci. Technol.*, vol. 44, no. 12, pp. 1370–1421, 2014, doi: 10.1080/10643389.2013.781936.
- [23] A. Murray and D. Lantagne, “Accuracy, precision, usability, and cost of free chlorine residual testing methods,” *J. Water Health*, vol. 13, no. 1, pp. 79–90, 2015, doi: 10.2166/wh.2014.195.
- [24] Y. Qin *et al.*, “Integrated water quality monitoring system with pH, free chlorine, and temperature sensors,” *Sensors Actuators, B Chem.*, vol. 255, pp. 781–790, 2018, doi: 10.1016/j.snb.2017.07.188.
- [25] G. Gordon, D. L. Sweetin, K. Smith, and G. E. Pacey, “Improvements in the N,N-diethyl-p-phenylenediamine method for the determination of free and combined residual chlorine through the use of FIA,” vol. 38, no. 2, pp. 145–149, 1991.
- [26] L. Moberg and B. Karlberg, “An improved N, N-diethyl-p -phenylenediamine (DPD) method for the determination of free chlorine based on multiple wavelength detection,” vol. 407, pp. 127–133, 2000.
- [27] F. J. Del Campo, O. Ordeig, and F. J. Muñoz, “Improved free chlorine amperometric sensor chip for drinking water applications,” *Anal. Chim. Acta*, vol. 554, no. 1–2, pp. 98–104, 2005, doi: 10.1016/j.aca.2005.08.035.
- [28] K. Singh and S. K. Mehta, “Luminescent ZnO quantum dots as an efficient sensor for free chlorine detection in water,” *Analyst*, vol. 141, no. 8, pp. 2487–2492, 2016, doi: 10.1039/c5an02599k.
- [29] J. Shang, L. Yu, Y. Sun, X. Chen, Q. Kang, and D. Shen, “On site determination of free chlorine in water samples by a smartphone-based colorimetric device with improved sensitivity and reliability,” *New J. Chem.*, vol. 43, no. 36, pp. 14409–14416, 2019, doi: 10.1039/c9nj03954f.
- [30] J. Dou, J. Shang, Q. Kang, and D. Shen, “Field analysis free chlorine in water samples by a smartphone-based colorimetric device with improved sensitivity and accuracy,” *Microchem. J.*, vol. 150, p. 104200, 2019, doi: 10.1016/j.microc.2019.104200.
- [31] Y. Ding *et al.*, “A carbon dot-based hybrid fluorescent sensor for detecting free chlorine in water medium,” *Anal. Methods*, vol. 8, no. 5, pp. 1157–1161, 2016, doi: 10.1039/c5ay03143e.
- [32] D. B. Gunjal *et al.*, “Sustainable carbon nanodots synthesised from kitchen derived waste

- tea residue for highly selective fluorimetric recognition of free chlorine in acidic water: A waste utilization approach,” *J. Taiwan Inst. Chem. Eng.*, vol. 95, pp. 147–154, 2019, doi: 10.1016/j.jtice.2018.10.014.
- [33] Y. Dong, G. Li, N. Zhou, R. Wang, Y. Chi, and G. Chen, “Graphene Quantum Dot as a Green and Facile Sensor for Free Chlorine in Drinking Water,” *Anal. Chem.*, vol. 84, no. 19, pp. 8378–8382, 2012, doi: <https://doi.org/10.1021/ac301945z>.
- [34] W. C. Chen, P. Venkatesan, and S. P. Wu, “A highly selective turn-on fluorescent probe for hypochlorous acid based on hypochlorous acid-induced oxidative intramolecular cyclization of boron dipyrromethene-hydrazone,” *Anal. Chim. Acta*, vol. 882, pp. 68–75, 2015, doi: 10.1016/j.aca.2015.04.012.
- [35] H. E. Moore, M. J. Garmendla, and W. J. Cooper, “Kinetics of Monochloramine Oxidation of N, N-Diethyl-p-phenylenediamine,” *Environ. Sci. Technol.*, vol. 18, no. 5, pp. 348–353, 1984, doi: 10.1021/es00123a011.
- [36] A. U. Alam *et al.*, “Polymers and organic materials-based pH sensors for healthcare applications,” *Prog. Mater. Sci.*, vol. 96, pp. 174–216, 2018, doi: 10.1016/j.pmatsci.2018.03.008.
- [37] A. J. Bard, R. Parsons, and J. Jordan, *Standard Potentials in Aqueous Solutions*. New York: Marcel Dekker, 1985.
- [38] J. A. Harrison and Z. A. Khan, “The reduction of chlorine in alkaline solution,” *J. Electroanal. Chem.*, vol. 30, no. 1, pp. 87–92, 1971, doi: 10.1016/0368-1874(71)85036-0.
- [39] A. U. Alam, D. Clyne, H. Jin, N. X. Hu, and M. J. Deen, “Fully Integrated, Simple, and Low-Cost Electrochemical Sensor Array for in Situ Water Quality Monitoring,” *ACS Sensors*, vol. 5, no. 2, pp. 412–422, 2020, doi: 10.1021/acssensors.9b02095.
- [40] F. Kodera, R. Saito, H. Ishikawa, A. Miyakoshi, and M. Umeda, “Electrochemical Detection of Free Chlorine Using Ni Metal Nanoparticles Combined with Multilayered Graphene Nanoshells,” *Electroanalysis*, vol. 31, no. 7, pp. 1245–1248, 2019, doi: 10.1002/elan.201800326.
- [41] C. M. Bishop, *Pattern Recognition and Machine Learning*. New York: Springer Science+Business Media, 2006.
- [42] N. Ketkar, *Deep Learning with Python: A Hands-on Introduction*. Bangalore: Nikhil Ketkar, 2017.

- [43] F. Chollet, *Deep Learning with Python*, 1st ed. Manning Publications Co., 2018.
- [44] A. Rosebrock, *Deep Learning for Computer Vision with Python*, 1st ed. PyImageSearch, 2017.
- [45] Y. S. Abu-Mostafa, M. Magdon-Ismail, and H.-T. Lin, *Learning from Data: A Short Course*. Abu-Mostafa, Yaser S. Magdon-Ismail, Malik Lin, Hsuan-Tien, 2012.
- [46] O. Voznyy *et al.*, “Machine Learning Accelerates Discovery of Optimal Colloidal Quantum Dot Synthesis,” *ACS Nano*, vol. 13, pp. 11122–11128, 2019, doi: 10.1021/acsnano.9b03864.
- [47] K. Watanabe *et al.*, “Microreactor combinatorial system for nanoparticle synthesis with multiple parameters,” *Chem. Eng. Sci.*, vol. 75, pp. 292–297, 2012, doi: 10.1016/j.ces.2012.03.006.
- [48] A. Shafaei and G. Reza Khayati, “A predictive model on size of silver nanoparticles prepared by green synthesis method using hybrid artificial neural network-particle swarm optimization algorithm,” *Measurement*, vol. 151, p. 107199, 2020, doi: 10.1016/j.measurement.2019.107199.
- [49] J. Siddiqui, M. Taheri, A. U. Alam, and M. J. Deen, “Nanomaterials in Smart Packaging Applications: A Review,” *Small*, vol. 18, no. 1, p. 2101171, 2022, doi: 10.1002/sml.202101171.
- [50] D. Chen, L. Tang, and J. Li, “Graphene-based materials in electrochemistry,” *Chem. Soc. Rev.*, vol. 39, no. 8, pp. 3157–3180, 2010, doi: 10.1039/b923596e.
- [51] R. E. P. Meyler, M. A. Edwards, and J. V. Macpherson, “Exploring the suitability of different electrode materials for hypochlorite quantification at high concentration in alkaline solutions,” *Electrochem. commun.*, vol. 86, pp. 21–25, 2018, doi: 10.1016/j.elecom.2017.11.004.
- [52] H. Cheng *et al.*, “Recent advances in intelligent food packaging materials: Principles, preparation and applications,” *Food Chem.*, vol. 375, p. 131738, 2022, doi: 10.1016/j.foodchem.2021.131738.
- [53] L. Manjakkal, D. Szwagierczak, and R. Dahiya, “Metal oxides based electrochemical pH sensors: Current progress and future perspectives,” *Prog. Mater. Sci.*, vol. 109, no. February 2019, p. 100635, 2020, doi: 10.1016/j.pmatsci.2019.100635.
- [54] A. Nasture, E. I. Ionete, F. A. Lungu, S. I. Spiridon, and L. G. Patularu, “Water Quality

- Carbon Nanotube-Based Sensors Technological Barriers and Late Research Trends: A Bibliometric Analysis,” *Chemosensors*, vol. 10, no. 5, p. 161, 2022, doi: doi.org/10.3390/chemosensors10050161.
- [55] A. J. Bard and L. R. Faulkner, *Electrochemical Methods: Fundamentals and Applications*, 2nd ed. John Wiley and Sons, 2001.
- [56] I. Seymour, B. O’Sullivan, P. Lovera, J. F. Rohan, and A. O’Riordan, “Electrochemical detection of free-chlorine in Water samples facilitated by in-situ pH control using interdigitated microelectrodes,” *Sensors Actuators, B Chem.*, vol. 325, no. May, p. 128774, 2020, doi: 10.1016/j.snb.2020.128774.
- [57] K. A. S. Pathiratne, S. S. Skandaraja, and E. M. C. M. Jayasena, “Linear sweep voltammetric determination of free chlorine in waters using graphite working electrodes,” *J. Natl. Sci. Found. Sri Lanka*, vol. 36, no. 1, pp. 25–31, 2008, doi: 10.4038/jnsfsr.v36i1.130.
- [58] J. F. Júnior *et al.*, “Driver behavior profiling: An investigation with different smartphone sensors and machine learning,” *PLoS One*, vol. 12, no. 4, pp. 1–16, 2017, doi: 10.1371/journal.pone.0174959.
- [59] V. Selamneni, K. Gohel, N. Bokka, S. Sharma, and P. Sahatiya, “MoS₂-Based Multifunctional Sensor for Both Chemical and Physical Stimuli and Their Classification Using Machine Learning Algorithms,” *IEEE Sens. J.*, vol. 21, no. 3, pp. 3694–3701, 2021, doi: 10.1109/JSEN.2020.3023309.
- [60] V. V. Kornienko *et al.*, “Machine Learning for Optical Gas Sensing: A Leaky-Mode Humidity Sensor as Example,” *IEEE Sens. J.*, vol. 20, no. 13, pp. 6954–6963, 2020, doi: 10.1109/JSEN.2020.2978931.
- [61] P. Khatri, K. K. Gupta, and R. K. Gupta, “Drift compensation of commercial water quality sensors using machine learning to extend the calibration lifetime,” *J. Ambient Intell. Humaniz. Comput.*, vol. 12, pp. 3091–3099, 2021, doi: 10.1007/s12652-020-02469-y.
- [62] M. Yan, J. Tylczak, Y. Yu, G. Panagakos, and P. Ohodnicki, “Multi-component optical sensing of high temperature gas streams using functional oxide integrated silica based optical fiber sensors,” *Sensors Actuators B. Chem.*, vol. 255, no. 1, pp. 357–365, 2017, doi: 10.1016/j.snb.2017.08.026.
- [63] S. Feng *et al.*, “Review on Smart Gas Sensing Technology,” *Sensors*, vol. 19, no. 17, p.

- 3760, 2019, doi: 10.3390/s19173760.
- [64] M. A. Rahman, P. Kumar, D. S. Park, and Y. B. Shim, “Electrochemical sensors based on organic conjugated polymers,” *Sensors*, vol. 8, no. 1, pp. 118–141, 2008, doi: 10.3390/s8010118.
- [65] P. T. Kissinger and W. R. Heineman, “Cyclic voltammetry,” *J. Chem. Educ.*, vol. 60, no. 9, pp. 702–706, 1983, doi: 10.1021/ed060p702.
- [66] G. Bontempelli, N. Dossi, and R. Toniolo, “Linear Sweep and Cyclic,” *Encyclopedia of Analytical Science*, no. 2005. Elsevier Inc., pp. 188–197, 2016, doi: 10.1016/b978-0-12-409547-2.12200-0.
- [67] A. J. Lucio and J. V. Macpherson, “Combined Voltammetric Measurement of pH and Free Chlorine Speciation Using a Micro-Spot sp² Bonded Carbon-Boron Doped Diamond Electrode,” *Anal. Chem.*, vol. 92, no. 24, pp. 16072–16078, 2020, doi: 10.1021/acs.analchem.0c03692.
- [68] S. C. Silva, R. M. Cardoso, E. M. Richter, R. A. A. Munoz, and E. Nossol, “Reduced graphene oxide/multi-walled carbon nanotubes/prussian blue nanocomposites for amperometric detection of strong oxidants,” *Mater. Chem. Phys.*, vol. 250, p. 123011, 2020, doi: 10.1016/j.matchemphys.2020.123011.
- [69] F. Abd-wahab, H. Farhana, A. Guthoos, W. Wardatul, and A. Wan, “Solid-State rGO-PEDOT: PSS Transducing Material for Cost-Effective Enzymatic Sensing,” *Biosensors*, vol. 9, no. 1, p. 36, 2019, doi: 10.3390/bios9010036.
- [70] R. G. Compton and C. E. Banks, *Understanding Voltammetry*. Hackensack: World Scientific Publishing Europe Ltd, 2007.
- [71] N. Elgrishi, K. J. Rountree, B. D. McCarthy, E. S. Rountree, T. T. Eisenhart, and J. L. Dempsey, “A Practical Beginner’s Guide to Cyclic Voltammetry,” *J. Chem. Educ.*, vol. 95, no. 2, pp. 197–206, 2018, doi: 10.1021/acs.jchemed.7b00361.
- [72] S. G. Bratsch, “Standard Electrode Potentials and Temperature Coefficients in Water at 298.15 K,” *J. Phys. Chem. Ref. Data*, vol. 18, no. 1, pp. 1–21, 1989, doi: 10.1063/1.555839.
- [73] T. Soundappan, K. Haddad, and S. Kavadiya, “Crumpled graphene oxide decorated SnO₂ nanocolumns for the electrochemical detection of free chlorine,” *Appl. Nanosci.*, vol. 7, no. 8, pp. 645–653, 2017, doi: 10.1007/s13204-017-0603-x.

- [74] J. Islam, H. Shao, M. M. R. Badal, K. M. Razeeb, and M. Jamal, “Pencil graphite as electrode platform for free chlorine sensors and energy storage devices,” *PLoS One*, vol. 16, no. 3, p. e0248142, Mar. 2021, doi: 10.1371/journal.pone.0248142.
- [75] D. Guo *et al.*, “A novel label-free hypochlorite amperometric sensor based on target-induced oxidation of benzenboronic acid pinacol ester,” *Chem. Eng. J.*, vol. 373, no. May, pp. 1–7, 2019, doi: 10.1016/j.cej.2019.05.027.
- [76] D. R. Kumar, S. Kesavan, T. T. Nguyen, J. Hwang, C. Lamiel, and J. Shim, “Polydopamine@electrochemically reduced graphene oxide-modified electrode for electrochemical detection of free-chlorine,” *Sensors Actuators B. Chem.*, vol. 240, pp. 818–828, 2017, doi: 10.1016/j.snb.2016.09.025.
- [77] A. Amine and H. Mohammadi, “Amperometry,” *Encyclopedia of Analytical Science*. Elsevier Inc., pp. 85–98, 2018, doi: 10.1016/B978-0-12-409547-2.14204-0.
- [78] J. Wang and Z. Taha, “Batch Injection Analysis,” *Anal. Chem.*, vol. 63, no. 10, pp. 1053–1056, 1991.
- [79] E. Barbolani, G. Piccardi, and F. Pantani, “Use of potentiometry with imposed current for the determination of chlorine in breakpoint chlorination,” *Anal. Lett.*, vol. 16, no. 13, pp. 987–998, 1983, doi: 10.1080/00032718308067956.
- [80] D. Midgley, “A bromide-selective electrode-redox electrode cell for the potentiometric determination of bromine and free residual chlorine,” *Talanta*, vol. 30, no. 8, pp. 547–554, 1983, doi: 10.1016/0039-9140(83)80132-5.
- [81] S. Lal and G. D. Christian, “Potentiometric Studies with an Ion Permselective Membrane,” *Anal. Chem.*, vol. 43, no. 3, pp. 410–421, 1971, doi: 10.1021/ac60298a014.
- [82] B. J. Hernlem and L. S. Tsai, “Titration of chlorine: Amperometric versus potentiometric,” *Am. Water Work. Assoc.*, vol. 92, no. 12, pp. 101–107, 2000, doi: 10.1002/j.1551-8833.2000.tb09075.x.
- [83] L. C. Adam and G. Gordon, “Direct and Sequential Potentiometric Determination of Hypochlorite, Chlorite, and Chlorate Ions When Hypochlorite Ion Is Present in Large Excess,” *Anal. Chem.*, vol. 67, no. 3, pp. 535–540, 1995.
- [84] Y. Zhang, Z. Li, X. Guo, G. Liu, and S. Zhang, “Potentiometric Sensor Based on Carbon Paste Electrode for Monitoring Total Residual Chlorine in Electrolytically-Treated Ballast Water,” *Sensors*, vol. 21, no. 2, p. 350, 2021, doi: <https://doi.org/10.3390/s21020350>.

- [85] E. Grygołowicz-Pawlak, K. Wyglądacz, S. Sęk, R. Bilewicz, Z. Brzózka, and E. Malinowska, “Studies on ferrocene organothiol monolayer as an intermediate phase of potentiometric sensors with gold inner contact,” *Sensors Actuators, B Chem.*, vol. 111–112, pp. 310–316, 2005, doi: 10.1016/j.snb.2004.12.038.
- [86] X. H. Dai, J. Zhang, X. J. Pang, J. P. Zhou, G. Z. Liu, and S. Y. Zhang, “Ferrocene-enhanced polyvinyl chloride-coated electrode for the potentiometric detection of total residual chlorine in simulated ballast water,” *J. Electroanal. Chem.*, vol. 760, pp. 158–164, 2016, doi: 10.1016/j.jelechem.2015.11.036.
- [87] A. Määttänen *et al.*, “A low-cost paper-based inkjet-printed platform for electrochemical analyses,” *Sensors Actuators, B Chem.*, vol. 177, pp. 153–162, 2013, doi: 10.1016/j.snb.2012.10.113.
- [88] C. A. Li, K. N. Han, X. H. Pham, and G. H. Seong, “A single-walled carbon nanotube thin film-based pH-sensing microfluidic chip,” *Analyst*, vol. 139, no. 8, pp. 2011–2015, 2014, doi: 10.1039/c3an02195e.
- [89] M. Taheri and J. Deen, “Green Approach Using RuO₂/GO Nanocomposite for Low Cost and Highly Sensitive pH Sensing,” *J. Electrochem. Soc.*, vol. 169, p. 047501, 2022, doi: 10.1149/1945-7111/ac5f1f.
- [90] E. Hoque, L. H. H. Hsu, A. Aryasomayajula, P. R. Selvaganapathy, and P. Kruse, “Pencil-Drawn Chemiresistive Sensor for Free Chlorine in Water,” *IEEE Sensors Lett.*, vol. 1, no. 4, pp. 1–4, 2017, doi: 10.1109/lsens.2017.2722958.
- [91] L. H. H. Hsu, E. Hoque, P. Kruse, and P. Ravi Selvaganapathy, “A carbon nanotube based resettable sensor for measuring free chlorine in drinking water,” *Appl. Phys. Lett.*, vol. 106, no. 6, p. 063102, 2015, doi: 10.1063/1.4907631.
- [92] V. Patel, P. Kruse, and P. R. Selvaganapathy, “Flexible chemiresistive sensor with xurographically patterned gold leaf as contact electrodes for measuring free chlorine,” *FLEPS 2021 - IEEE Int. Conf. Flex. Printable Sensors Syst.*, no. Step d, pp. 14–17, 2021, doi: 10.1109/FLEPS51544.2021.9469787.
- [93] Y. K. Yen, K. Y. Lee, C. Y. Lin, S. T. Zhang, C. W. Wang, and T. Y. Liu, “Portable Nanohybrid Paper-Based Chemiresistive Sensor for Free Chlorine Detection,” *ACS Omega*, vol. 5, no. 39, pp. 25209–25215, 2020, doi: 10.1021/acsomega.0c03366.
- [94] A. Zubiarraín-Laserna, S. Angizi, M. A. Akbar, R. Divigalpitiya, P. R. Selvaganapathy,

- and P. Kruse, “Detection of free chlorine in water using graphene-like carbon based chemiresistive sensors,” *RSC Adv.*, vol. 12, no. 4, pp. 2485–2496, 2022, doi: 10.1039/d1ra08264g.
- [95] W. Göpel and K. D. Schierbaum, “SnO₂ sensors: current status and future prospects,” *Sensors Actuators B*, vol. 26, no. 1–3, pp. 1–12, 1995, doi: doi.org/10.1016/0925-4005(94)01546-T.
- [96] A. J. Oostra, K. H. W. Van Den Bos, P. W. M. Blom, and J. J. Michels, “Disruption of the electrical conductivity of highly conductive poly(3,4-ethylenedioxythiophene):poly(styrene sulfonate) by hypochlorite,” *J. Phys. Chem. B*, vol. 117, no. 37, pp. 10929–10935, 2013, doi: 10.1021/jp4050836.
- [97] N. Lei, P. Li, W. Xue, and J. Xu, “Simple graphene chemiresistors as pH sensors: fabrication and characterization,” *Meas. Sci. Technol.*, vol. 22, p. 107002, 2011, doi: 10.1088/0957-0233/22/10/107002.
- [98] A. Mohtasebi and P. Kruse, “Chemical sensors based on surface charge transfer,” in *Physical Sciences Reviews*, 2018, vol. 3, no. 2, pp. 1–13, doi: 10.1515/psr-2017-0133.
- [99] K. Mopoung *et al.*, “A Real-Time Free Chlorine Monitoring by Graphene Field-Effect Transistor,” *Proc. 14th Annu. IEEE Int. Conf. Nano/Micro Eng. Mol. Syst. NEMS 2019*, pp. 64–67, 2019, doi: 10.1109/NEMS.2019.8915664.
- [100] H. Kabir, P. Y. Ma, N. Renn, N. W. Nicholas, and I. F. Cheng, “Electrochemical determination of free chlorine on pseudo-graphite electrode,” *Talanta*, vol. 205, p. 120101, 2019, [Online]. Available: <https://doi.org/10.1016/j.talanta.2019.06.101>.
- [101] C. Xiong *et al.*, “Highly sensitive solution-gated graphene transistor based sensor for continuous and real-time detection of free chlorine,” *Anal. Chim. Acta*, vol. 1033, pp. 65–72, 2018, doi: 10.1016/j.aca.2018.06.041.
- [102] R. Olivé-Monllau, C. S. Martínez-Cisneros, J. Bartrolí, M. Baeza, and F. Céspedes, “Integration of a sensitive carbon nanotube composite electrode in a ceramic microanalyzer for the amperometric determination of free chlorine,” *Sensors Actuators, B Chem.*, vol. 151, no. 2, pp. 416–422, 2011, doi: 10.1016/j.snb.2010.10.017.
- [103] K. Senthilkumar and J. M. Zen, “Free chlorine detection based on EC’ mechanism at an electroactive polymelamine-modified electrode,” *Electrochem. commun.*, vol. 46, pp. 87–90, 2014, doi: 10.1016/j.elecom.2014.06.018.

- [104] S. Pan, M. J. Deen, and R. Ghosh, “Low-Cost Graphite-Based Free Chlorine Sensor,” *Anal. Chem.*, vol. 87, no. 21, pp. 10734–10737, 2015, doi: 10.1021/acs.analchem.5b03164.
- [105] J. Muñoz, F. Céspedes, and M. Baeza, “Modified multiwalled carbon nanotubes/epoxy amperometric nanocomposite sensors with CuO nanoparticles for electrocatalytic detection of free chlorine,” *Microchem. J.*, vol. 122, pp. 189–196, 2015, doi: 10.1016/j.microc.2015.05.001.
- [106] K. S. Novoselov *et al.*, “Two-dimensional atomic crystals,” vol. 102, no. 30, pp. 10451–10453, 2005.
- [107] J. C. Meyer, A. K. Geim, M. I. Katsnelson, K. S. Novoselov, T. J. Booth, and S. Roth, “The structure of suspended graphene sheets,” *Nature*, vol. 446, pp. 60–63, 2007, doi: 10.1038/nature05545.
- [108] E. Stolyarova *et al.*, “High-resolution scanning tunneling microscopy imaging of mesoscopic graphene sheets on an insulating surface,” *PNAS*, vol. 104, no. 22, pp. 9209–9212, 2007, doi: 10.1073/pnas.0703337104.
- [109] D. Wei *et al.*, “Scalable Synthesis of Few-Layer Graphene Ribbons with Controlled Morphologies by a Template Method and Their Applications in Nanoelectromechanical Switches,” *J. Am. Chem. Soc.*, vol. 131, no. 31, pp. 11147–11154, 2009, doi: doi.org/10.1021/ja903092k.
- [110] Z. Jin, J. R. Lomeda, B. K. Price, W. Lu, Y. Zhu, and J. M. Tour, “Mechanically Assisted Exfoliation and Functionalization of Thermally Converted Graphene Sheets,” *Chem. Mater.*, vol. 21, no. 14, pp. 3045–3047, 2009, doi: 10.1021/cm901601g.
- [111] D. Saini, “Synthesis and functionalization of graphene and application in electrochemical biosensing,” *Nanotechnol. Rev.*, vol. 5, no. 4, pp. 393–416, 2016, doi: 10.1515/ntrev-2015-0059.
- [112] H. Touhara and F. Okino, “Property Control of Carbon Materials by Fluorination,” *Carbon Alloy. Nov. Concepts to Dev. Carbon Sci. Technol.*, vol. 38, pp. 485–498, 2003, doi: 10.1016/B978-008044163-4/50030-9.
- [113] T. Fujimori and M. Takaoka, “Direct chlorination of carbon by copper chloride in a thermal process,” *Environ. Sci. Technol.*, vol. 43, no. 7, pp. 2241–2246, 2009, doi: 10.1021/es802996a.

- [114] L. G. Bulusheva *et al.*, “Bromination of double-walled carbon nanotubes,” *Chem. Mater.*, vol. 24, no. 14, pp. 2708–2715, 2012, doi: 10.1021/cm3006309.
- [115] H. L. Poh, F. Šaněk, Z. Sofer, and M. Pumera, “High-pressure hydrogenation of graphene: Towards graphane,” *Nanoscale*, vol. 4, no. 22, pp. 7006–7011, 2012, doi: 10.1039/c2nr31962d.
- [116] A. Vijaya Bhaskar Reddy, M. Moniruzzaman, Y. Veera Manohara Reddy, and G. Madhavi, “Graphene-based nanomaterials for the removal of pharmaceuticals in drinking water sources,” in *Graphene-Based Nanotechnologies for Energy and Environmental Applications*, Elsevier Inc., 2019, pp. 329–358.
- [117] H. W. Wanzlick, “Aspects of Nucleophilic Carbene Chemistry,” *Angew. Chemie Int. Ed.*, vol. 1, no. 2, pp. 75–80, 1962, doi: 10.1002/anie.196200751.
- [118] J. Mu, J. Bastos-arrieta, M. Mu, D. Muraviev, and C. Francisco, “Simple green routes for the customized preparation of sensitive carbon nanotubes / epoxy nanocomposite electrodes with functional metal nanoparticles,” *RSC Adv.*, vol. 4, pp. 44517–44524, 2014, doi: 10.1039/C4RA07294D.
- [119] J. Siddiqui and M. J. Deen, “Biodegradable asparagine-graphene oxide free chlorine sensors fabricated using solution-based processing,” *Analyst*, 2022, doi: 10.1039/D2AN00533F.
- [120] A. Olean-Oliveira, J. C. Pacheco, P. M. Seraphim, and M. F. S. Teixeira, “Synergistic effect of reduced graphene oxide/azo-polymer layers on electrochemical performance and application as nonenzymatic chemiresistor sensors for detecting superoxide anion radicals,” *J. Electroanal. Chem.*, vol. 852, p. 113520, 2019, doi: 10.1016/j.jelechem.2019.113520.
- [121] Y. Shao, J. Wang, H. Wu, J. Liu, I. A. Aksay, and Y. Lin, “Graphene Based Electrochemical Sensors and Biosensors: A Review,” *Electroanalysis*, vol. 22, no. 10, pp. 1027–1036, 2010, doi: 10.1002/elan.200900571.
- [122] D. N. H. Tran, S. Kabiri, and D. Losic, “A green approach for the reduction of graphene oxide nanosheets using non-aromatic amino acids,” *Carbon N. Y.*, vol. 76, pp. 193–202, 2014, doi: 10.1016/j.carbon.2014.04.067.
- [123] A. J. Downard, “Electrochemically assisted covalent modification of carbon electrodes,” *Electroanalysis*, vol. 12, no. 14, pp. 1085–1096, 2000, doi: 10.1002/1521-

- 4109(200010)12:14<1085::AID-ELAN1085>3.0.CO;2-A.
- [124] H. Maeda *et al.*, “Direct Covalent Modification of Glassy Carbon Surfaces with 1-Alkanols by Electrochemical Oxidation,” *Chem. Pharm. Bull.*, vol. 42, no. 9, pp. 1870–1873, 1994, doi: <https://doi.org/10.1248/cpb.42.1870>.
- [125] S. Uchiyama, H. Watanabe, H. Yamazaki, A. Kanazawa, H. Hamana, and Y. Okabe, “Electrochemical Introduction of Amino Group to a Glassy Carbon Surface by the Electrolysis of Carbamic Acid,” *J. Electrochem. Soc.*, vol. 154, no. 2, pp. F31–F35, 2007, doi: [10.1149/1.2402127](https://doi.org/10.1149/1.2402127).
- [126] R. S. Deinhammer, M. Ho, J. W. Anderegg, and M. D. Porter, “Electrochemical Oxidation of Amine-Containing Compounds: A Route to the Surface Modification of Glassy Carbon Electrodes,” *Langmuir*, vol. 10, no. 4, pp. 1306–1313, 1994, doi: [10.1021/la00016a054](https://doi.org/10.1021/la00016a054).
- [127] C. Berger *et al.*, “Electronic Confinement and Coherence in Patterened Epitaxial Graphene,” *Science (80-.)*, vol. 312, no. 5777, pp. 1191–1197, 2006, doi: [10.1126/science.1125925](https://doi.org/10.1126/science.1125925).
- [128] B. H. Duan, E. Xie, L. Han, and Z. Xu, “Turning PMMA Nanofibers into Graphene Nanoribbons by In Situ Electron Beam Irradiation,” *Adv. Mater.*, vol. 20, no. 17, pp. 3284–3288, 2008, doi: [10.1002/adma.200702149](https://doi.org/10.1002/adma.200702149).
- [129] J. Wu, W. Pisula, and K. Mullen, “Graphenes as Potential Material for Electronics,” vol. 107, no. 3, pp. 718–747, 2007, doi: [10.1021/cr068010r](https://doi.org/10.1021/cr068010r).
- [130] G. Eda, G. Fanchini, and M. Chhowalla, “Large-area ultrathin films of reduced graphene oxide as a transparent and flexible electronic material,” vol. 3, no. May, pp. 1–5, 2008, doi: [10.1038/nnano.2008.83](https://doi.org/10.1038/nnano.2008.83).
- [131] C. Xie *et al.*, “Monolayer graphene film/silicon nanowire array Schottky junction solar cells,” *Appl. Phys. Lett.*, vol. 99, no. 13, pp. 2011–2014, 2011, doi: [10.1063/1.3643473](https://doi.org/10.1063/1.3643473).
- [132] M. Ahmad and S. R. P. Silva, “Low temperature growth of carbon nanotubes – A review,” *Carbon N. Y.*, vol. 158, pp. 24–44, 2020, doi: [10.1016/j.carbon.2019.11.061](https://doi.org/10.1016/j.carbon.2019.11.061).
- [133] M. R. Tomei, F. Arduini, D. Neagu, and D. Moscone, “Carbon black-based disposable sensor for an on-site detection of free chlorine in swimming pool water,” *Talanta*, vol. 189, pp. 262–267, Nov. 2018, doi: [10.1016/j.talanta.2018.07.005](https://doi.org/10.1016/j.talanta.2018.07.005).
- [134] M. R. Tomei, E. Marcoccio, D. Neagu, D. Moscone, and F. Arduini, “A Miniaturized Carbon Black-based Electrochemical Sensor for Chlorine Dioxide Detection in Swimming

- Pool Water,” *Electroanalysis*, vol. 32, no. 5, pp. 986–991, 2019, doi: 10.1002/elan.201900667.
- [135] S. Chatterjee, J. Byun, K. Dutta, R. U. Pedersen, A. Pottathil, and H. (Qi) Xie, “Designing an Internet-of-Things (IoT) and sensor-based in-home monitoring system for assisting diabetes patients: iterative learning from two case studies,” *Eur. J. Inf. Syst.*, vol. 27, no. 6, pp. 670–685, 2018, doi: 10.1080/0960085X.2018.1485619.
- [136] K. Janeczek, “Composite materials for printed electronics in Internet of Things applications,” *Bull. Mater. Sci.*, vol. 43, no. 1, pp. 1–10, 2020, doi: 10.1007/s12034-020-02101-x.
- [137] M. Maksimović and Vladimir Vujović, “Application of internet of things in food packaging and transportation,” vol. 1, no. 4, pp. 333–350, 2015.
- [138] M. Mäntysalo, L. Xie, F. Jonsson, Y. Feng, A. L. Cabezas, and L. R. Zheng, “System integration of smart packages using printed electronics,” in *Proceedings - Electronic Components and Technology Conference*, 2012, pp. 997–1002, doi: 10.1109/ECTC.2012.6248957.
- [139] H. Yang, X. Huo, T. A. Yekeen, Q. Zheng, M. Zheng, and X. Xu, “Effects of lead and cadmium exposure from electronic waste on child physical growth,” *Environ. Sci. Pollut. Res.*, vol. 20, pp. 4441–4447, 2013, doi: 10.1007/s11356-012-1366-2.
- [140] O. A. Alabi, Y. M. Adeoluwa, X. Huo, X. Xu, and A. A. Bakare, “Environmental contamination and public health effects of electronic waste: an overview,” *J. Environ. Heal. Sci. Eng.*, vol. 19, no. 1, pp. 1209–1227, 2021, doi: 10.1007/s40201-021-00654-5.
- [141] W. Wu *et al.*, “Ecological effects of soil properties and metal concentrations on the composition and diversity of microbial communities associated with land use patterns in an electronic waste recycling region,” *Sci. Total Environ.*, vol. 601–602, pp. 57–65, 2017, doi: 10.1016/j.scitotenv.2017.05.165.
- [142] J. O. Okeme and V. H. Arrandale, “Electronic Waste Recycling: Occupational Exposures and Work-Related Health Effects,” *Curr. Environ. Heal. reports*, vol. 6, no. 4, pp. 256–268, 2019, doi: 10.1007/s40572-019-00255-3.
- [143] R. Chandra and R. Rustgi, “Biodegradable Polymers,” *Prog. Polym. Sci.*, vol. 23, pp. 1273–1335, 1998.
- [144] I. Vroman and L. Tighzert, “Biodegradable Polymers,” *Materials (Basel)*, vol. 2, no. 2,

- pp. 307–344, 2009, doi: 10.3390/ma2020307.
- [145] J. Hyun, H. Seok, S. Rim, K. Park, and J. Kim, “Biodegradable poly(asparagine) grafted with poly(caprolactone) and the effect of substitution on self-aggregation,” *Colloids Surfaces A Physicochem. Eng. Asp.*, vol. 264, no. 1–3, pp. 187–194, 2005, doi: 10.1016/j.colsurfa.2005.05.019.
- [146] J. Hyun, H. Seok, S. Rim, and J. Kim, “Polymer micelle-like aggregates of novel amphiphilic biodegradable poly (asparagine) grafted with poly (caprolactone),” *Polymer (Guildf.)*, vol. 44, no. 3, pp. 583–591, 2003.
- [147] C. Martín *et al.*, “A Biodegradable Multifunctional Graphene Oxide Platform for Targeted Cancer Therapy,” *Adv. Funct. Mater.*, vol. 29, no. 39, p. 1901761, 2019, doi: 10.1002/adfm.201901761.
- [148] E. Watanabe, N. Tomoshige, and H. Uyama, “New Biodegradable and Thermoresponsive Polymers Based on Amphiphilic Poly(asparagine) Derivatives,” *Macromol. Symp.*, vol. 249–250, no. 1, pp. 509–514, 2007, doi: 10.1002/masy.200750428.
- [149] T. Kuila, S. Bose, A. Kumar, and P. Khanra, “Chemical functionalization of graphene and its applications,” *Prog. Mater. Sci.*, vol. 57, no. 7, pp. 1061–1105, 2012, doi: 10.1016/j.pmatsci.2012.03.002.
- [150] Q. Tang, Z. Zhou, and Z. Chen, “Graphene-related nanomaterials: Tuning properties by functionalization,” *Nanoscale*, vol. 5, no. 11, pp. 4541–4583, 2013, doi: 10.1039/c3nr33218g.
- [151] E. Llobet, “Gas sensors using carbon nanomaterials: A review,” *Sensors Actuators B. Chem.*, vol. 179, pp. 32–45, 2012, doi: doi.org/10.1016/j.snb.2012.11.014.
- [152] D. Voet and J. G. Voet, *Biochemistry*. Danvers: John Wiley & Sons Inc., 1990.
- [153] A. Piñeiro-García, F. Tristan, D. Meneses-Rodríguez, V. Semetey, and S. M. Vega-Díaz, “Tuning the nucleophilic attack and the reductive action of glycine on graphene oxide under basic medium,” *Mater. Today Chem.*, vol. 19, 2021, doi: 10.1016/j.mtchem.2020.100386.
- [154] S. Mallakpour, A. Abdolmaleki, and S. Borandeh, “Covalently functionalized graphene sheets with biocompatible natural amino acids,” *Appl. Surf. Sci.*, vol. 307, pp. 533–542, 2014, doi: 10.1016/j.apsusc.2014.04.070.
- [155] L. Ma, G. Wang, and J. Dai, “Influence of structure of amines on the properties of amines-

- modified reduced graphene oxide/polyimide composites,” *J. Appl. Polym. Sci.*, vol. 133, no. 34, pp. 1–9, 2016, doi: 10.1002/app.43820.
- [156] M. M. Gudarzi and F. Sharif, “Enhancement of dispersion and bonding of graphene-polymer through wet transfer of functionalized graphene oxide,” *Express Polym. Lett.*, vol. 6, no. 12, pp. 1017–1031, 2012, doi: 10.3144/expresspolymlett.2012.107.
- [157] B. Dehghanzad, M. K. Razavi Aghjeh, O. Rafeie, A. Tavakoli, and A. Jameie Oskooie, “Synthesis and characterization of graphene and functionalized graphene via chemical and thermal treatment methods,” *RSC Adv.*, vol. 6, no. 5, pp. 3578–3585, 2016, doi: 10.1039/c5ra19954a.
- [158] F. Z. Dörwald, *Side Reactions in Organic Synthesis: A Guide to Successful Synthesis Design*. Weinheim: 2005 WILEY-VCH Verlag GmbH & Co. KGaA, 2006.
- [159] H. Jungbluth, M. Marending, G. De-Deus, B. Sener, and M. Zehnder, “Stabilizing sodium hypochlorite at high pH: Effects on soft tissue and dentin,” *J. Endod.*, vol. 37, no. 5, pp. 693–696, 2011, doi: 10.1016/j.joen.2011.02.019.
- [160] K. Huang, K. P. Reber, M. D. Toomey, H. Haflich, J. A. Howarter, and A. D. Shah, “Reactivity of the polyamide membrane monomer with free chlorine: Reaction kinetics, mechanisms, and the role of chloride,” *Environ. Sci. Technol.*, vol. 53, no. 14, pp. 8167–8176, 2019, doi: 10.1021/acs.est.9b01446.
- [161] S. Mallakpour, A. Abdolmaleki, and S. Borandeh, “Fabrication of amino acid-based graphene-zinc oxide (ZnO) hybrid and its application for poly(ester-amide)/graphene-ZnO nanocomposite synthesis,” *J. Thermoplast. Compos. Mater.*, vol. 30, no. 3, pp. 358–380, 2017, doi: 10.1177/0892705715598365.
- [162] H. Tao, T. Wu, M. Aldeghi, T. C. Wu, A. Aspuru-Guzik, and E. Kumacheva, “Nanoparticle synthesis assisted by machine learning,” *Nat. Rev. Mater.*, vol. 6, pp. 701–716, 2021, doi: 10.1038/s41578-021-00337-5.
- [163] Y. Orimoto *et al.*, “Application of Artificial Neural Networks to Rapid Data Analysis in Combinatorial Nanoparticle Syntheses,” *J. Phys. Chem.*, vol. 116, no. 33, pp. 17885–17896, 2012, doi: <https://doi.org/10.1021/jp3031122>.
- [164] Q. Liu, X. Li, M. Ye, S. S. Ge, and X. Du, “Drift Compensation for Electronic Nose by Semi-Supervised Domain Adaption,” *IEEE Sens. J.*, vol. 14, no. 3, pp. 657–665, 2014, doi: 10.1109/JSEN.2013.2285919.

- [165] U. Yaqoob and Mohammad I. Younis, “Chemical Gas Sensors: Recent Developments, Challenges, and the Potential of Machine Learning—A Review,” *Sensors*, vol. 21, no. 8, p. 2877, 2021, doi: <https://doi.org/10.3390/s21082877>.
- [166] A. M. M. Gherman, N. Tosa, M. V. Cristea, V. Tosa, S. Porav, and P. S. Agachi, “Artificial neural networks modeling of the parameterized gold nanoparticles generation through photo-induced process,” *Mater. Res. Express*, vol. 5, no. 8, p. 085011, 2018.

Appendix A Copyright Permissions

Biodegradable asparagine–graphene oxide free chlorine sensors fabricated using solution-based processing

J. Siddiqui and M. Jamal Deen, *Analyst*, 2022, **147**, 3643 DOI:
10.1039/D2AN00533F

To request permission to reproduce material from this article, please go to the [Copyright Clearance Center request page](#).

If you are **an author contributing to an RSC publication, you do not need to request permission** provided correct acknowledgement is given.

If you are **the author of this article, you do not need to request permission to reproduce figures and diagrams** provided correct acknowledgement is given. If you want to reproduce the whole article in a third-party publication (excluding your thesis/dissertation for which permission is not required) please go to the [Copyright Clearance Center request page](#).

Read more about [how to correctly acknowledge RSC content](#).

Combined Voltammetric Measurement of pH and Free Chlorine Speciation Using a Micro-Spot sp² Bonded Carbon–Boron Doped Diamond Electrode

Author: Anthony J. Lucio, Julie V. Macpherson



Publication: Analytical Chemistry

Publisher: American Chemical Society

Date: Dec 1, 2020

Copyright © 2020, American Chemical Society

PERMISSION/LICENSE IS GRANTED FOR YOUR ORDER AT NO CHARGE

This type of permission/license, instead of the standard Terms and Conditions, is sent to you because no fee is being charged for your order. Please note the following:

- Permission is granted for your request in both print and electronic formats, and translations.
- If figures and/or tables were requested, they may be adapted or used in part.
- Please print this page for your records and send a copy of it to your publisher/graduate school.
- Appropriate credit for the requested material should be given as follows: "Reprinted (adapted) with permission from {COMPLETE REFERENCE CITATION}. Copyright {YEAR} American Chemical Society." Insert appropriate information in place of the capitalized words.
- One-time permission is granted only for the use specified in your RightsLink request. No additional uses are granted (such as derivative works or other editions). For any uses, please submit a new request.

If credit is given to another source for the material you requested from RightsLink, permission must be obtained from that source.

BACK

CLOSE WINDOW

Rights and permissions

Open Access This article is distributed under the terms of the Creative Commons Attribution 4.0 International License (<http://creativecommons.org/licenses/by/4.0/>), which permits unrestricted use, distribution, and reproduction in any medium, provided you give appropriate credit to the original author(s) and the source, provide a link to the Creative Commons license, and indicate if changes were made.

[Reprints and Permissions](#)

About this article



Check for updates

Cite this article

Soundappan, T., Haddad, K., Kavadiya, S. *et al.* Crumpled graphene oxide decorated SnO₂ nanocolumns for the electrochemical detection of free chlorine. *Appl Nanosci* **7**, 645–653 (2017). <https://doi.org/10.1007/s13204-017-0603-x>

[Download citation](#) ↓

Fully Integrated, Simple, and Low-Cost Electrochemical Sensor Array for in Situ Water Quality Monitoring

Author: Arif U. Alam, Dennis Clyne, Hao Jin, et al

Publication: ACS Sensors

Publisher: American Chemical Society

Date: Feb 1, 2020



Copyright © 2020, American Chemical Society

PERMISSION/LICENSE IS GRANTED FOR YOUR ORDER AT NO CHARGE

This type of permission/license, instead of the standard Terms and Conditions, is sent to you because no fee is being charged for your order. Please note the following:

- Permission is granted for your request in both print and electronic formats, and translations.
- If figures and/or tables were requested, they may be adapted or used in part.
- Please print this page for your records and send a copy of it to your publisher/graduate school.
- Appropriate credit for the requested material should be given as follows: "Reprinted (adapted) with permission from (COMPLETE REFERENCE CITATION). Copyright (YEAR) American Chemical Society." Insert appropriate information in place of the capitalized words.
- One-time permission is granted only for the use specified in your RightsLink request. No additional uses are granted (such as derivative works or other editions). For any uses, please submit a new request.

If credit is given to another source for the material you requested from RightsLink, permission must be obtained from that source.

[BACK](#)
[CLOSE WINDOW](#)


Chapter: Linear Sweep and Cyclic
 Book: Reference Module in Chemistry, Molecular Sciences and Chemical Engineering
 Author: G. Bontempelli, N. Dossi, R. Tonolo
 Publisher: Elsevier
 Date: 2016
 Copyright © 2016 Elsevier Inc. All rights reserved.

Review Order

Please review the order details and the associated [terms and conditions](#).

No royalties will be charged for this reuse request although you are required to obtain a license and comply with the license terms and conditions. To obtain the license, click the Accept button below.

Licensed Content

Licensed Content Publisher: Elsevier
 Licensed Content Publication: Elsevier Books
 Licensed Content Title: Reference Module in Chemistry, Molecular Sciences and Chemical Engineering
 Licensed Content Author: G. Bontempelli, N. Dossi, R. Tonolo
 Licensed Content Date: 2016
 Licensed Content Pages: 1

Order Details

Type of Use: reuse in a thesis/dissertation
 Portion: figures/tables/illustrations
 Number of figures/tables/illustrations: 1
 Format: electronic
 Are you the author of this Elsevier chapter?: No
 Will you be translating?: No

About Your Work

Title: DESIGN OF A TIME-TO-DIGITAL CONVERTER AND MULTI-TIME-GATED SPAD ARRAYS TOWARDS BIOMEDICAL IMAGING APPLICATIONS
 Institution name: McMaster University
 Expected presentation date: Dec 2022

Additional Data

Order reference number: 123456789
 Portions: Figures 1 (A), (B)

Requestor Location

Requestor Location: McMaster University
 91 Old Finch Avenue
 Scarborough, ON M1B5G5
 Canada
 Attn: McMaster University

Tax Details

Publisher Tax ID: GB 494 6272 12

Price

Total: 0.00 CAD



Chapter: Amperometry
 Book: Encyclopedia of Analytical Science
 Author: Aziz Amine, Hasna Mohammadi
 Publisher: Elsevier
 Date: 2019
 Copyright © 2019 Elsevier Ltd. All rights reserved.

Order Completed

Thank you for your order.

This Agreement between McMaster University – Junaid Siddiqui ("You") and Elsevier ("Elsevier") consists of your license details and the terms and conditions provided by Elsevier and Copyright Clearance Center.

Your confirmation email will contain your order number for future reference.

License Number 5411961492785

[Printable Details](#)

License date Oct 18, 2022

Licensed Content

Licensed Content Publisher Elsevier
 Licensed Content Publication Elsevier Books
 Licensed Content Title Encyclopedia of Analytical Science
 Licensed Content Author Aziz Amine, Hasna Mohammadi
 Licensed Content Date Jan 1, 2019
 Licensed Content Pages 14

Order Details

Type of Use reuse in a thesis/dissertation
 Portion figures/tables/illustrations
 Number of figures/tables/illustrations 1
 Format electronic
 Are you the author of this Elsevier chapter? No
 Will you be translating? No

About Your Work

Title DESIGN OF A TIME-TO-DIGITAL CONVERTER AND MULTI-TIME-GATED SPAD ARRAYS TOWARDS BIOMEDICAL IMAGING APPLICATIONS
 Institution name McMaster University
 Expected presentation date Dec 2022

Additional Data

Order reference number 1234567890
 Portions Figure 1 (A) - (C)

Requestor Location

McMaster University
 91 Old Finch Avenue

Tax Details

Publisher Tax ID GB 494 6272 12

Requestor Location

Scarborough, ON M1B5G5
 Canada
 Attn: McMaster University

Price

Total 0.00 USD

Paper-Based, Hand-Drawn Free Chlorine Sensor with Poly(3,4-ethylenedioxythiophene):Poly(styrenesulfonate)

Author: Yiheng Qin, Si Pan, Matlar M. R. Howlader, et al

Publication: Analytical Chemistry

Publisher: American Chemical Society

Date: Nov 1, 2016

Copyright © 2016, American Chemical Society



PERMISSION/LICENSE IS GRANTED FOR YOUR ORDER AT NO CHARGE

This type of permission/license, instead of the standard Terms and Conditions, is sent to you because no fee is being charged for your order. Please note the following:

- Permission is granted for your request in both print and electronic formats, and translations.
- If figures and/or tables were requested, they may be adapted or used in part.
- Please print this page for your records and send a copy of it to your publisher/graduate school.
- Appropriate credit for the requested material should be given as follows: "Reprinted (adapted) with permission from (COMPLETE REFERENCE CITATION). Copyright (YEAR) American Chemical Society." Insert appropriate information in place of the capitalized words.
- One-time permission is granted only for the use specified in your RightsLink request. No additional uses are granted (such as derivative works or other editions). For any uses, please submit a new request.

If credit is given to another source for the material you requested from RightsLink, permission must be obtained from that source.

[BACK](#)

[CLOSE WINDOW](#)

Appendix B Code Bases

Machine Learning Code Base

https://github.com/siddij3/Machine_Learning_for_Asparagine_GO_FCI

Firmware Code Base

https://github.com/siddij3/WQM_FreeChlorine

Android App